DYNAMIC RESOURCE ALLOCATION AND OPTIMIZATION IN WIRELESS NETWORKS

By

YANG SONG

A DISSERTATION PRESENTED TO THE GRADUATE SCHOOL
OF THE UNIVERSITY OF FLORIDA IN PARTIAL FULFILLMENT
OF THE REQUIREMENTS FOR THE DEGREE OF
DOCTOR OF PHILOSOPHY

UNIVERSITY OF FLORIDA

2010

To my beloved parents and friends

ACKNOWLEDGMENTS

I would like to gratefully and sincerely thank my Ph.D. advisor Prof. Yuguang Fang for his invaluable guidance, understanding, patience, and most importantly, his continual faith and confidence in me during my Ph.D. studies at the University of Florida. I feel extremely fortunate to have him as my advisor, who is always willing to help me both academically and personally. Thanks for everything. I also owe my wholehearted gratitude to my Ph.D. committee members, Prof. Pramod P. Khargonekar, Prof. Sartaj Sahni, Prof. Tan Wong, and Prof. Shigang Chen, for their constructive suggestions and valuable comments on my Ph.D. research and dissertation.

I have been fortunate to have many friends in WINET. I specially thank Chi Zhang, Xiaoxia Huang, Yun Zhou, Shushan Wen, Jianfeng Wang, Hongqiang Zhai, Yanchao Zhang, Feng Chen, Pan Li, Jinyuan Sun, Miao Pan, Rongsheng Huang, Yue Hao for many valuable discussions and good memories.

Last but definitely not least, this work would not have been achieved without the support and understanding of my parents. They have always supported me in every choice I have chosen in my life.

TABLE OF CONTENTS

LIST OF TABLES

LIST OF FIGURES

Abstract of Dissertation Presented to the Graduate School
of the University of Florida in Partial Fulfillment of the
Requirements for the Degree of Doctor of Philosophy

DYNAMIC RESOURCE ALLOCATION AND OPTIMIZATION IN WIRELESS NETWORKS

By

Yang Song

August 2010

Chair: Yuguang “Michael” Fang
Major: Electrical and Computer Engineering

Due to the hostile wireless medium and the limited resources in wireless networks, how well wireless networks can perform and how to make wireless networks provide better service are critical and challenging problems. These motivate our research in both theoretical analysis and protocol designs in time-varying wireless networks. In this dissertation, we aim to address the dynamic resource allocation and optimization problems in wireless networks, spanning wireless ad hoc networks, wireless mesh networks, wireless sensor networks, wireless local area networks, and cognitive radio networks.

Our contributions can be summarized as follows. First, we propose an online dynamic pricing scheme which maximizes the network revenue subject to stability in multi-hop wireless networks with multiple QoS-specific flows. Secondly, we design a novel green scheduling algorithm in multi-hop wireless networks with stochastic arrivals and time-varying channel conditions which minimizes the energy expenditure subject to network stability. Thirdly, we develop a negotiation-based algorithm which attains an ϵ-optimal solution to the non-convex joint power and frequency allocation problem in cooperative wireless mesh access networks. In addition, we analyze the existence and the inefficiency of the Nash equilibrium in non-cooperative wireless mesh access networks and proposed pricing schemes to improve the equilibrium efficiency. Fourthly, we propose a queueing based model to capture the cross layer

interactions in multi-hop wireless sensor networks and designed a joint rate admission control, traffic engineering, dynamic routing and scheduling scheme to maximize the overall network utility. Fifthly, we analyze the thresholds-based rate adaptation algorithms in IEEE 802.11 WLANs from a reverse engineering perspective and propose a threshold optimization algorithm to enhance the performance of IEEE 802.11 WLANs. Finally, we investigate the stochastic traffic engineering problem in multi-hop cognitive radio networks and derive a distributed algorithm based on the stochastic primal-dual approach for convex scenarios as well as a general solution based on the learning automata techniques for non-convex scenarios.

CHAPTER 1
INTRODUCTION

WANETs are self-configuring and stand-alone networks of nodes connected by wireless links. They have attracted extensive attention as ideal networking solutions for scenarios where fixed network infrastructures are not available or reliable. In addition, multimedia transmissions have become an indispensable component of network traffic nowadays. However, the issue of QoS provisioning for multimedia transmissions is remarkably challenging in multi-hop wireless ad hoc networks. Time varying channel conditions among wireless links impose severe adverse impact on the QoS of multimedia transmissions. Therefore, while wired networks have mature solutions and established protocols for providing QoS, novel solutions which incorporate salient features of wireless transmissions need to be developed to support multimedia transmissions in multi-hop wireless networks. In addition, from the network provider's perspective, it is imperative to design a pricing mechanism which maximizes the network revenue while addressing the QoS requirements of users. Such a scheme should also ensure a network-wide stability under stochastic traffic arrivals and time varying channel conditions. In Chapter 2, we proposed a QoS-aware dynamic pricing scheme which provably ensures the network-wide stability while attaining a solution which is arbitrarily close to the global maximum revenue, with a controllable tradeoff with the average delay in the network. Moreover, a weight assignment mechanism is devised to address the service differentiation issue for multiple flows in the network with different delay priorities.

In Chapter 3, we investigate the issue of *Green Computing* in wireless networks, which is an important concern raised from computer scientists and engineers that attempts to utilize the computing resources efficiently while introducing minimum impact on the environment. In multi-hop wireless networks, we first identify that the well-established MaxWeight, or back-pressure scheduling algorithm, is not energy-optimal. The scheduling process of the MaxWeight algorithm neglects the

enormous energy consumption in retransmissions which are not negligible in wireless networks with fading channels. To address this, we proposed a minimum energy scheduling algorithm which significantly reduced the overall energy expenditure compared to the original MaxWeight algorithm. The energy consumption induced by the proposed algorithm can be pushed arbitrarily close to the global minimum solution. Moreover, the improvement on the energy efficiency is achieved without losing the throughput-optimality.

A wireless mesh network is characterized by a multi-hop wireless backbone connecting wired Internet entry points, or gateways, and wireless access points (AP) which provide network access to end users. In a WMN, how to assign multiple channels and power levels to each AP is of great importance to maximize the overall network utilization and the aggregated throughput. In Chapter 4, we investigate the non-convex throughput maximization problem in WMNs for both cooperative and non-cooperative scenarios. In the cooperative case, we model the interactions among all APs as an *identical interest game* and present a decentralized negotiation-based throughput maximizing algorithm for the joint frequency and power assignment problem. We prove that this algorithm converges to the optimal frequency and power assignment solution, which maximizes the overall throughput of the wireless mesh network, with arbitrarily high probability. In the case of non-cooperative APs, we prove the existence of Nash equilibria and show that the overall throughput performance is noticeably inferior to the cooperative scenario. To bridge the performance gap, we develop a pricing scheme to combat the selfish behaviors of non-cooperative APs. The overall network performance in term of aggregated throughput is significantly improved.

Recent years have witnessed a surge in research and development of WSNs for their broad applications in both military and civilian operations. Before the wide deployment of wireless sensor networks, a systematic understanding about the performance of multi-hop wireless sensor networks is desired. However, finding a

suitable and accurate analytical model for wireless sensor networks is particularly challenging. An appropriate model should reflect the realistic network operations with emphasis on the distinguishing features of wireless sensor networks such as the challenge of automatic load balancing among multiple sink nodes, the task of dynamic network scheduling and routing under time varying channel conditions, and the instantaneous decision-making on the number of admitted packets in order to ensure the network-wide stability. To capture the cross layer interactions of multi-hop wireless sensor networks, in Chapter 5, we proposed a constrained queueing model to investigate the joint rate admission control, dynamic routing, adaptive link scheduling, and automatic load balancing in wireless sensor networks through a set of interconnected queues. To demonstrate the effectiveness of the proposed constrained queueing model, we investigate the stochastic network utility maximization problem in multi-hop wireless sensor networks. Based on the proposed queueing model, we develop an adaptive network resource allocation scheme which yields a near-optimal solution to the stochastic network utility maximization problem. The proposed scheme consists of multiple layer components such as joint rate admission control, traffic splitting, dynamic routing, and an adaptive link scheduling algorithm. Our proposed scheme is essentially an online algorithm which only requires the instantaneous information of the current time slot and hence remarkably reduces the computational complexity.

IEEE 802.11 WLAN has become the dominating technology for indoor wireless Internet access. In order to maximize the network throughput, IEEE 802.11 devices, i.e., stations, need to adaptively change the data rate to combat the time varying channel environments. However, the specification of rate adaptation algorithms is not provided by the IEEE 802.11 standard. This intentional omission encourages the studies on this active area where a variety of rate adaptation algorithms have been proposed. Due to its simplicity, the thresholds-based rate adaptation algorithm is predominantly adopted by vendors. The data rate increases if a certain number of

consecutive transmissions are successful. Although widely deployed, the obscure objective function of this type of rate adaptation algorithms, commonly based on the heuristic up/down mechanism, is less comprehended. In Chapter 6, we study the thresholds-based rate adaptation algorithm from a reverse engineering perspective. The implicit objective function, which the rate adaption algorithm is maximizing, is unveiled. Our results provide an analytical model from which the heuristics-based rate adaptation algorithm, such as ARF, can be better understood. Moreover, we propose a threshold optimization algorithm which dynamically adapts the up/down thresholds. Our algorithm provably converges to the set of stochastic optimum thresholds in arbitrary stationary yet potentially fast-varying channel environments and the performance in term of throughput is enhanced remarkably.

In Chapter 7, we investigate the stochastic traffic engineering (STE) problem in multi-hop cognitive radio networks. More specifically, we are particularly interested in how the traffic in the multi-hop cognitive radio networks should be steered, under the influence of random returns of primary users. It is worth noting that given a routing strategy, the corresponding networks performance, e.g., the average queueing delay encountered, is a random variable. In multi-hop cognitive radio networks, this distinguishing feature of randomness, induced by the unpredictable behaviors of primary users, must be taken into account in protocol designs. We formulate the STE problem in a stochastic network utility maximization framework. For the case where convexity holds, we derive a distributed cross layer algorithm via the stochastic primal-dual approach, which provably converges to the global optimum solution. For the scenarios where convexity is not attainable, we propose an alternative decentralized algorithmic solution based on the learning automata techniques. We show that the algorithm converges to the global optimum solution asymptotically under mild conditions. Finally, Chapter 8 concludes this dissertation.

CHAPTER 2
REVENUE MAXIMIZATION IN MULTI-HOP WIRELESS NETWORKS

2.1 Introduction

In recent years, multi-hop wireless networks have made significant advance in both academic and industrial aspects. Besides traditional data services, multimedia transmissions become an indispensable component of network traffic nowadays. For example, people can watch live games while listening to online musical stations at the same time. Therefore, supporting multimedia services in multi-hop wireless networks effectively and efficiently has received intensive attention from the community. However, the issue of QoS provisioning for multimedia transmissions is remarkably challenging in multi-hop wireless networks. Time varying channel conditions among wireless links impose severe adverse impact on the QoS of multimedia transmissions. Therefore, while wired networks have mature solutions and established protocols for providing QoS, novel solutions which incorporate salient features of wireless transmissions, need to be developed to support multimedia transmissions in multi-hop wireless networks.

Multimedia flows usually impose application-specific requirements on the minimum average attainable data rates from the network. Furthermore, different multimedia flows may have distinct rate requirements. For example, multimedia streams for high quality video-on-demand (VoD) movie transmissions usually require larger minimum data rates on average than those of online music transmissions. Consequently, a natural question arises that how the network resource should be allocated such that all the minimum rate constraints are satisfied simultaneously. In addition, due to the nature of wireless transmissions, decentralized solution with low complexity is strongly desired. In this chapter, we investigate the resource allocation problem in multi-hop wireless networks, from a network administrator's perspective. For each flow, the network charges a certain amount of admission fee in order to build up a system-wide revenue. The price imposed on each flow is subject to adaptation in order to obtain the optimum revenue. Hence, a

dynamic pricing policy is desired by the network administrator to maximize the overall network revenue subject to the stability of the network. To achieve this, we propose a QoS-aware dynamic pricing algorithm, namely, QADP, which provably accumulates a network revenue that is arbitrarily close to the optimum solution while maintaining network stability under stochastic traffic arrivals and time varying channel conditions. Meanwhile, the minimum date rate requirements from all multimedia flows are satisfied simultaneously.

Besides minimum data rates, multimedia flows, especially wireless video transmissions, usually impose additional requirements on maximum end-to-end delays. For example, a multimedia stream for video surveillance may need a lower data transmission rate compared to high quality video-on-demand movie transmissions, whereas a much more stringent delay requirement is imposed. Therefore, the network inclines to allocate more network resource to those delay-imperative multimedia transmissions provided that the minimum data rate requirements of all flows are satisfied. Unfortunately, however, an *absolute* guarantee for arbitrary delay requirements is extremely difficult, if not impossible, due to the lack of accurate delay analysis in multi-hop wireless networks. For example, [1] derives a lower bound on the delay performance of arbitrary scheduling policy in multi-hop wireless networks. However, the upper bound of delay is unspecified. In fact, it is shown that in wireless scenarios, even to decide whether a set of delay requirements can be supported by the network is an $\mathcal{NP}$-hard problem and thus is intrinsically difficult to solve [2]. Even worse yet, time varying wireless channel conditions and stochastic traffic arrivals significantly exacerbate the hardness of sheer delay guarantees. In light of this, in this work, we alternatively aim to provide a *service differentiation* solution for the delay requirements of all flows. More specifically, the network provides a set of *service levels*, denoted by $\ell = 1, \cdots, L$ where level one has the highest priority in the system with respect to delay guarantees. Note that L can be arbitrarily large. Each multimedia flow, according to the upper layer application, proposes a service level request to the

network. For example, a background traffic for movie downloading is associated with level ten whereas a VoD online movie transmission demands a service level of two[1] . By meticulously assigning weights to multimedia flows, QADP algorithm provides a service differentiation solution in a way that the guaranteed maximum average end-to-end delay for service level one traffic is j times less than that of level j transmissions, where $j = 1, \cdots, L$. In other words, level one transmissions have the minimum upper bound for end-to-end delay and thus represent the highest priority. Therefore, by following QADP, a QoS-aware revenue maximization solution, subject to the stability of the network, is provided. QADP algorithm is inherently an online dynamic control based algorithm which is self-adaptive to the changes of statistical characteristics of traffic arrivals. Moreover, our scheme enjoys a decoupled structure and hence is suitable for decentralized implementation which is of great interest for protocol design in multi-hop wireless networks. Note that our results are applicable to some special interesting cases of network topology such as single-hop wireless cellular networks.

The rest of this chapter is organized as follows. Section 2.2 compares our work with other existing solutions on network optimization with multiple flows. System model and problem formulation are provided in Section 2.3. Our proposed solution, i.e., QADP algorithm, is introduced in Section 2.4 followed by the performance analysis in Section 2.5. Simulation results are provided in Section 2.6 and Section 2.7 concludes this chapter.

2.2 Related Work

There exists a rich literature on how the network resource should be allocated efficiently among multiple competitive transmitting flows. According to the network model, they can be roughly divided into two categories, i.e., *fluid based* approach and

[1] We emphasize that this application-to-service-level mapping is arbitrary and can be specified by the network before transmissions.

queue based approach. In fluid based algorithms, e.g., [3–7], the characteristics of a particular flow are uniquely associated with fluid variables. For example, the flow injection rate is a commonly used fluid variable which is determined by the source node. However, whenever a change of the flow injection rate occurs, it is usually assumed that all the nodes on the path will perceive this change instantaneously. In addition, the knowledge of up-to-date local information on intermediate nodes, e.g., shadow prices [4, 6, 7], is usually vital for the flow control algorithm implemented on the source node. Simply put, state information of a particular flow is usually assumed to be shared and known by all nodes on its path instantaneously and accurately, although some exceptions are discussed, e.g., [8]. In general, fluid based approach does not consider the practical queue dynamics in real networks. Moreover, fluid based algorithms usually utilize a dual decomposition framework, such as in [3, 4, 7] which heavily relies on convex optimization techniques [9]. Consequently, a fixed point solution is attained. However, in time varying environments such as wireless networks, a fixed operating point is hardly optimal[2] . On the contrary, queue based approach models the network as a set of interconnected queues. Each source node injects packets into the network which traverse through the network hop by hop until reach the destination. Every packet needs to wait for service in the queues of intermediate nodes along the path, which reflects the reality in practical networks. In addition, queue based approach usually adopts a dynamic control based solution where responsive actions are adjusted on the fly by which a long term average optimum is achieved. In this work, we utilize a queue based network model where an optimal dynamic pricing policy is developed. For more discussions on fluid based algorithms, refer to [10, 11] and the references therein.

[2] In fact, in the work, we analytically show that the imposed price needs to be adjusted dynamically in order to achieve the optimum.

The interconnected queue network model has attracted significant attention since the seminal work of [12] where the well-known *MaxWeight* scheduling algorithm is proposed. Neely extends the results into a general time varying setting in [13, 14], based on which a pioneering stochastic network optimization technique is developed [15, 16]. For a comprehensive treatment on this area, refer to [17] and the references therein. Unfortunately, in the literature, few work has been devoted to addressing the issue of QoS provisioning in practical wireless settings, which is of special interest in supporting multimedia transmissions in multi-hop wireless networks. For example, [18–20] investigate the delay constraints by assuming that the queue behaves as an M/M/1 queue. However, this may not be realistic due to the complex interaction of queues induced by the scheduling algorithm. In [2, 21, 22], delay guaranteed scheduling algorithms are studied. However, the derived delay bound is up to a logarithmic factor of the proposed delay requirement, given that the delay requirements satisfy certain per-server and per-session conditions [2]. Finding a general policy that is able to achieve arbitrary feasible delay requirements is still an open problem. In addition, while existing solutions on prioritized transmissions are available, e.g., [23, 24], the question of how to achieve a minimum data rate guarantee concurrently, as well as maximizing a system-wide revenue, is unspecified. In [25, 26], lazy packet scheduling algorithms are proposed. However, they require the knowledge on future stochastic arrivals as a priori, while in our scheme, a.k.a., QADP algorithm, such information is not needed.

Revenue maximization problem has been studied extensively in the literature for many different settings. Nevertheless, in general, either QoS provisioning is not particularly addressed[27–30], or the network model is restricted to wired networks where the channel conditions of the system are assumed to be time-invariant and remain unchanged [31, 32]. Our work is inspired by [33]. However, our work differs from [33] in the following crucial aspects. First, [33] studies a single hop network with only one access point (AP) while our work investigates a general multi-hop wireless ad

hoc network where exogenous arrivals may enter the network via any node. Secondly, [33] assumes a Markovian user traffic demand while our work is applicable to arbitrary traffic demands. Thirdly and most importantly, [33] does not consider the issue of QoS provisioning for multiple transmission flows, which is the main focus of our work. To the best of our knowledge, this work is the first work to address the problem of revenue maximization, subject to network stability while providing QoS differentiations to quality-sensitive traffics such as multimedia video transmissions.

2.3 Revenue Maximization with QoS (Quality of Service) Requirements

2.3.1 System Model

We consider a static multi-hop wireless network represented by a directed graph $\mathcal{G} = (\mathcal{N}, \mathcal{E})$, illustrated in Figure 2-1, where $\mathcal{N}$ is the set of nodes and $\mathcal{E}$ is the set of links. The numbers of nodes and links in the network are denoted by N and E, respectively. A link is denoted either by $e \in \mathcal{E}$ or $(a, b) \in \mathcal{E}$ where a and b are the transmitter and the receiver of the link. Time is slotted, i.e., $t = 0, 1, \cdots$. For link (a, b), the instantaneous channel condition at time slot t is denoted by $S_{a,b}(t)$. For example, $S_{a,b}(t)$ can represent the time varying fading factor on link (a, b) at time t. Denote $\mathbf{S}(t)$ as the channel condition vector on all links. We assume that $\mathbf{S}(t)$ remains constant during a time slot. However, $\mathbf{S}(t)$ may change on slot boundaries. We assume that there are a finite but arbitrarily large number of possible channel condition vectors and $\mathbf{S}(t)$ evolves following a finite state irreducible Markovian[3] chain with well defined steady state distribution. However, the steady state distribution itself and the transition probabilities are unknown. At each time slot t, given the channel state vector $\mathbf{S}(t)$, the network controller chooses a *link schedule*, denoted by $I(t)$, from a feasible set $\Upsilon_{\mathbf{S}(t)}$, which is restricted by factors such as underlying interference model, duplex constraints

[3] Note that the Markovian channel state assumption is not essential and can be relaxed to a more general setting as in [14].

or peak power limitations. For a wireless link (a, b), the link data rate $\mu_{a,b}(t)$ is a function of $I(t)$ and $\mathbf{S}(t)$. We denote $\boldsymbol{\mu}(t)$ as the vector of link rates of all links at time slot t.

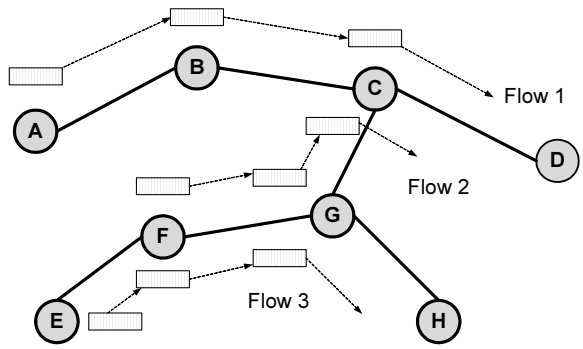

Figure 2-1. An example of multi-hop wireless networks

There are C commodities, a.k.a., flows, in the network, where each commodity, say $c, c = 1, 2, \cdots, C$, is associated with a routing path $P_c = \{c(0), c(1), \cdots, c(\kappa_c)\}$ where $c(0)$ and $c(\kappa_c)$ are the source and the destination node of flow c while $c(j)$ denotes the j-th hop node on its path. Without loss of generality, we assume that every node in the network initiates at most one flow[4] . However, multiple flows can intersect at any node in the network. Each node maintains a separate queue for every flow that passes through it. For each flow c, denote $A_c(t)$ as the exogenous arrival to the *transport layer* of node $c(0)$ during time slot t. We assume that the stochastic arrival process, i.e., $A_c(t)$, has an expected average rate of λ_c. More specifically, we have

$$\lim_{t\to\infty} \frac{1}{t} \sum_{\tau=0}^{t-1} E(A_c(\tau)) = \lambda_c \quad \forall c. \tag{2–1}$$

For a single queue, define the *overflow function* [13] as

$$g(B) = \limsup_{t\to\infty} \frac{1}{t} \sum_{\tau=0}^{t-1} Pr(Q(\tau) > B) \tag{2–2}$$

[4] If a node initiates more than one flow in the network, we can replace this node with multiple duplicate nodes and the following analysis still holds.

where $Q(\tau)$ is the *queue backlog* at time τ. We say the queue is *stable* if [13, 14]

$$\lim_{B\to\infty} g(B) \to 0. \tag{2–3}$$

A network is stable if all the queues in this network are stable.

Denote $\boldsymbol{\lambda} = \{\lambda_1, \cdots, \lambda_C\}$ as the *arrival rate vector* of the network. Note that all the arrival rate vectors are defined in an average sense. A flow control mechanism is implemented where during time slot t, an amount of $R_c(t)$ traffic is admitted to the network layer for flow c. Apparently, we have $R_c(t) \leq A_c(t)$. For simplicity, we assume that there are no reservoirs to hold the excessive traffic, i.e., incoming packets are dropped if not admitted. However, we emphasize that our analysis can be applied to general cases where transport layer reservoirs are deployed to buffer the un-admitted traffic. The *network capacity region*, a.k.a., the *network stability region*, denoted by Ω, is defined as all the admission rate vectors that can be supported by the network, in the sense that there exists a policy that stabilizes the network under this admission rate. Moreover, we are particularly interested in multimedia transmissions where each flow c has specific QoS requirements. To be specific, each flow c has a minimum data rate requirement α_c as well as an application-dependent prioritized service level request, denoted by $\ell_c, 1 \leq \ell_c \leq L$. Denote $\boldsymbol{\alpha} = \{\alpha_1, \cdots, \alpha_C\}$ and $\boldsymbol{\ell} = \{\ell_1, \cdots, \ell_C\}$ as the *minimum rate vector* and the *service level request vector* of the network where ℓ_1 has the highest priority in terms of the delay guarantees provided by the network. In addition, we assume that the minimum rate vector, i.e., $\boldsymbol{\alpha}$, is *inside* of the network capacity region Ω. Since that if $\boldsymbol{\alpha}$ is inherently not feasible, we cannot expect to find any policy to meet those demands and the only solution is to increase the network's information-theoretic capacity by traditional methods such as adding more channels, radios, enabling network coding, or utilizing MIMO techniques with multiple antennas. Nevertheless, in this work, we restrict ourselves to the specific question of how to find a simple yet optimal policy for the network if such requirements are indeed theoretically attainable. We

emphasize that, however, the answer to this question is by no means straightforward due to the intractability of quantifying the underlying network capacity region. Moreover, time varying channel conditions and stochastic exogenous arrivals make the problem even more challenging. It is our main objective to develop an optimum policy without knowing the network capacity region and the statistical characteristics of random arrival processes as well as time varying channels. We will formulate the QoS-aware revenue maximization problem next.

2.3.2 Problem Formulation

Denote the *queue backlog* of node n for flow c as $Q_n^c(t)$. Note that $Q_{c(\kappa_c)}^c \equiv 0$ since whenever a packet reaches the destination, it is considered as leaving the network. The queue updating dynamic of $Q_n^c(t)$ is given as follows. For $j = 1, \cdots, \kappa_c - 1$, we have

$$Q_{c(j)}^c(t+1) \leq [Q_{c(j)}^c(t) - \mu_{c(j),c}^{out}(t)]^+ + \mu_{c(j),c}^{in}(t) \tag{2–4}$$

and for $j = 0$,

$$Q_{c(j)}^c(t+1) = [Q_{c(j)}^c(t) - \mu_{c(j),c}^{out}(t)]^+ + R_c(t) \tag{2–5}$$

where $[x]^+$ denotes $\max(x, 0)$ and $\mu_{n,c}^{in}(t)$, $\mu_{n,c}^{out}(t)$ represent the allocated data rate of the incoming link and the outgoing link of node n, by the scheduling algorithm, with respect to flow c. Note that (2–4) is an inequality since the previous hop node may have less packets to transmit than the allocated data rate $\mu_{c(j),c}^{in}(t)$.

During time slot t, $p_c(t)$ is charged for flow c as the *per unit flow* price. The functionality of the price is not only to control the admitted flows, but also, more importantly, to build up a system-wide revenue from the network's perspective. We further assume that each flow is associated with a particular user and thus we will use *flow* and *user* interchangeably. Every user c is assumed to have a concave, differentiable utility function $\mathcal{O}_c(R_c(t))$ which reflects the degree of satisfaction by transmitting with data rate $R_c(t)$. At time slot t, user c selects a data rate which

optimizes the net income, a.k.a., *surplus*, i.e.,

$$R_c(t) = \text{argmax}_r \left(\mathcal{O}_c(r) - r \times p_c(t)\right) \quad \forall c = 1, \cdots, C. \tag{2–6}$$

Without loss of generality, we assume that

$$\mathcal{O}_c(r) = \log(1 + r). \tag{2–7}$$

However, we stress that the following analysis can be extended to other heterogeneous forms of utility functions straightforwardly. Note that the fairness issue of multiple flows can be solved by choosing utility functions properly. For example, a utility function of $\log(r)$ represents the proportional fairness among competitive flows. For more discussions, refer to [4] and [10].

From the network administrator's perspective, the overall network-wide revenue is the target to be maximized. Meanwhile, the stability of the network as well as the QoS requirements from multimedia flows need to be addressed. Formally speaking, the objective of the network is to find an optimal policy to

<u>QoS-Aware Revenue Maximization Problem:</u>

$$\text{maximize} \quad D = \liminf_{t \to \infty} \frac{1}{t} \sum_{\tau=0}^{t-1} O(\tau) \tag{2–8}$$

s.t.

(a) the network is stable,

(b) the minimum data rate requirements, i.e., $\boldsymbol{\alpha}$, are satisfied,

(c) the guaranteed maximum end-to-end delays for multiple multimedia flows are prioritized according to the service levels of $\boldsymbol{\ell}$,

where

$$O(t) = E(\sum_c R_c(t) p_c(t)) \tag{2–9}$$

is the *expected* overall network revenue during time slot t, with respected to the randomness of arrival processes and channel variations.

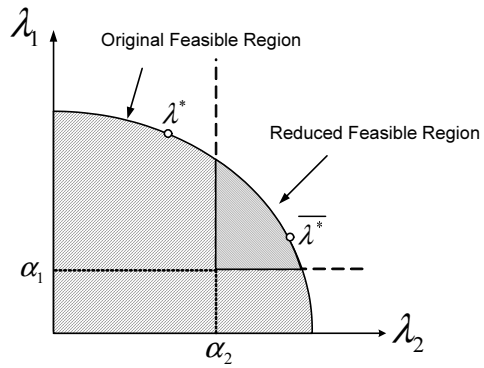

Figure 2-2. A conceptual example of the network capacity region with two multimedia flows. The minimum data rate requirements reduce the feasible region of the optimum solution

However, the QoS-aware revenue maximization problem is inherently challenging due to unawareness of future random arrivals and stochastic time varying channel conditions. Even worse yet, the QoS requirements significantly complicate the problem, as illustrated in Figure 2-2. In unconstrained cases, the feasible region of the optimum solution $\boldsymbol{\lambda}^*$ is essentially the whole network capacity region. However, as shown in Figure 2-2, the original optimum solution may not even be feasible under the minimum data rate requirements. Besides, finding a policy which achieves the new constrained optimum solution, denoted by $\overline{\boldsymbol{\lambda}^*}$, is a nontrivial task as well. In addition, due to the multi-hop nature of wireless transmissions, decentralized solutions with low complexity are remarkably favorable. To address the aforementioned concerns, in next section, we will propose an optimal online policy, namely, QADP, which provably generates a network revenue that is arbitrarily close to the optimum solution of (2–8). Meanwhile, the imposed requirements of the problem, i.e., (a), (b) and (c), are achieved on the fly.

In the following, we first assume that the arrival rate vector $\boldsymbol{\lambda}$ lies outside of the capacity region Ω for all time slots, i.e., a heave traffic scenario.

2.4 QoS-Aware Dynamic Pricing (QADP) Algorithm

In this section, we propose an online policy, i.e., QADP algorithm, which solves the QoS-aware revenue maximization problem in (2–8).

We first introduce some system-wide parameters to facilitate our analysis. Define $R_c^{\max}$ as the upper bound of admitted traffic of flow c during one time slot, i.e., $R_c(t) \leq R_c^{\max}, \forall c, t$. For example, $R_c^{\max}$ can represent the hardware limitation on the maximum volume of traffic that a node can admit during one time slot, or simply the peak arrival rate within one time slot if such information is available. Let μ^{max} be the maximum data rate on *any* link of the network, which may be determined by factors such as the number of antennas, modulation schemes and coding policies. In addition, for each flow c, we introduce a *virtual queue* $Y_c(t)$ which is initially empty, and the queue updating dynamic is defined as

$$Y_c(t+1) = [Y_c(t) - R_c(t)]^+ + \alpha_c \quad \forall c. \tag{2–10}$$

Note that virtual queues are easy to implement. For example, the source node of flow c, i.e., $c(0)$, can maintain a software based counter to measure the backlog updates of virtual queue $Y_c(t)$. In addition, for each flow c, we define

$$\delta_c = N(\mu^{\max})^2 + (R_c^{\max})^2 + \frac{1}{2}(\alpha_c)^2 \quad \forall c. \tag{2–11}$$

Denote $\theta^1, \cdots, \theta^C$ as the weights which will be calculated and assigned to all flows, where C denotes the number of flows in the network. Let J be a tunable[5] positive large number determined by the network. In addition, we assume a maximum value of the allocated weight, denoted by $\theta^{\max}$, i.e., $\theta^c \leq \theta^{\max}, \forall c$. The proposed QADP algorithm is given as follows.

QADP ALGORITHM:

- ***Part I: Weight Assignment***
  For all multimedia transmissions, find the flow with the minimum value of $\alpha_c \times \ell_c, c = 1, \cdots, C$, say, flow j. For each flow c, assign an associated *weight*, denoted

[5] The impact of J on the performance of QADP algorithm will be clarified shortly.

by θ^c, which is calculated by

$$\theta^c = \frac{\theta^{\max} \times \alpha_j \times \ell_j}{\alpha_c \times \ell_c}, \quad \forall c = 1, \cdots, C. \tag{2–12}$$

- ***Part II: Dynamic Pricing***
  For every time slot t, the source node of flow c, i.e., $c(0)$, measures the value of $Q^c_{c(0)}(t)$ and $Y_c(t)$. If $Q^c_{c(0)}(t) > Y_c(t)$, the instantaneous admission price is set as

$$p_c(t) = \sqrt{\frac{\theta^c \left(Q^c_{c(0)}(t) - Y_c(t) \right)}{J}} \tag{2–13}$$

  and $p_c(t) = 0$ otherwise.

- ***Part III: Scheduling***
  For every time slot t, find a link schedule $I^*(t)$, from the feasible set $\Upsilon_{S(t)}$, which solves

$$\max_{I(t) \in \Upsilon_{S(t)}} \sum_{(a,b) \in \mathcal{E}} \mu_{a,b}(t) \xi_{a,b} \tag{2–14}$$

  where

$$\xi_{a,b} = \max_{c:(a,b) \in P_c} \left(\theta^c (Q^c_a(t) - Q^c_b(t)) \right) \tag{2–15}$$

  if $\exists c$, such that $(a, b) \in P_c$, and $\xi_{a,b} = 0$ otherwise.

END

It is worth noting that Part I of QADP can be precalculated before actual transmissions. The weight assignment can be implemented either by the network controller which knows the QoS requirements of all flows, or by mutual information exchanges among multiple multimedia flows, in a decentralized fashion. The value of θ^c represents the QoS-wise "importance" of flow c and remains unchanged unless the QoS requirements from flows, i.e., $(\boldsymbol{\alpha}, \boldsymbol{\ell})$, are updated, by which a new weight calculation is triggered.

The dynamic pricing part is the crucial component of QADP. By following (2–13), not only the incoming admitted rates can be regulated effectively, but also the overall average network revenue can be maximized, as will be shown shortly. Note that after the weight assignment, in order to compute $p_c(t)$, the source node of flow c, i.e., $c(0)$, which is considered as the edge node of the network, requires only local information, i.e., current backlogs of the source data queue and the virtual queue. It is interesting

to observe that if $Q^c_{c(0)}(t) \leq Y_c(t)$, the admission is free! Intuitively, a small value of $Q^c_{c(0)}(t)$ indicates a deficient arrival rate of flow c. On the contrary, a large value of $Y_c(t)$ means that the average "service rate" is less than the average "arrival rate" and thus the virtual queue is building up. Note in (2–10) that this indicates that the average of $R_c(t)$ falls below the arrival rate, i.e., α_c. Therefore, when $Q^c_{c(0)}(t) \leq Y_c(t)$, the network provides free admission to encourage more incoming packets in order to satisfy the QoS constraints. We will make this intuition precise and rigorous in the following section.

The third part of QADP is a *weighted* extension to the well-known *MaxWeight* scheduling algorithm [12, 13, 34]. Instead of the *exact difference* of queue backlogs, we deliberately select the *weighted difference* of queue backlogs as the weight of a particular link in the scheduling algorithm. Intuitively, if a flow is assigned with a larger value of θ^c, the links associated with it will have a higher possibility of being selected for transmissions by QADP. Therefore, by assigning proper values of θ^c to flows with different QoS requirements, a *service differentiation* can be achieved which provides more flexibility to previous schemes in the literature, e.g., [13, 15, 16]. In addition, as indicated by (2–13), a higher priority needs to pay at a higher price. Note that to calculate (2–14), QADP needs to solve a complex optimization problem which requires a global information on channel states, i.e., $\mathbf{S}(t)$. However, availed of the prosperous development of distributed scheduling schemes, such as [35–38], the difficulty of centralized computation can be circumvented, which provides QADP algorithm the amenability for decentralized implementations.

2.5 Performance Analysis

In this section, we provide the main result on the performance of QADP algorithm.

Theorem 2.1. *Define D^* as the optimum solution of (2–8). For QADP algorithm, we have*

(a) *Revenue Maximization*

$$\liminf_{t\to\infty} \frac{1}{t}\sum_{\tau=0}^{t-1} O(\tau) \geq D^* - \frac{K}{J} \tag{2–16}$$

where K is a constant and is given by

$$K = \sum_{c} \theta^c \delta_c \tag{2–17}$$

and δ_c is defined in (2–11).

(b) *Network Stability*
The network is stable under QADP algorithm, i.e., for every queue in the network, (2–3) is satisfied.

(c) *QoS Provisioning*
By following QADP algorithm, any feasible *minimum data rate requirements $\boldsymbol{\alpha}$ can be satisfied. In addition, the guaranteed maximum average end-to-end delays for multimedia flows with service level j are j times larger than that of level one transmissions.*

It is of great importance to observe that in (2–16), the achieved performance of QADP algorithm can be pushed arbitrarily close to the optimum solution D^* by selecting a sufficiently large value of J. The proof of Theorem 2.1 is provided in the rest of this section.

2.5.1 Proof of Revenue Maximization

Recall that the minimum rate vector $\boldsymbol{\alpha}$ is assumed to lie *inside* the capacity region Ω. Therefore, there exists a small positive number $\tilde{\epsilon} > 0$ such that $\boldsymbol{\alpha} + \tilde{\epsilon}\mathbf{1} \in \Omega$ where $\mathbf{1}$ is a unity vector with dimension C.

Lemma 1. *For any* feasible *input rate vector $\boldsymbol{\vartheta}$, there exists a stationary*[6] *randomized policy, denoted by* RAND*, which generates*

$$E\left(\mu_{n,c}^{out} - \mu_{n,c}^{in} - \vartheta_n^c(t)\right) = 0 \quad \forall n, c, t \tag{2–18}$$

[6] Stationary means that the probabilistic structure of the randomized policy does not change with different values of queue backlogs.

and

$$E(\vartheta^c_{c(0)}(t)) \geq \alpha_c + \tilde{\epsilon} \quad \forall t, c \tag{2–19}$$

where $\vartheta^c_n(t)$ *is the exogenous arrival on node* n *for flow* c *during time slot* t*.*

Proof. (Sketch) The proof of Lemma 1 utilizes standard techniques as in [13, 15, 16]. The basic idea is to reduce the exponentially large dimension of extreme points to a finite set with dimension $E + 1$ by Caratheodory's Theorem. Then a randomized link schedule selection is implemented among all reduced $E+1$ extreme points. The detailed proof is omitted.

We emphasize that Lemma 1 is only an existence proof in the sense that the randomized algorithm *RAND* cannot be implemented in practice. This is because that *RAND* requires a prior knowledge on the network capacity region, i.e., the underlying steady state distribution of Markovian channels, and hence is computationally prohibitive. However, the existence of *RAND* plays a crucial role for the performance analysis of QADP algorithm, which, in contrast, is an online adaptive policy and does not require the statistical characteristics of the stochastic arrivals and time varying channel conditions.

Recall that a virtual queue $Y_c(t)$ is introduced for every flow c and the queue updating dynamic is given by (2–10). As a result, the minimum data rate requirement is converted to a queue stability problem since if the virtual queue $Y_c(t)$ is stable, the average service rate, i.e., the time average of $R_c(t)$, needs to be greater than the average arrival rate, i.e., α_c. Define $\boldsymbol{Z}(t) = [\boldsymbol{Q}(t); \boldsymbol{Y}(t)]$ as all the real data queues and virtual queues at time slot t. If we can ensure that the network is stable with respect to $\boldsymbol{Z}(t)$, the backlogs of real queues are bounded and the minimum rate requirements are achieved at the same time.

Define a system-wide *potential function (PF)* as

$$PF(\boldsymbol{Z}(t)) = \sum_c PF^c(\boldsymbol{Z}(t)) \tag{2–20}$$

where

$$PF^c(\boldsymbol{Z}(t)) = \frac{1}{2}\left(\sum_n \theta^c(Q_n^c(t))^2 + \theta^c(Y_c(t))^2\right). \tag{2–21}$$

Note that $PF(\boldsymbol{Z}(t))$ is a scalar-valued nonnegative function. Define

$$\Delta(\boldsymbol{Z}(t)) = E\left(PF(\boldsymbol{Z}(t+1)) - PF(\boldsymbol{Z}(t))|\boldsymbol{Z}(t)\right) \tag{2–22}$$

as the *drift* of the potential function $PF(\boldsymbol{Z}(t))$.

For flow c, we take the square of both sides of (2–4) and (2–5) and obtain[7]

$$\begin{aligned}\left(Q_{c(j)}^c(t+1)\right)^2 &\leq \left(Q_{c(j)}^c(t)\right)^2 + \left(\mu_{c(j),c}^{out}(t)\right)^2 \\ &+ \left(\mu_{c(j),c}^{in}(t)\right)^2 - 2Q_{c(j)}^c(t)\left(\mu_{c(j),c}^{out}(t) - \mu_{c(j),c}^{in}(t)\right)\end{aligned}$$

for $j = 1, \cdots, \kappa_c - 1$, and

$$\begin{aligned}\left(Q_{c(j)}^c(t+1)\right)^2 &\leq \left(Q_{c(j)}^c(t)\right)^2 + \left(\mu_{c(j),c}^{out}(t)\right)^2 \\ &+ \left(R_c(t)\right)^2 - 2Q_{c(j)}^c(t)\left(\mu_{c(j),c}^{out}(t) - R_c(t)\right)\end{aligned} \tag{2–23}$$

for $j = 0$. Similarly, for (2–10), we have

$$\begin{aligned}(Y_c(t+1))^2 &\leq (Y_c(t))^2 + (R_c(t))^2 + (\alpha_c)^2 \\ &\quad -2Y_c(t)(R_c(t) - \alpha_c).\end{aligned} \tag{2–24}$$

[7] We use the fact that for nonnegative real numbers a, b, c, d, if $a \leq [b-c]^+ + d$, then $a^2 \leq b^2 + c^2 + d^2 - 2b(c-d)$, as given in Lemma 4.3 on [17].

By combining the inequalities above, we have

$$
\begin{aligned}
& PF^c(\boldsymbol{Z}(t+1)) - PF^c(\boldsymbol{Z}(t)) \\
& \leq \Xi_c + \theta^c Q^c_{c(0)}(t) R_c(t) - \theta^c Y_c(t)(R_c(t) - \alpha_c) \\
& - \sum_n \theta^c Q^c_n(t) \left(\mu^{out}_{n,c}(t) - \mu^{in}_{n,c}(t)\right)
\end{aligned} \tag{2–25}
$$

where

$$
\Xi_c = \theta^c \left(N(\mu^{\max})^2 + (R^{\max}_c)^2 + \frac{1}{2}(\alpha_c)^2 \right). \tag{2–26}
$$

Note that (2–25) is summed over the whole network. If node n is not on the path of flow c, $\mu^{in}_{n,c}(t) = \mu^{out}_{n,c}(t) = 0$. Moreover, $\mu^{in}_{n,c}(t) = 0$ for the source node of flow c and $\mu^{out}_{n,c}(t) = 0$ for the destination node of flow c. Next, we sum over all flows to derive the network-wide *potential function difference* as

$$
\begin{aligned}
& PF(\boldsymbol{Z}(t+1)) - PF(\boldsymbol{Z}(t)) \\
& \leq K - \sum_{n,c} \theta^c Q^c_n(t)(\mu^{out}_{n,c}(t) - \mu^{in}_{n,c}(t)) \\
& + \sum_c \theta^c Q^c_{c(0)}(t) R_c(t) - \sum_c \theta^c Y_c(t)(R_c(t) - \alpha_c)
\end{aligned}
$$

where $K = \sum_c \Xi_c$. Therefore, we have

$$
\begin{aligned}
\Delta(\boldsymbol{Z}(t)) \;\; \leq \;\; & K - \sum_{n,c} \theta^c Q^c_n(t) E\left(\mu^{out}_{n,c}(t) - \mu^{in}_{n,c}(t) | \boldsymbol{Z}(t)\right) \\
+ \;\; & \sum_c \theta^c Q^c_{c(0)}(t) E(R_c(t) | \boldsymbol{Z}(t)) \\
- \;\; & \sum_c \theta^c Y_c(t) E(R_c(t) - \alpha_c | \boldsymbol{Z}(t)).
\end{aligned} \tag{2–27}
$$

Next, for a positive constant J, we subtract both sides of (2–27) by $JE\left(\sum_c R_c(t)p_c(t)|\boldsymbol{Z}(t)\right)$ and have

$$\begin{aligned}
&\Delta(\boldsymbol{Z}(t)) - JE\left(\sum_c R_c(t)p_c(t)|\boldsymbol{Z}(t)\right) \\
&\leq K - \sum_{n,c} \theta^c Q_n^c(t) E\left(\mu_{n,c}^{out}(t) - \mu_{n,c}^{in}(t)|\boldsymbol{Z}(t)\right) \\
&+ \sum_c \theta^c Q_{c(0)}^c(t) E(R_c(t)|\boldsymbol{Z}(t)) \\
&- \sum_c \theta^c Y_c(t) E(R_c(t) - \alpha_c|\boldsymbol{Z}(t)) \\
&- JE\left(\sum_c R_c(t)p_c(t)|\boldsymbol{Z}(t)\right). \qquad (2\text{–}28)
\end{aligned}$$

Note that (2–28) is general and holds for any possible policy.

For an arbitrarily small positive constant $0 < \epsilon \leq \epsilon^{\max}$, define the ϵ-*reduced network capacity region*, Ω_ϵ, as all possible input rate vectors such that

$$\Omega_\epsilon = \{\boldsymbol{\lambda}|\lambda_c + \epsilon \in \Omega \quad \forall c\} \qquad (2\text{–}29)$$

where Ω is the original network capacity region. We will discuss about how to obtain $\epsilon^{\max}$ shortly.

Define D_ϵ^* as the optimum value of the *reduced problem* to (2–8) where Ω is replaced by Ω_ϵ. It can be verified that [14]

$$\lim_{\epsilon \to 0} D_\epsilon^* \to D^* \qquad (2\text{–}30)$$

where D^* is the optimum value of the original revenue maximization problem in (2–8), i.e., the target of QADP algorithm.

Specifically, we denote $r_{\epsilon,c}^*(0), r_{\epsilon,c}^*(1), \cdots, r_{\epsilon,c}^*(t), \cdots$ and $p_{\epsilon,c}^*(0), p_{\epsilon,c}^*(1), \cdots, p_{\epsilon,c}^*(t), \cdots$ as the optimum sequences of admitted rates and prices, for flow c, which achieve D_ϵ^*. Define $\widetilde{r_c^\epsilon}$ as the time average of the optimum sequence of $r_{\epsilon,c}^*(0), r_{\epsilon,c}^*(1), \cdots, r_{\epsilon,c}^*(t), \cdots$. Therefore, following the definition of (2–29), we have $\widetilde{r_c^\epsilon} + \epsilon \in \Omega$. By Lemma 1, we claim

that there exists a randomized policy, denoted by *RAND*, which yields

$$E(\mu_{n,c}^{out}(t) - \mu_{n,c}^{in}(t) - r_{\epsilon,c}^{*}(t)) = \epsilon \quad \forall c, n = c(0) \tag{2–31}$$

and

$$E(\mu_{n,c}^{out}(t) - \mu_{n,c}^{in}(t)) = \epsilon \quad \forall c, n \neq c(0) \tag{2–32}$$

and

$$E(r_{\epsilon,c}^{*}(t) + \epsilon) \geq \alpha_c + \tilde{\epsilon} \quad \forall c. \tag{2–33}$$

Denote the RHS of (2–28) as Ψ. Without loss of generality, we assume $\epsilon \leq \tilde{\epsilon}$. Therefore, for randomized policy *RAND*, we have

$$\begin{aligned}\Psi^{RAND} \leq K - \epsilon \left(\sum_{n,c} \theta^c Q_n^c(t) + \sum_c \theta^c Y_c(t) \right) \\ -JE \left(\sum_c (r_{\epsilon,c}^{*}(t) + \epsilon) \widetilde{p_{\epsilon,c}^{*}(t)} | \boldsymbol{Z}(t) \right)\end{aligned} \tag{2–34}$$

where $\widetilde{p_{\epsilon,c}^{*}(t)}$ is the corresponding price which induces a rate of $r_{\epsilon,c}^{*}(t) + \epsilon$ by (2–6).

Lemma 2. *QADP algorithm minimizes the RHS of (2–28) over all possible policies.*

Proof. The scheduling part of QADP algorithm in Section 2.4 is a weighted version of *MaxWeight* algorithm [12, 13, 34] which maximizes $\sum_{n,c} \theta^c Q_n^c(t)(\mu_{n,c}^{out}(t) - \mu_{n,c}^{in}(t)) = \sum_{(a,b)\in\mathcal{E}} \mu_{a,b}(t)\xi_{a,b}$ if $\exists c$, such that $(a, b) \in P_c$, for every time slot t. The dynamic pricing part of QADP is essentially maximizing

$$\sum_c \left(\theta^c (Y_c(t) - Q_{c(0)}^c(t)) R_c(t) + J R_c(t) p_c(t) \right) \tag{2–35}$$

for every time slot. By (2–6) and (2–7), we see that QADP finds an optimum price $p_c^{*}(t)$ which maximizes

$$M = \theta^c (Y_c(t) - Q_{c(0)}^c(t))(\frac{1}{p_c(t)} - 1) + J(1 - p_c(t)). \tag{2–36}$$

Define $W = \theta^c (Q_{c(0)}^c(t) - Y_c(t))$.

Case 1: If $W > 0$, we have

$$M = J + W - (Jp_c(t) + W\frac{1}{p_c(t)}). \tag{2–37}$$

Take the first order derivative, we have

$$M' = \frac{W}{(p_c(t))^2} - J. \tag{2–38}$$

The second order derivative brings us

$$M'' = -\frac{W}{(p_c(t))^3} < 0. \tag{2–39}$$

Therefore, M is a concave function and the optimum value is achieved by

$$p_c^*(t) = \sqrt{\frac{W}{J}}. \tag{2–40}$$

Case 2: If $W \leq 0$, M is a decreasing function with respect to $p_c(t)$. Therefore, $p_c^*(t) = 0$.

Following Lemma 2, we conclude that for QADP algorithm,

$$\begin{aligned}
&\Delta(\boldsymbol{Z}(t)) - JE\left(\sum_c R_c(t)p_c(t)|\boldsymbol{Z}(t)\right) \leq \Psi^{QADP} \\
&\leq \Psi^{RAND} \leq K - \epsilon\left(\sum_{n,c}\theta^c Q_n^c(t) + \sum_c \theta^c Y_c(t)\right) \\
&-JE\left(\sum_c (r_{\epsilon,c}^*(t) + \epsilon)\widetilde{p_{\epsilon,c}^*(t)}|\boldsymbol{Z}(t)\right).
\end{aligned} \tag{2–41}$$

We take expectation with the distribution of $\boldsymbol{Z}(t)$, on both sides of (2–41). By the fact that $E_Y(E(X|Y)) = E(X)$, we have

$$\begin{aligned}
&E(PF(\boldsymbol{Z}(t+1))) - E(PF(\boldsymbol{Z}(t))) \\
&\leq K + JO(t) - \epsilon E\left(\sum_{n,c}\theta^c Q_n^c(t) + \sum_c \theta^c Y_c(t)\right) \\
&-JE\left(\sum_c (r_{\epsilon,c}^*(t) + \epsilon)\widetilde{p_{\epsilon,c}^*(t)}\right).
\end{aligned} \tag{2–42}$$

Note that (2–42) is satisfied for all time slots. Therefore, we take a sum on time slots $\tau = 0, \cdots, T-1$ and have

$$
\begin{aligned}
&E(PF(\boldsymbol{Z}(T))) - E(PF(\boldsymbol{Z}(0))) \leq TK + \sum_{\tau=0}^{T-1} JO(\tau) \\
&- \sum_{\tau=0}^{T-1} \epsilon E\left(\sum_{n,c} \theta^c Q_n^c(\tau) + \sum_c \theta^c Y_c(\tau)\right) \\
&- \sum_{\tau=0}^{T-1} JE\left(\sum_c (r_{\epsilon,c}^*(\tau) + \epsilon)\widetilde{p_{\epsilon,c}^*(\tau)}\right).
\end{aligned} \tag{2–43}
$$

Divide (2–43) by T and rearrange terms to obtain

$$
\begin{aligned}
&\frac{1}{T}\sum_{\tau=0}^{T-1} \epsilon E\left(\sum_{n,c} \theta^c Q_n^c(\tau) + \sum_c \theta^c Y_c(\tau)\right) \\
&+\frac{1}{T}\sum_{\tau=0}^{T-1} JE\left(\sum_c (r_{\epsilon,c}^*(\tau) + \epsilon)\widetilde{p_{\epsilon,c}^*(\tau)}\right) \\
&\leq K + \frac{1}{T}\sum_{\tau=0}^{T-1} JO(\tau) + \frac{E(PF(\boldsymbol{Z}(0)))}{T}
\end{aligned} \tag{2–44}
$$

where the nonnegativity of the potential function is utilized. We first take $\liminf_{T\to\infty}$ on both sides of (2–44) and have[8]

$$
\begin{aligned}
&\liminf_{T\to\infty} \frac{1}{T}\sum_{\tau=0}^{T-1} \epsilon E\left(\sum_{n,c} \theta^c Q_n^c(\tau) + \sum_c \theta^c Y_c(\tau)\right) \\
&+ \liminf_{T\to\infty} \frac{1}{T}\sum_{\tau=0}^{T-1} JE\left(\sum_c (r_{\epsilon,c}^*(\tau) + \epsilon)\widetilde{p_{\epsilon,c}^*(\tau)}\right) \\
&\leq K + \liminf_{T\to\infty} \frac{1}{T}\sum_{\tau=0}^{T-1} JO(\tau).
\end{aligned} \tag{2–45}
$$

[8] We assume that the initial queue sizes of real data queues and virtual queues are bounded.

Note that the first term of (2–45) is nonnegative and thus we have

$$\begin{aligned}&\liminf_{T\to\infty}\frac{1}{T}\sum_{\tau=0}^{T-1}O(\tau)\\&\geq\liminf_{T\to\infty}\frac{1}{T}\sum_{\tau=0}^{T-1}E\left(\sum_{c}(r^*_{\epsilon,c}(\tau)+\epsilon)\widetilde{p^*_{\epsilon,c}(\tau)}\right)-\frac{K}{J}.\end{aligned}$$

Recall that the analysis above applies to arbitrarily small $0<\epsilon\leq\epsilon^{\max}$. We observe that

$$\lim_{\epsilon\to 0}\liminf_{T\to\infty}\frac{1}{T}\sum_{\tau=0}^{T-1}E\left(\sum_{c}(r^*_{\epsilon,c}(\tau)+\epsilon)\widetilde{p^*_{\epsilon,c}(\tau)}\right)\to D^*_{\epsilon}. \tag{2–46}$$

Therefore, by (2–30), taking the limit of $\epsilon\to 0$ yields the performance bound of (2–16) in Theorem 2.1.

2.5.2 Proof of Network Stability

To prove the stability of the network, we take $\limsup$ on (2–44) and obtain

$$\begin{aligned}&\limsup_{T\to\infty}\frac{1}{T}\sum_{\tau=0}^{T-1}\epsilon E\left(\sum_{n,c}\theta^c Q^c_n(\tau)+\sum_{c}\theta^c Y_c(\tau)\right)\\&\leq K+J\left(\limsup_{T\to\infty}\frac{1}{T}\sum_{\tau=0}^{T-1}O(\tau)\right)\end{aligned} \tag{2–47}$$

since the second term of (2–44) is also nonnegative. Note that if it satisfies that $O(t)\leq O^{\max}$ for all time slot t, (2–47) becomes

$$\begin{aligned}&\limsup_{T\to\infty}\frac{1}{T}\sum_{\tau=0}^{T-1}E\left(\sum_{n,c}\theta^c Q^c_n(\tau)+\sum_{c}\theta^c Y_c(\tau)\right)\\&\leq\frac{K+JO^{\max}}{\epsilon}.\end{aligned} \tag{2–48}$$

Recall that the above analysis applies to any $0<\epsilon\leq\epsilon^{\max}$. In addition, by the definition of (2–29), we have

$$\epsilon^{\max}=\mu^{\max}-\max_{i}\alpha_i \text{ where } i=1,\cdots,C \tag{2–49}$$

where $\mu^{\max}$ is the maximum possible data rate on a link. Moreover, by (2–6) and (2–7), we have $O^{\max} = C$ where C is the number of flows in the network. Therefore, we have

$$\limsup_{T\to\infty} \frac{1}{T} \sum_{\tau=0}^{T-1} E\left(\sum_{n,c} \theta^c Q_n^c(\tau) + \sum_c \theta^c Y_c(\tau)\right) \leq \frac{K + JC}{\epsilon^{\max}}.$$

Using the fact that

$$X(t) \leq Y(t)\ \forall t \Rightarrow \limsup X(t) \leq \limsup Y(t), \tag{2–50}$$

we have, for every flow c, the average queue length on its routing path is bounded by

$$\limsup_{T\to\infty} \frac{1}{T} \sum_{\tau=0}^{T-1} E\left(\sum_{j=0}^{\kappa_c} Q_{c(j)}^c(\tau)\right) \leq \frac{K + JC}{\theta^c \epsilon^{\max}}. \tag{2–51}$$

Finally, by applying Markov Inequality, we conclude that all data queues in the network are stable, based on the fact that the RHS of (2–51) is bounded.

2.5.3 Proof of QoS Provisioning

Similar to (2–51), for every virtual queue $Y_c(t)$, we can obtain

$$\limsup_{T\to\infty} \frac{1}{T} \sum_{\tau=0}^{T-1} E(Y_c(\tau)) \leq \frac{K + JC}{\theta^c \epsilon^{\max}}. \tag{2–52}$$

Therefore, by similar analysis and the definition of virtual queues, we conclude that the virtual queues are stable and thus the minimum data rate requirements imposed by multimedia flows are achieved.

Next, we show that QADP indeed provides a service differentiation solution on the guaranteed maximum end-to-end delays for all multimedia flows. Denote the actual experienced average delay of flow c as ω_c. By Little's Law, ω_c is approximated[9] by

[9] Note that we consider a heavy loaded network. Propagation delays are assumed to be negligible compared to queueing delays and thus are omitted.

$$\begin{aligned}\omega_c &= \frac{\text{average overall queue length on the path of flow } c}{\text{average incoming rate of flow } c} \\ &= \frac{\limsup_{T\to\infty} \frac{1}{T}\sum_{\tau=0}^{T-1} E\left(\sum_{j=0}^{\kappa_c} Q_{c(j)}^{c}(\tau)\right)}{\limsup_{T\to\infty} \frac{1}{T}\sum_{\tau=0}^{T-1} E(R_c(\tau))}. \end{aligned} \tag{2–53}$$

In light of the stability of virtual queue $Y_c(t)$, we have $\limsup_{T\to\infty} \frac{1}{T}\sum_{\tau=0}^{T-1} E(R_c(\tau)) \geq \alpha_c$. Hence, we can obtain

$$\omega_c \leq \frac{K + JC}{\theta^c \epsilon^{\max} \alpha_c}. \tag{2–54}$$

Equivalently speaking, to differentiate the guaranteed maximum delay bound, we need to find a set of weights such that

$$\theta^c \alpha_c \ell_c = \theta^d \alpha_d \ell_d \tag{2–55}$$

is satisfied for any pair of multimedia flows c and d. Therefore, it is straightforward to verify that the weight assignment algorithm in QADP indeed provides a service differentiation solution where the guaranteed maximum end-to-end delays of multimedia flows are distinguished according to application-dependent service level requests, which completes the proof of Theorem 2.1. The performance of QADP algorithm will be evaluated numerically in Section 2.6.

2.6 Simulations

2.6.1 Single-Hop Wireless Cellular Networks

We first consider a single-hop wireless cellular network with downlink multimedia transmissions, as shown in Figure 2-3. The base station (BS) is associated with three users with infinite backlogged traffic. A separate queue is maintained by the base station for every user. In addition, at each time slot, BS can only transmit to one particular user. A wireless link is assumed to have three equally possible channel states, i.e., *Good, Medium, Bad*. The corresponding transmission rates for three channel states are 20, 15 and 10 bits per slot, respectively. Therefore, the base station encounters a complex

opportunistic scheduling problem where the revenue maximization problem, network stability as well as the QoS requirements need to be addressed simultaneously.

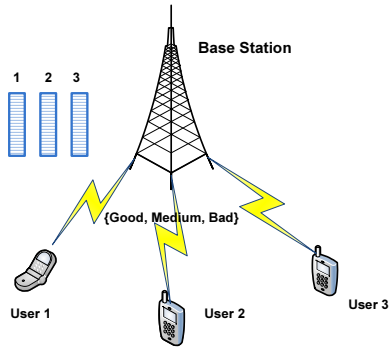

Figure 2-3. A single-hop wireless cellular network with three users

Without loss of generality, we assume that the minimum average rate requirements for user $1, 2, 3$ are $\boldsymbol{\alpha} = [1, 2, 3]$ bits per slot. In addition, to provide service differentiation, the network offers three prioritized service levels, e.g., *Platinum, Gold* and *Silver*, where level *Platinum* possesses the highest priority in terms of end-to-end delay upper bound. We assume that user 1 has a service level request for *Platinum* while user 2 and 3 demand for level *Gold* and *Silver*, respectively, according to the upper layer applications. Other system parameters are assumed to be $R_c^{\max} = 20$ bits per slot for all flows and $\theta^{\max} = 100$. We next implement QADP algorithm for different values of J where $J = [50, 100, 500, 1000, 5000, 10000, 20000, 50000, 100000]$. Every experiment is simulated for 500000 time slots.

Figure 2-4 depicts the system revenue, i.e., the solution of (2–8) by QADP algorithm, with respect to different values of J. As shown in (2–16) and demonstrated pictorially in Figure 2-4, the achieved system revenue by QADP converges gradually to the optimum solution as J grows. Note that the values of system revenues are almost indistinguishable when $J \geq 50000$. Figure 2-5 illustrates the actual experienced average delays of all three flows with different values of J, where the delays of user 1 to user 3 are compared from left to right. It is worth noting that, not only the maximum guaranteed end-to-end delays are distinguished analytically by QADP, but also the

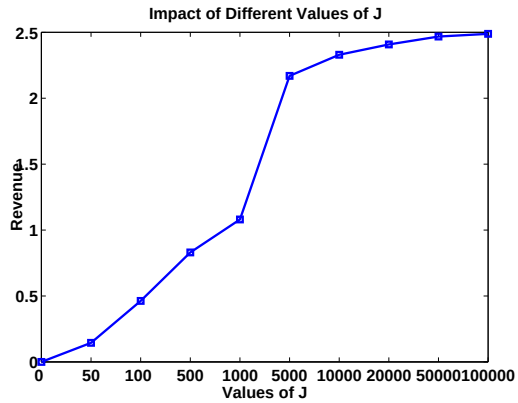

Figure 2-4. Impact of different values of J on the performance of QADP

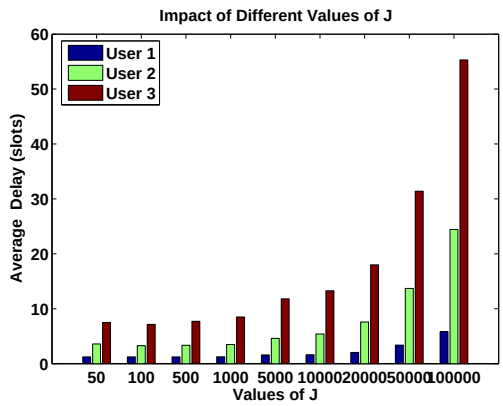

Figure 2-5. Impact of different values of J on the average experienced delays

actual experienced average delays are prioritized for all three flows with distinct service level requests. More specifically, user 1, i.e., the *Platinum* user, enjoys a delay which is less than half of that of user 2 and one third of that of user 3, for all values of J, as demonstrated in Figure 2-5. However, as shown by Figure 2-4 and Figure 2-5 jointly, while a larger value of J yields an improvement on the performance of QADP, the end-to-end delays of all three flows are augmented concurrently. Therefore, by tuning J, a tradeoff between optimality and average delays can be achieved. The time average admitted rates of multimedia flows are shown in Table 2-1. We observe that in all cases, the average rates of flows exceed the minimum data rate requirements specified by $\boldsymbol{\alpha}$.

The sample paths of price adaptations and queue backlog evolutions are illustrated in Figure 2-7 and Figure 2-6, respectively, for the first 100 time slots with $J = 50000$.

Table 2-1. Average admitted rates for multimedia flows

	Flow 1	Flow 2	Flow 3
J = 50	4.01	2.71	3.07
J = 100	4.04	2.72	3.09
J = 500	4.05	2.91	3.11
J = 1000	4.31	3.07	3.16
J = 5000	4.51	3.57	3.42
J = 10000	4.63	3.94	3.62
J = 20000	4.75	4.28	4.09
J = 50000	5.09	4.71	4.61
J = 100000	5.13	4.88	4.85

Note that, in Figure 2-7, the prices imposed for three users are dynamically adjusted at every time slot. It is worth noting that whenever a data queue in Figure 2-6 has a tendency to build up, the price imposed by QADP algorithm, as shown in Figure 2-7, rises correspondingly, which in turn discourages the excessive admitted rate and thus all queues in the network remain bounded. As a result, the stability of the network is achieved.

2.6.2 Multi-Hop Wireless Networks

We next consider a multi-hop wireless network with a topology shown in Figure 2-1. There are three multimedia flows exist in the network, denoted by *Flow 1, 2, 3*. The routing paths of flows are specified by $P_1 = \{A, B, C, D\}$, $P_2 = \{F, G, C, D\}$ and $P_3 = \{E, F, G, H\}$. Without loss of generality, we assume a two-hop interference model which represents the general IEEE 802.11 MAC protocols [36, 37]. Other configurations are the same as the single-hop scenario described above except that the possible link rates are assumed to be $40, 30, 20$ bits per slot for three channel conditions. We observe that in this network topology, link $C \rightarrow D$ and link $F \rightarrow G$ are shared by two different flows. Therefore, in the scheduling part of QADP, the particular flow with a larger weighted queue backlog difference should be selected.

In Figure 2-8, we specifically depict the dynamics of three virtual queues for the first 400 time slots with $J = 50000$. Unlike the single-hop case in Figure 2-6, the virtual

Figure 2-6. Queue backlog dynamics for all users

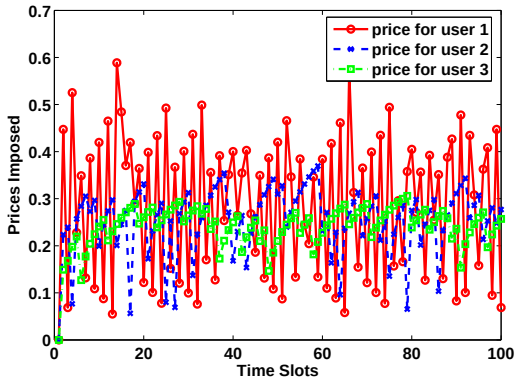

Figure 2-7. Price dynamics in QADP for all users

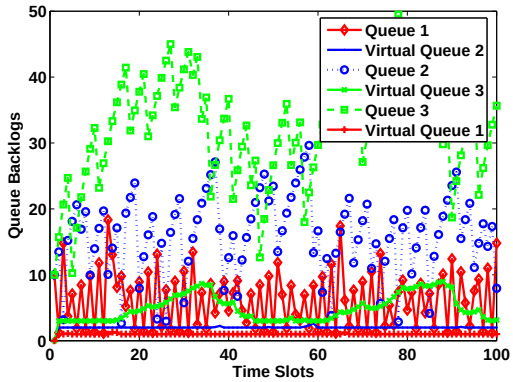

queues behave remarkably different in this multi-hop scenario. It is worth noting that while the virtual queues of user 1 and 3 have relatively low occupancies, the virtual queue associated with user 2 suffers a larger average backlog. Intuitively, due to the underlying two-hop interference model, link $G \rightarrow C$ needs to be scheduled exclusively in the network for successful transmissions. In other words, link $G \rightarrow C$ is the bottleneck of the network. Therefore, to ensure network-wide stability, a much more stringent regulation is enforced on the admitted rate of flow 2. As a consequence, although remains bounded, the virtual queue of flow 2 accumulates more backlogs compared to other competitive flows. In addition, we compare the time average queue backlogs of all data queues in the network, from left to right, in Figure 2-9. We can observe that the data queues on the path of flow 1 have fewer average backlogs due to the highest

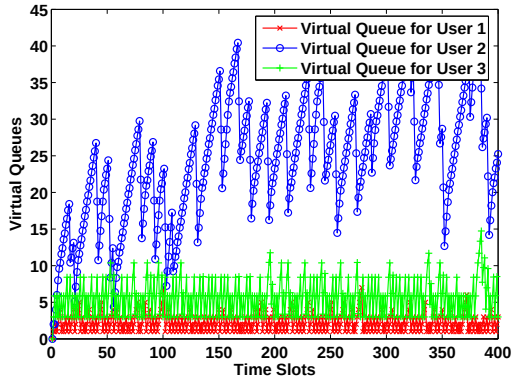

Figure 2-8. Virtual queue backlog updates in QADP for $J = 50000$

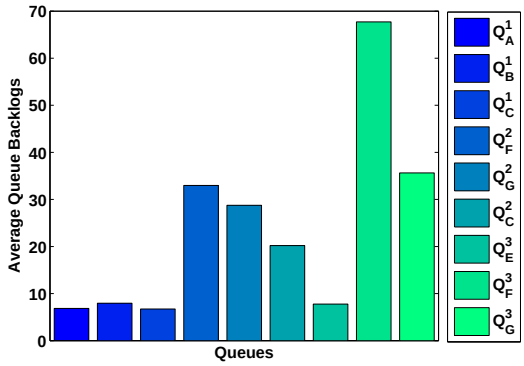

Figure 2-9. Average queue backlogs in the network for J = 50000

priority with respect to the service level, i.e., *Platinum*. On the contrary, the queues on the path of flow 3 have larger backlogs compared to other two flows. It is noticeable that Q_F^3 and Q_G^3 have considerably larger average queue sizes. This is because that Q_F^3 has to share the link rate of $F \rightarrow G$ with Q_F^2. Nevertheless, Q_F^3 possesses a smaller share of bandwidth than Q_F^2 due to the lower prioritized service level associated with flow 3. Even worse yet, both link $F \rightarrow G$ and $G \rightarrow H$ have less opportunity to be scheduled due to their locations and the underlying interference model. Therefore, the average backlogs on the path of user 3 has higher occupancies compared to other two competitive flows. The average data rates are provided in Table 2-2. Note that the minimum average rate requirements of all multimedia flows are satisfied simultaneously, as expected. The tradeoff between optimality and average delay, which is controlled by different values of

J, as well as the network service differentiation in terms of delays are analogous to the single-hop scenario discussed above. Duplicated simulation figures are omitted.

Table 2-2. Average admitted rates for multimedia flows

	Flow 1	Flow 2	Flow 3
J = 50	3.04	2.08	3.88
J = 100	3.12	2.03	3.98
J = 500	3.17	2.04	4.60
J = 1000	3.30	2.03	5.04
J = 5000	4.13	2.01	6.45
J = 10000	4.36	2.02	7.32
J = 20000	5.08	2.03	8.12
J = 50000	6.43	2.01	9.18
J = 100000	7.63	2.01	9.89

2.7 Conclusions

We consider a multi-hop wireless network where multiple QoS-specific multimedia flows share the network resource jointly. To maximize the overall network revenue, we propose a dynamic pricing based algorithm, namely, QADP, which achieves a solution that is arbitrarily close to the optimum, subject to network stability. Moreover, a weight assignment mechanism is introduced to address the service differentiation issue for multimedia flows with different delay priorities. In tandem with the virtual queue technique which provides minimum average data rate guarantees, the QoS requirements of multiple multimedia streams are addressed effectively.

In this work, the application-dependent service level requests and the users' utility functions are assumed to be attained *truthfully*. The mechanism design for strategy-proof user information acquisition seems interesting and needs further investigation. Moreover, in this work, we assume that the information of channel states, i.e., $\mathbf{S}(t)$, is available for QADP algorithm, which is either acquired by the central base station or approximated by the distributed local scheduling algorithms. As a future work, an online channel probing mechanism needs to be incorporated into QADP, as suggested in [39].

CHAPTER 3
ENERGY-CONSERVING SCHEDULING IN WIRELESS NETWORKS

3.1 Introduction

There has been a lot of interest over the past few years in characterizing the network capacity region as well as designing efficient scheduling algorithms in multi-hop wireless networks. Due to the stochastic traffic arrivals and time-varying channel conditions, supporting high throughput and high quality communications in multi-hop wireless networks is inherently challenging. To utilize the scarce wireless bandwidth resource effectively, scheduling algorithms which can dynamically allocate the network resource, i.e., select active links, are investigated intensively in the community. For example, *MaxWeight* algorithm, a.k.a., *back-pressure* algorithm, has been extensively studied in the literature, e.g., [5, 14, 34, 37, 40], following the seminal work of [12]. The *MaxWeight* algorithm enjoys the merit of self-adaptability due to its online nature. In addition, *MaxWeight* algorithm is known to be throughput optimal [17]. That is to say, the *MaxWeight* algorithm can stabilize the network under arbitrary traffic load that can be stabilized by any other possible scheduling algorithms. Therefore, the *MaxWeight* algorithm attracts significant attention and becomes an indispensable component for link scheduling in network protocol designs, e.g., [41–43].

While the throughput-optimality of the *MaxWeight* algorithm is well understood, the energy consumption induced by the *MaxWeight* algorithm is less studied in the literature. However, due to the scarcity of energy supplies in wireless nodes, it is imperative to study the energy consumption of the scheduling algorithm which is of special interest in energy-constrained wireless networks such as wireless sensor networks. Is the throughput optimal *MaxWeight* scheduling algorithm also energy optimal? In this work, we show that the answer to this question is *no*. The reason is that the vast energy consumptions during packet retransmissions are completely neglected by the *MaxWeight* algorithm. For example, in [16], an energy optimal control scheme

is proposed where a minimum power expenditure is achieved. However, as in other related works, e.g., [17], the wireless channels in [16] are assumed to be *error-free*, i.e., all the transmissions are assumed to be successful. Nevertheless, in practice, wireless channels are error-prone and data transmissions are subject to random failures due to the hostile channel conditions. Therefore, before a packet can be successfully removed from the transmitter's queue, several transmissions may have occurred, including the original attempt and the posterior retransmissions, which deplete a significant amount of energy for the transmitter. However, in the traditional *MaxWeight* algorithm, such energy-consuming retransmissions induced by channel errors are overlooked. Intuitively, from energy-saving perspective, the possibility that a particular link is selected for transmissions should rely on not only the queue difference between the transmitter and the receiver, which is the design rationale of the traditional *MaxWeight* algorithm, but also the potential energy consumptions of retransmissions induced by erroneous channels. We will make this intuition precise and rigorous in the following sections.

In this work, we propose a minimum energy scheduling (MES) algorithm which consumes an amount of energy that can be pushed arbitrarily close to the global minimum solution. In addition, the energy efficiency attained by the MES algorithm incurs no loss of throughput-optimality. The proposed MES algorithm significantly reduces the overall energy consumption compared to the traditional *MaxWeight* algorithm and remains throughput optimal. Therefore, our proposed MES algorithm is more favorable for dynamic link scheduling and network protocol designs in energy-constrained wireless networks such as wireless sensor networks.

The rest of this chapter is organized as follows. Section 3.2 describes the system model used in this work. The proposed MES algorithm is introduced in Section 3.3 where the performance analysis is provided. Simulation results are shown in Section 3.4 and Section 3.5 concludes this chapter.

3.2 System Model

We consider a static multi-hop wireless network denoted by a directed graph $(\mathcal{N}, \mathcal{L})$ where $\mathcal{N}$ is the set of nodes and $\mathcal{L}$ denotes the set of links in the network. We use $|X|$ to represent the cardinality of set X. Time is slotted by $t = 0, 1, 2, \cdots$ and in every time slot, the instantaneous channel state of a link $(a, b) \in \mathcal{L}$ is denoted by $S_{a,b}(t)$ where a and b are the transmitter and the receiver of the link. In this work, we use $\mathbf{S}(t)$ to denote the channel state vector of the whole network. Note that $\mathbf{S}(t)$ remains constant within one time slot, however, it is subject to changes on time slot boundaries. We assume that $\mathbf{S}(t)$ has a finite but potentially large number of possible values and evolves following an irreducible Markovian chain with well defined steady state distributions. Nevertheless, the steady state distribution and the transition probabilities are unknown to the network. Given an instantaneous channel state $S_{a,b}(t)$, the transmission of a packet on link (a, b) is successful with a probability of $p_{a,b}(t)$, if link (a, b) is active and suffers no interference from concurrent transmissions. From the network's perspective, at each time slot t, an interference-free link schedule, denoted by $I(t)$, is selected from a feasible set $\Omega(t)$, which is constrained by the underlying interference model, e.g., K-hop interference model [44], as well as other limitations such as duplex constraints and peak power limitations. Denote $\widetilde{u_{a,b}}(t)$ as the *nominal* link rate if link (a, b) is selected by the network and the channel is error-free, i.e., $p_{a,b}(t) = 1$. The *actual* data rate of link (a, b) is hence represented by $u_{a,b}(t) = \widetilde{u_{a,b}}(t)p_{a,b}(t)$. We assume that $u_{a,b}(t)$ is upper bounded by a constant $u^{\max}$ for all $(a, b) \in \mathcal{L}$. In practice, $u^{\max}$ can be determined by the number of antennas equipped in a single node as well as the coding/modulation schemes available to the network. We denote $\mathbf{u}(t)$ as the link rate vector of the network at time t. Apparently, $\mathbf{u}(t)$ is a function of both $I(t)$ and $\mathbf{S}(t)$.

The network consists of $|\mathcal{F}|$ flows indexed by $f = 1, 2, \cdots, |\mathcal{F}|$. Each flow f is associated with a routing path $R_f = [n_0^f, n_1^f, \cdots, n_{\iota_f}^f]$ where $n_j^f, j = 0, \cdots, \iota_f$ denotes the nodes on the path of flow f. At each time slot t, the stochastic exogenous arrivals

of flow f, i.e., the number of new packets that are initiated by node n_0^f, is denoted by $A_f(t)$. For the ease of exposition, we assume that $A_f(t)$ is i.i.d. for every time slot with an average rate of λ_f. In addition, the arrival processes of all flows are assumed to be independent. We further assume that the maximum number of new packets generated by a flow during one time slot is upper bounded, i.e., $A_f(t) \leq A^{\max}, \forall f, t$. We emphasize that the i.i.d. assumption incurs no loss of generality and our model can be extended to cases where $A_f(t)$ is non-stationary in a straightforward fashion, as in [14].

Every node in the network maintains a separate queue for each flow that passes through it. Denote $Q_n^f(t)$ as the queue backlog at time t, for node n, where f is one of the flows that traverses through n, i.e., $n \in R_f$. We assume that $Q_n^f(t) = 0, \forall t$ if $n = n_{\iota_f}^f$. That is to say, if a packet reaches the destination, we consider the packet as leaving the network immediately. Define the *overflow function* of Q_n^f as

$$O(M) = \limsup_{t\to\infty} \frac{1}{t} \sum_{\tau=0}^{t-1} \Pr(Q_n^f(\tau) > M). \tag{3–1}$$

The queue is stable if [14]

$$\lim_{M\to\infty} O(M) \to 0 \tag{3–2}$$

and the network is stable if all individual queues are stable concurrently.

For notation brevity, we define the network admission rate vector as $\boldsymbol{\lambda} = \{\lambda_{n,f}, \forall n, f\}$ where $\lambda_{n,f}$ is the average exogenous arrival rate of flow f on queue[1] Q_n^f. We have $\lambda_{n,f} = \lambda_f$ if $n = n_0^f$ and $\lambda_{n,f} = 0$ otherwise. Denote Λ as the *network capacity region* [12], namely, the set of all feasible admission rate vectors, i.e., $\boldsymbol{\lambda}$, that the network can support, in the sense that there exists a scheduling algorithm which stabilizes the network under traffic load $\boldsymbol{\lambda}$. It is shown in [12] and [14] that Λ is convex, closed and bounded.

[1] Note that with a slight abuse of notation, we use Q_n^f to denote both the queue itself and the number of packets in the queue.

Without loss of generality, we consider an energy consumption model as follows. Recall that the successful transmission probability of link (a, b) is $p_{a,b}(t)$. Therefore, for a particular packet to be transmitted from a to b, on average, a number of $\frac{1}{p_{a,b}(t)}$ transmissions are needed in order to "erase" this packet from the queue of node a. From the transmitter's perspective, however, every transmission, either the original attempt or retransmissions, costs the same amount of energy. Denote $\alpha_{a,b}$ as the energy needed to transmit a packet on link (a, b). For example, $\alpha_{a,b}$ can be proportional to the distance between node a and b. Therefore, in order to transmit a packet successfully on (a, b), node a needs to spend a total energy of $\frac{\alpha_{a,b}}{p_{a,b}(t)}$ on average. For the receiver b, we assume that the energy depletion on *successful* packets receptions are dominant, i.e., the energy spent for overhearing and short ACK messages are neglected. Denote $\beta_{a,b}$ as the energy consumed for a successful packet reception in demodulation and decoding on node b. With a data rate[2] of $u_{a,b}(t)$ on link (a, b), the overall energy spent during time slot t is given by

$$\begin{aligned} G_{a,b}(t) &= u_{a,b}(t)\left(\frac{\alpha_{a,b}}{p_{a,b}(t)} + \beta_{a,b}\right) \\ &= \widetilde{u_{a,b}}(t)\left(\alpha_{a,b} + \beta_{a,b}p_{a,b}(t)\right). \end{aligned} \tag{3–3}$$

Note that due to the stochastic nature of wireless channels, $G_{a,b}$ is a random variable. We stress that the simple energy consumption model above is not essential and our analysis can be extended to other more complex forms of energy models straightforwardly, as will be shown in the next section.

[2] The unit of data rate in this work is defined as packets/slot. It is worth noting that other units such as bits/slot are also applicable.

In addition, we assume that the energy consumption of the whole network during one single time slot is upper bounded, i.e.,

$$\sum_{(a,b)\in\mathcal{L}} G_{a,b}(t) \leq G^{\max}, \forall t. \tag{3–4}$$

Therefore, to minimize the energy consumption, the objective of the network is to find a scheduling algorithm which solves

<u>Minimum Energy Scheduling Problem:</u>

$$\text{minimize} \quad C = \limsup_{T\to\infty} \frac{1}{T} \sum_{t=0}^{T-1} \overline{G}(t) \tag{3–5}$$

s.t.

the network remains stable, and

$$\overline{G}(t) = E\left(\sum_{(a,b)\in\mathcal{L}} h_{a,b}(t)\left(\frac{\alpha_{a,b}}{p_{a,b}(t)} + \beta_{a,b}\right)\right) \tag{3–6}$$

is the *expected* overall network energy consumption during time slot t, with respect to the randomness of arrival processes and channel variations. Note that $h_{a,b}(t)$ is the actual number of successfully transmitted packets on link (a, b) during time slot t and[3] $h_{a,b}(t) \leq u_{a,b}(t)$.

In the next section, we will propose a minimum energy scheduling (MES) algorithm which minimizes the average network energy consumption asymptotically subject to network stability. In addition, the proposed MES algorithm is throughput optimal, in the sense that the MES algorithm can ensure the network stability for all feasible network admission rate vectors in the network capacity region. Restated, the set of feasible arrival rates supported by the MES algorithm is the superset of all other possible

[3] The inequality holds when node a has less packets to transmit than the allocated data rate $u_{a,b}(t)$.

scheduling algorithms, including those with a priori knowledge on the futuristic arrivals and channel conditions.

3.3 Minimum Energy Scheduling Algorithm

3.3.1 Algorithm Description

The minimum energy scheduling (MES) algorithm is given as follows.

MES ALGORITHM:

At every time slot t:

- Every link $(a, b) \in \mathcal{L}$ finds the flow f^* which maximizes

$$\max_{f:(a,b)\in R_f} \left(2Q_a^f(t) - \frac{J\alpha_{a,b}}{p_{a,b}(t)} - 2Q_b^f(t) - J\beta_{a,b}\right) \tag{3–7}$$

  where J is a positive constant which is tunable as a system parameter.

- Every link $(a, b) \in \mathcal{L}$ calculates the link weight as

$$H_{a,b}(t) = \left[2Q_a^{f^*}(t) - \frac{J\alpha_{a,b}}{p_{a,b}(t)} - 2Q_b^{f^*}(t) - J\beta_{a,b}\right]^+ \tag{3–8}$$

  where $[x]^+$ denotes $\max(x, 0)$.

- For the network, a link schedule $I^*(t)$ is selected which solves

$$\max_{I(t)\in\Omega(t)} \sum_{(a,b)\in\mathcal{L}} u_{a,b}(t)H_{a,b}(t) \tag{3–9}$$

END

Note that the proposed MES algorithm is different from the *MaxWeight* algorithm proposed in [12, 13]. In the original *MaxWeight* algorithm, the weight of a particular link (a, b) is the queue difference between node a and b. However, in the MES algorithm, as indicated by (3–8), the link weight $H_{a,b}(t)$ is related to the potential energy consumptions on this link under the current channel condition as well. More specifically, the link weight in the MES algorithm is the queue difference subtracted by a weighted energy consumption factor, i.e., $J\left(\frac{\alpha_{a,b}}{p_{a,b}(t)} + \beta_{a,b}\right)$, where J represents the weight. Intuitively, if the current channel is unfavorable, i.e., $p_{a,b}(t)$ is small, the energy required for a successful

transmission is remarkably large due to the retransmissions and thus the link should be selected less likely. Therefore, the link weight in the MES algorithm, i.e., $H_{a,b}(t)$, can be viewed as a balance between the queue difference and the energy consumptions under the current channel condition. More specifically, in the original *MaxWeight* algorithm, if a link has a larger queue difference, the link is more likely to be selected for transmissions. However, in the MES algorithm, both the queue difference and the energy expenditure are taken into consideration. In addition, as indicated by (3–7), by replacing $J\left(\frac{\alpha_{a,b}}{p_{a,b}(t)}+\beta_{a,b}\right)$ with other metrics, our MES algorithm can incorporate other forms of energy consumption models straightforwardly.

Observe that if $J = 0$, the MES algorithm reduces to the original *MaxWeight* algorithm, i.e., the energy consumptions during retransmissions are omitted. Therefore, the *MaxWeight* algorithm is a special case of our MES algorithm. On the other hand, if we let $J \to \infty$, the performance of the MES algorithm can be pushed arbitrarily close to the global minimum solution, as will be shown analytically in Section 3.3.3. However, as illustrated in (3–7) and (3–8), when J increases, the network becomes more reluctant to transmissions, for the sake of energy conservation, unless the accumulated queue backlogs are significantly large. Intuitively, a larger average queue size induces a longer experienced delay for transmissions. Therefore, the system parameter J is essentially a control knob which provides a tradeoff between the energy-optimality and the experienced delay in the network.

Note that similar to the traditional *MaxWeight* algorithm, the calculation in (3–9) is centralized. However, following [12], much progress has been made in easing the computational complexity and deriving decentralized solutions for the centralized *MaxWeight* algorithm, e.g., [35–38, 40, 42–49]. It is worth noting that solving (3–9) is equivalent to finding the maximum weight independent set in the conflict graph, which is combinatorial in nature and thus is intrinsically difficult to solve. A natural heuristic, denoted by *GreedyMax*, is described as follows. First, the link with the highest weight

in the network is selected. Next, the link with the second highest weight which does not involve conflicts with any previously selected links, is selected and the iteration continues until no link can be added. Based on *GreedyMax*, a novel pre-partition based approach is introduced in [35]. The authors prove that if the topology of the network satisfies certain conditions, a.k.a., local pooling factor conditions, *GreedyMax* can achieve the same throughput as *MaxWeight*. Furthermore, tree based topology are shown to satisfy the local pooling conditions. In light of this, [35] utilizes graph algorithms to partition the whole network into trees where each tree is allocated an orthogonal channel. As a result, the whole network can operate with simple *GreedyMax* algorithm and achieve the same throughput as *MaxWeight*. This line of research is further simplified by [36] where the author proves that a *local* greedy maximal algorithm can obtain the same performance as the global *GreedyMax* algorithm. Specifically, in each time slot, a link only needs to compare its weight with local neighboring links to decide a feasible transmission schedule. Therefore, in tandem with the tree pre-partition method in [35], the complex scheduling algorithm in (3–9) can be implemented in a fully distributed fashion. Another feasible direction is to utilize the distributed random access approximation schemes, e.g., [37, 38, 42]. For example, in [42], each node in the network utilizes an IEEE 802.11 MAC protocol where the channel access probability is dynamically adjusted in accordance to the link weight, i.e., $H_{a,b}(t)$ in our scenario. The effectiveness of such random access based distributed approximations is studied extensively in [43] and [42] . We note that, although distributed implementation is not the focus of this work, our proposed MES algorithm can be approximated well by the solutions suggested in the above papers.

If an admission control mechanism is implemented in the network to regulate the overwhelming arrivals, in order to achieve an average minimum rate provision for each flow, we can utilize the concept of *virtual queues* introduced in [17, 34], where for each

flow f, we define a virtual queue $\mathcal{Y}_f(t)$ which is initially empty, i.e.,

$$\mathcal{Y}_f(0) = 0, \forall f \tag{3–10}$$

and the virtual queue updating dynamic is defined as

$$\mathcal{Y}_f(t+1) = [\mathcal{Y}_f(t) - R_f(t)]^+ + \delta_f \quad \forall f \tag{3–11}$$

where $R_f(t)$ is the admitted traffic for flow f at time slot t and δ_f is a feasible minimum rate requirement of flow f. Intuitively, if each of the virtual queues in the system is stable, the average arrival rate should be less than the average departure rate of the virtual queue and hence we have

$$\lim_{T\to\infty} \frac{1}{T} \sum_{t=0}^{T-1} R_f(t) \geq \delta_f, \forall f \tag{3–12}$$

which is exactly the desired minimum rate requirement for flow f. Moreover, the virtual queues are easy to implement. For example, the source node of flow f can maintain a software based counter to measure the backlog updates of virtual queue $\mathcal{Y}_f(t)$. Therefore, the minimum rate requirements can be incorporated into the proposed scheme straightforwardly.

3.3.2 Throughput-Optimality

We first show that the proposed MES algorithm is throughput optimal, as given in the following theorem.

Theorem 3.1. *The proposed MES algorithm is throughput optimal, i.e., for an arbitrary network admission rate vector $\boldsymbol{\lambda}$ which is inside of the network capacity region Λ, MES stabilizes the network under $\boldsymbol{\lambda}$.*

Proof. We first provide the queue updating equation of Q_n^f. Note that a packet is removed from the transmitter's queue if and only if it is received by the receiver successfully. Therefore, the queue updating dynamic is given by

$$Q_n^f(t+1) \leq [Q_n^f(t) - u_{n,f}^{out}(t)]^+ + u_{n,f}^{in}(t) + A_{n,f}(t) \tag{3–13}$$

where $u_{n,f}^{out}(t)$ and $u_{n,f}^{in}(t)$ are the allocated data rate on the outgoing link and the incoming link of node n, with respect to flow f. Note that $u_{n,f}^{out}(t) = \widetilde{u_{n,f}^{out}}(t)p_{n,c}^{out}(t)$ and $p_{n,c}^{out}(t)$ is the current successful transmission probability on this link. Note that $u_{n,f}^{out}(t) = 0, \forall t$ if node n is the destination node of flow f and $u_{n,f}^{in}(t) = 0, \forall t$ if node n is the source node of flow f. Furthermore, $A_{n,f}(t) = A_f(t)$ if n is the source node of flow f and $A_{n,f}(t) = 0$ otherwise.

From (3–13), we have

$$\begin{aligned}&(Q_n^f(t+1))^2 - (Q_n^f(t))^2 \leq \left((u^{\max})^2 + (u^{\max} + A^{\max})^2\right)\\&-2Q_n^f(t)\left(u_{n,f}^{out}(t) - u_{n,f}^{in}(t) - A_{n,f}(t)\right).\end{aligned} \tag{3–14}$$

Next, we sum (3–14) over the whole network on all data queues and obtain

$$\begin{aligned}&\sum_{n,f}(Q_n^f(t+1))^2 - \sum_{n,f}(Q_n^f(t))^2\\&\leq B - 2\sum_{n,f} Q_n^f(t)\left(u_{n,f}^{out}(t) - u_{n,f}^{in}(t) - A_{n,f}(t)\right)\end{aligned} \tag{3–15}$$

where

$$B = |\mathcal{N}||\mathcal{F}|\left((u^{\max})^2 + (u^{\max} + A^{\max})^2\right) \tag{3–16}$$

is a constant.

Denote $\boldsymbol{Q}(t) = \{Q_n^f(t), \forall f, n\}$ as the instantaneous queue backlogs in the network. We take the conditional expectation with respect to $\boldsymbol{Q}(t)$ on (3–15) and have

$$\begin{aligned}&E\left(\sum_{n,f}(Q_n^f(t+1))^2|\boldsymbol{Q}(t)\right) - E\left(\sum_{n,f}(Q_n^f(t))^2|\boldsymbol{Q}(t)\right)\\&\leq B - 2\sum_{n,f} Q_n^f(t)E\left(u_{n,f}^{out}(t) - u_{n,f}^{in}(t) - A_{n,f}(t)|\boldsymbol{Q}(t)\right).\end{aligned}$$

Define

$$G_Q^{MES}(t) = E\left(\sum_{n,f}\left(h_{n,f}^{out}(t)\frac{\alpha_{n,f}^{out}}{p_{n,f}^{out}(t)} + h_{n,f}^{in}(t)\beta_{n,f}^{in}\right)|\boldsymbol{Q}(t)\right)$$

where $\alpha_{n,f}^{out}$ ($\beta_{n,f}^{in}$) denotes the energy needed for a packet transmission (reception) on the outgoing (incoming) link of node n, with respect to flow f.

In addition, we define

$$\overline{G^{MES}}(t) = E\left(\sum_{n,f}\left(h_{n,f}^{out}(t)\frac{\alpha_{n,f}^{out}}{p_{n,f}^{out}(t)} + h_{n,f}^{in}(t)\beta_{n,f}^{in}\right)\right)$$

as the expected network-wide energy consumption during time slot t, by following the proposed MES algorithm. Apparently, we have

$$E\left(G_Q^{MES}(t)\right) = \overline{G^{MES}}(t).$$

Next, we add both sides by $JG_Q^{MES}(t)$ where J is a positive constant, and have

$$\begin{aligned}
&E\left(\sum_{n,f}(Q_n^f(t+1))^2|\boldsymbol{Q}(t)\right) - E\left(\sum_{n,f}(Q_n^f(t))^2|\boldsymbol{Q}(t)\right)\\
&+JG_Q^{MES}(t)\\
&\leq B - 2\sum_{n,f} Q_n^f(t)E\left(u_{n,f}^{out}(t) - u_{n,f}^{in}(t) - A_{n,f}(t)|\boldsymbol{Q}(t)\right)\\
&+JG_Q^{MES}(t)\\
&\leq B - 2\sum_{n,f} Q_n^f(t)E\left(u_{n,f}^{out}(t) - u_{n,f}^{in}(t) - A_{n,f}(t)|\boldsymbol{Q}(t)\right)\\
&+JE\left(\sum_{n,f}\left(u_{n,f}^{out}(t)\frac{\alpha_{n,f}^{out}}{p_{n,f}^{out}(t)} + u_{n,f}^{in}(t)\beta_{n,f}^{in}\right)|\boldsymbol{Q}(t)\right).
\end{aligned} \tag{3–17}$$

Denote the R.H.S. of (3–17) as Θ. It is of great importance to observe that, from the algorithm description of the MES algorithm above, at every time slot t, the MES algorithm essentially minimizes the R.H.S. of (3–17) over all possible scheduling algorithms.

Since $\boldsymbol{\lambda}$ lies in the interior of the network capacity region Λ, it immediately follows that there exists a small positive constant $\epsilon > 0$ such that

$$\boldsymbol{\lambda} + \boldsymbol{\epsilon} = \{(\lambda_{1,1} + \epsilon), \cdots, (\lambda_{n,f} + \epsilon), \cdots\} \in \Lambda. \tag{3–18}$$

By invoking Corollary 3.9 in [17], we claim that there exists a randomized scheduling policy, denoted by RA, which stabilizes the network while providing a data rate of

$$E\left(\overline{u_{n,f}^{out}}(t) - \overline{u_{n,f}^{in}}(t)|\boldsymbol{Q}(t)\right) = \lambda_{n,f} + \epsilon, \forall t \tag{3–19}$$

where $\overline{u_{n,c}^{out}}(t)$, $\overline{u_{n,c}^{in}}(t)$ are the link data rates induced by the randomized policy RA. Therefore, we have

$$\begin{aligned} \Theta^{RA} = B - 2\epsilon \textstyle\sum_{n,f} Q_n^f(t) \\ +JE\left(\textstyle\sum_{n,f}\left(\overline{u_{n,f}^{out}}(t)\frac{\alpha_{n,f}^{out}}{p_{n,f}^{out}(t)} + \overline{u_{n,f}^{in}}(t)\beta_{n,f}^{in}\right)|\boldsymbol{Q}(t)\right). \end{aligned} \tag{3–20}$$

Note that the last term in (3–20) is the actual energy consumption by RA algorithm during time slot t. Following (3–4), we have

$$\Theta^{RA} \leq B - 2\epsilon \sum_{n,f} Q_n^f(t) + JG^{\max}. \tag{3–21}$$

In light of (3–17), we have

$$\begin{aligned} E\left(\textstyle\sum_{n,f}(Q_n^f(t+1))^2|\boldsymbol{Q}(t)\right) - E\left(\textstyle\sum_{n,f}(Q_n^f(t))^2|\boldsymbol{Q}(t)\right) \\ +JG_Q^{MES}(t) \leq \Theta^{MES} \leq \Theta^{RA} \\ \leq B - 2\epsilon \textstyle\sum_{n,f} Q_n^f(t) + JG^{\max}. \end{aligned} \tag{3–22}$$

Next, we take the expectation with respect to $\boldsymbol{Q}(t)$ on (3–22) and have

$$\begin{aligned} E\left(\textstyle\sum_{n,f}(Q_n^f(t+1))^2\right) - E\left(\textstyle\sum_{n,f}(Q_n^f(t))^2\right) \\ +J\overline{G^{MES}}(t) \leq B - 2\epsilon E\left(\textstyle\sum_{n,f} Q_n^f(t)\right) + JG^{\max}. \end{aligned} \tag{3–23}$$

Note that the above inequality holds for any time slot t. Hence, we sum over from time slot 0 to $T-1$ and obtain

$$\begin{aligned} & E\left(\sum_{n,f}(Q_n^f(T))^2\right) - E\left(\sum_{n,f}(Q_n^f(0))^2\right) \\ & \quad + J\sum_{t=0}^{T-1}\overline{G^{MES}}(t) \\ & \leq TB - 2\epsilon\sum_{t=0}^{T-1}\sum_{n,f}E\left(Q_n^f(t)\right) + TJG^{\max}. \end{aligned} \tag{3–24}$$

Next, we rearrange terms and divide (3–24) by T and have

$$\begin{aligned} & 2\epsilon\frac{1}{T}\sum_{t=0}^{T-1}\sum_{n,f}E\left(Q_n^f(t)\right) \\ & \leq B + JG^{\max} + \frac{E\left(\sum_{n,f}(Q_n^f(0))^2\right)}{T} \\ & -J\frac{1}{T}\sum_{t=0}^{T-1}\overline{G^{MES}}(t) - \frac{E\left(\sum_{n,f}(Q_n^f(T))^2\right)}{T}. \end{aligned} \tag{3–25}$$

Note that the last two terms of (3–25) are both non-positive. By taking $\limsup_{T\to\infty}$ on both sides of (3–25), we attain

$$\limsup_{T\to\infty}\frac{1}{T}\sum_{t=0}^{T-1}\sum_{n,f}E\left(Q_n^f(t)\right) \leq \frac{B+JG^{\max}}{2\epsilon} < \infty. \tag{3–26}$$

Therefore, for every individual queue Q_n^f, we have

$$\limsup_{T\to\infty}\frac{1}{T}\sum_{t=0}^{T-1}E\left(Q_n^f(t)\right) \leq \frac{B+JG^{\max}}{2\epsilon} < \infty. \tag{3–27}$$

Finally, by invoking Markov inequality, we have

$$\limsup_{T\to\infty}\frac{1}{T}\sum_{t=0}^{T-1}\Pr\left(Q_n^f(t) > M\right) < \frac{B+JG^{\max}}{2\epsilon M}. \tag{3–28}$$

Therefore, by taking $\lim_{M\to\infty}$, we obtain the stability result of the MES algorithm and thus completes the proof.

3.3.3 Asymptotic Energy-Optimality

In this section, we show that the MES algorithm yields an asymptotic optimal solution to (3–5), i.e., the average energy consumption induced by the MES algorithm can be arbitrarily close to the global minimum solution of (3–5), by selecting a sufficiently large value of J.

Theorem 3.2. *Define C^{MES} and C^* as the average energy consumption induced by the MES algorithm and the optimal (minimum) solution of (3–5), respectively. The performance of the MES algorithm is given by*

$$C^{MES} \leq C^* + \frac{B}{J} \tag{3–29}$$

where B is defined in (3–16). Therefore, by choosing $J \to \infty$, the performance of the MES algorithm can be pushed arbitrarily close to the optimum solution C^*.

Proof. First, denote the optimal sequence of link rates, which generates the optimum solution C^*, as $\boldsymbol{u}^*(0), \boldsymbol{u}^*(1), \cdots, \boldsymbol{u}^*(t), \cdots$. Next, let us consider a *deterministic* policy, denoted by DE, which allocates exactly the optimum link data rates on every time slot t. Similar to (3–22), we have

$$\begin{aligned} &E\left(\textstyle\sum_{n,f}(Q_n^f(t+1))^2|\boldsymbol{Q}(t)\right) - E\left(\textstyle\sum_{n,f}(Q_n^f(t))^2|\boldsymbol{Q}(t)\right) \\ &\qquad + JG_Q^{MES}(t) \leq \Theta^{MES} \leq \Theta^{DE} \end{aligned} \tag{3–30}$$

where

$$\begin{aligned} &\Theta^{DE} \\ &= B - 2\sum_{n,f} Q_n^f(t) E\left(u_{n,f}^{*out}(t) - u_{n,f}^{*in}(t) - A_{n,f}(t)|\boldsymbol{Q}(t)\right) \\ &+ JE\left(\sum_{n,f}\left(u_{n,f}^{*out}(t)\frac{\alpha_{n,f}^{out}}{p_{n,f}^{out}(t)} + u_{n,f}^{*in}(t)\beta_{n,f}^{in}\right)|\boldsymbol{Q}(t)\right). \end{aligned} \tag{3–31}$$

It is worth noting in (3–31), only the data rates are replaced by the ones generated by the DE algorithm whereas all other values remain the same. Note that in this case, the

optimal data rates $u_{n,f}^{*out}(t)$ and $u_{n,f}^{*in}(t)$ are known as a priori by the DE algorithm and thus are constants with respect to $Q_n^f(t)$.

We take the expectation on both sides of (3–30) and have

$$\begin{aligned}
&E\left(\sum_{n,f}(Q_n^f(t+1))^2\right) - E\left(\sum_{n,f}(Q_n^f(t))^2\right) \\
&+J\overline{G^{MES}}(t) \leq B \\
&-2E\left(\sum_{n,f} Q_n^f(t) E\left(u_{n,f}^{*out}(t) - u_{n,f}^{*in}(t) - \lambda_{n,f} | \boldsymbol{Q}(t)\right)\right) \\
&+JE\left(\sum_{n,f}\left(u_{n,f}^{*out}(t)\frac{\alpha_{n,f}^{out}}{p_{n,f}^{out}(t)} + u_{n,f}^{*in}(t)\beta_{n,f}^{in}\right)\right).
\end{aligned} \tag{3–32}$$

We emphasize that, however, in this scenario, at arbitrary time slot t, the value of

$$u_{n,f}^{*out}(t) - u_{n,f}^{*in}(t) - \lambda_{n,f} \tag{3–33}$$

could be either non-positive or nonnegative. In other words, the relationship of (3–19) does not hold. To circumvent this, we first sum (3–32) over time slots $t = 0, \cdots, T-1$ and divide it by T. Thus, we attain

$$\begin{aligned}
&J\frac{1}{T}\sum_{t=0}^{T-1}\overline{G^{MES}}(t) \leq B \\
&+J\frac{1}{T}\sum_{t=0}^{T-1} E\left(\sum_{n,f}\left(u_{n,f}^{*out}(t)\frac{\alpha_{n,f}^{out}}{p_{n,f}^{out}(t)} + u_{n,f}^{*in}(t)\beta_{n,f}^{in}\right)\right) \\
&+\frac{E\left(\sum_{n,f}(Q_n^f(0))^2\right)}{T} - 2\frac{1}{T}\sum_{t=0}^{T-1}\Xi(t)
\end{aligned}$$

where

$$\Xi(t) = E\left(\sum_{n,f} Q_n^f(t) E\left(u_{n,f}^{*out}(t) - u_{n,f}^{*in}(t) - \lambda_{n,f} | \boldsymbol{Q}(t)\right)\right). \tag{3–34}$$

By taking $\limsup_{T\to\infty}$, we have

$$J \limsup_{T\to\infty} \frac{1}{T} \sum_{t=0}^{T-1} \overline{G^{MES}}(t) \leq B + JC^*$$
$$-2 \limsup_{T\to\infty} \frac{1}{T} \sum_{t=0}^{T-1} \Xi(t). \tag{3–35}$$

Note that

$$\lim(AB) = \lim(A) \lim(B) \tag{3–36}$$

if $\lim(A)$ and $\lim(B)$ exist and are bounded. Recall that in the previous section, we have shown that

$$\limsup_{T\to\infty} \frac{1}{T} \sum_{t=0}^{T-1} \sum_{n,f} E\left(Q_n^f(t)\right) \tag{3–37}$$

exists and is finite. Moreover, since $u_{n,f}^{*out}(t)$ and $u_{n,f}^{*in}(t)$ are the optimum solution to (3–5), the network stability is achieved under $\boldsymbol{\lambda}$. Therefore, we have

$$\limsup_{T\to\infty} \frac{1}{T} \sum_{t=0}^{T-1} u_{n,f}^{*out}(t) \geq \limsup_{T\to\infty} \frac{1}{T} \sum_{t=0}^{T-1} u_{n,f}^{*in}(t) + \lambda_{n,f}$$

since otherwise, the network stability cannot be ensured by $\boldsymbol{u}^*$. Finally, we conclude that

$$\limsup_{T\to\infty} \frac{1}{T} \sum_{t=0}^{T-1} \Xi(t) \tag{3–38}$$

is nonnegative and thus the last term of (3–35) can be omitted. Consequently, by dividing J on both sides of (3–35), we have

$$\limsup_{T\to\infty} \frac{1}{T} \sum_{t=0}^{T-1} \overline{G^{MES}}(t) \leq \frac{B}{J} + C^*. \tag{3–39}$$

Therefore, Theorem 3.2 holds.

3.4 Simulations

We consider a multi-hop wireless network illustrated in Figure 3-1. There are three flows in the network, denoted by *Flow 1, 2, 3*. The routing paths of flows are specified by $R_1 = \{A, B, C, D\}$, $R_2 = \{F, G, C, D\}$ and $R_3 = \{E, F, G, H\}$. The exogenous

arrival processes are Bernoulli processes with an average rate of 5 packets per slot for all three flows. Without loss of generality, we assume a two-hop interference model which represents the general IEEE 802.11 MAC protocols [36, 37]. The nominal link rate of a wireless link is assumed to be 20 packets per slot. For a particular link, there are three equally possible channel states, i.e., *Good, Medium, Bad* where the corresponding successful transmission probabilities are $0.8, 0.6, 0.3$, respectively.

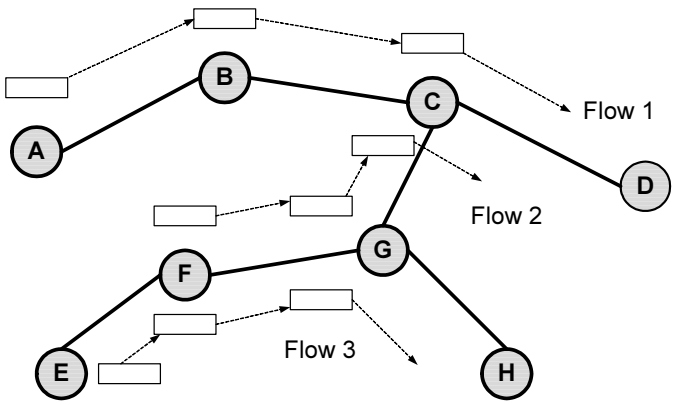

Figure 3-1. Network topology with interconnected queues

For the ease of exposition, we assume that $\alpha_{a,b} = \beta_{a,b} = 50\mu J$ for all links in the network [50]. We investigate the average energy consumption induced by the *MaxWeight* algorithm and the proposed MES algorithm with different values of J, i.e., 50, 100, 200, 500, 800, 1000, 2000, 5000, 8000, 10000, 12000, 14000, 16000, 18000, 20000, 25000. Every simulation is executed for 10000 time slots.

Figure 3-2 depicts the average energy consumption per time slot for the *MaxWeight* algorithm and the MES algorithm with different values of J. As illustrated in Figure 3-2, when $J = 0$, the MES algorithm reduces to the original *MaxWeight* algorithm and yields the same amount of energy expenditure. However, as J increases, the energy consumption induced by the MES algorithm decreases remarkably. In addition, as shown analytically in Theorem 3.2, the MES algorithm approaches to the global minimum energy expenditure gradually as J increases. To achieve a better understanding on the impact of larger values of J, we compare the average queue backlogs of all data

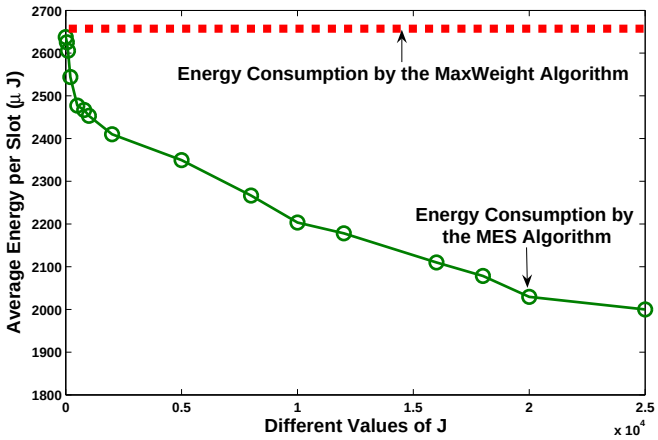

Figure 3-2. Comparison of the energy consumptions of the *MaxWeight* algorithm and the MES algorithm

queues, with $J = 50$, 150, 350 and 500, in Figure 3-3 and Figure 3-4, where the queues in the network are indexed by 1 to 9 in the order of Q_A^1, Q_B^1, Q_C^1, Q_F^2, Q_G^2, Q_C^2, Q_E^3, Q_F^3 and Q_G^3. It is worth noting that, as J grows, the average queue backlogs in the network increases correspondingly. Following Little's Law, larger queue backlogs yield longer network delays. Therefore, while the network-wide energy expenditure is noticeably reduced, a larger value of J yields a longer average delay in the network. As a consequence, a tradeoff between the energy-optimality and the experienced delay can be attained by tuning J properly.

So far, throughout this work, we have assumed that the energy in each node is constrained yet sufficiently large. Next, we investigate the performance of the MES algorithm in multi-hop wireless networks where each node has a limited and finite amount of energy. More specifically, the same network in Figure 3-1 is considered, however, we assume that each node in the network has a battery with an initial energy of 1 Joule. We compare the performance of the *MaxWeight* algorithm with the MES algorithm for different values of J, in terms of the *network lifetime*, which is defined as the time instance when the first node in the network depletes the battery completely. The values of J are 50, 200, 500, 800, 1000, 2000, 5000, 8000, 10000, 15000 and 20000.

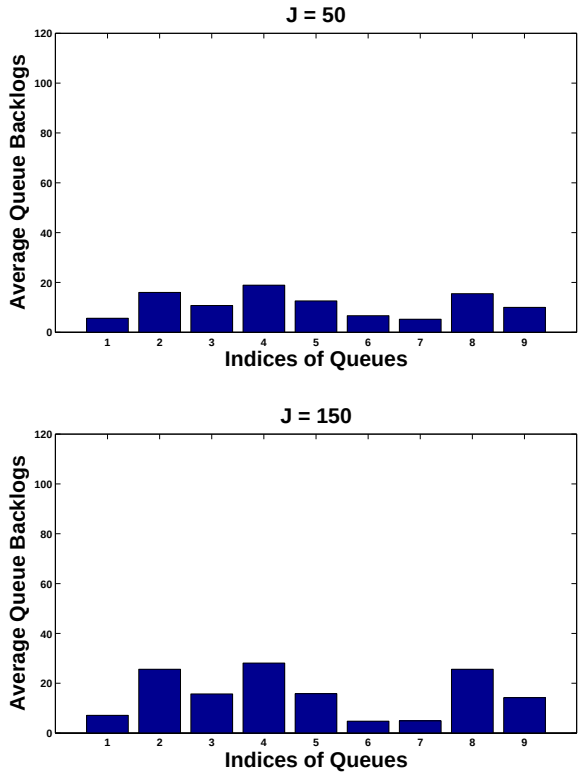

Figure 3-3. The average queue backlogs in the network for $J = 50$ and 150

Figure 3-5 pictorially compares the network lifetime induced by the *MaxWeight* algorithm and that of the MES algorithm for different values of J. Similar to the previous scenario, when J is small, the MES algorithm yields similar performance, in terms of the network lifetime, compared to the *MaxWeight* algorithm. However, when J increases, the MES algorithm significantly outperforms the traditional *MaxWeight* algorithm. It is worth noting that when $J = 20000$, the MES algorithm prolongs the network lifetime by more than twice as much as that of the *MaxWeight* algorithm! By the same token, a tradeoff between the network lifetime and the experienced delay of the network can be controlled effectively by tuning the value of J.

3.5 Conclusions

In this chapter, we investigate the energy consumption issue of the scheduling algorithms in multi-hop wireless networks. We show that the traditional *MaxWeight* algorithm, which is well known to be throughput optimal, is not energy optimal due to

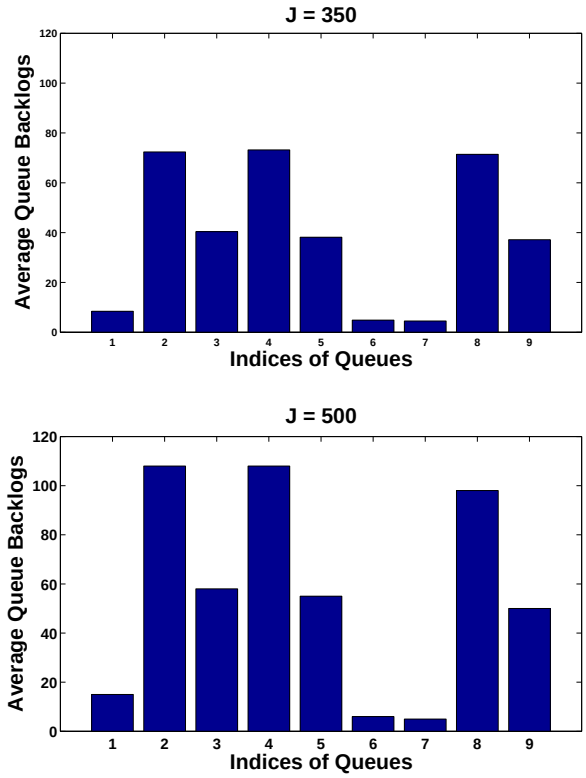

Figure 3-4. The average queue backlogs in the network for $J = 350$ and 500

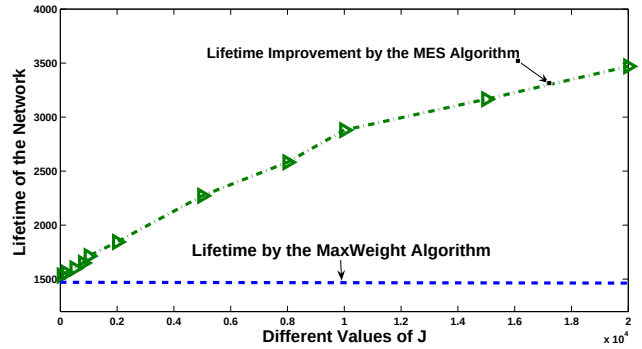

Figure 3-5. Comparison of the lifetime of the *MaxWeight* algorithm and the MES algorithm

the overlook of the energy consumptions induced by inevitable packet retransmissions. In light of this, we propose a minimum energy scheduling (MES) algorithm which significantly reduces the energy consumption compared to the original *MaxWeight* algorithm. In addition, we analytically show that the MES algorithm is essentially energy optimal in the sense that the average energy expenditure of the MES algorithm can be

pushed arbitrarily close to the global minimum solution. Moreover, the improvement on the energy efficiency is achieved without losing the throughput-optimality. Therefore, the proposed MES algorithm is of great importance for network protocol designs in energy-constrained multi-hop wireless networks such as wireless sensor networks.

CHAPTER 4
CHANNEL AND POWER ALLOCATION IN WIRELESS MESH NETWORKS

4.1 Introduction

Metropolitan wireless mesh networks gain enormous popularity recently [51]. The deployment of wireless mesh networks not only facilitates the data communication by removing cumbrous wires and cables, but also provides a means of Internet access scheme, which is a further step towards the goal of “communicating anywhere anytime”. No matter where the location is or the purpose that the wireless mesh network is deployed, the same conceptual layered architecture is utilized. Figure 4-1 illustrates the hierarchical structure of wireless mesh networks. The peripheral nodes are the access points (AP) which provide wireless access for the end users, or *clients*. Each AP is associated with a mesh router. They can be manufactured in a single device with two separate functional radios [52] [53], or simply connected with Ethernet cables [54]. The mesh routers are capable of communicating with each other via the wireless backbone. The central node is a gateway mesh router which functions as an information exchange between the wireless mesh access network and other networks such as the Internet. Both the routing algorithmic design and channel assignment for backbone mesh routers are interesting issues and attract tremendous attention [55–57].

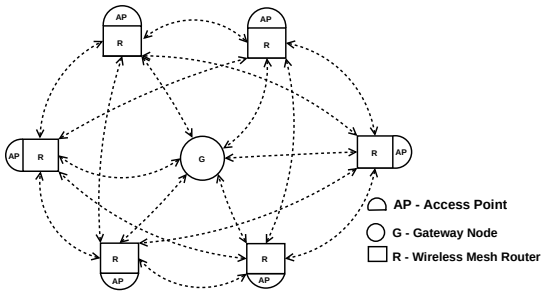

Figure 4-1. Hierarchical structure of wireless mesh access networks

In this work, we investigate an important issue which needs to be solved in wireless mesh networks. As in Figure 4-1, the AP and its associated clients form a regular WLAN *cell*, which operates with the *de facto* IEEE 802.11 standards.

The throughput of one cell depends on the signal-to-interference-plus-noise ratio (SINR) experienced at the receiver where the interference mainly comes from the other operating cells. For example, if each of the cells operates with IEEE 802.11b standard, we can utilize a different frequency band such as IEEE 802.11a or WiMAX [58], for the inter-cell communication among mesh routers and hence causes no interference to intra-cell transmissions. However, the co-channel interference from other operating cells is inevitable due to the limitation of available transmission channels, e.g., 3 non-overlapping channels in our example. Most current off-the-shelf APs are capable of adjusting the transmission rate according to the measured channel condition which is indicated by transmission bit error rate (BER). Given a particular modulation scheme, BER is uniquely determined by the SINR experienced by the receiver of the link. Generally speaking, higher SINR value yields lower BER and higher data rate. Therefore, the mutual interference dramatically degrades the transmission rate of each cell and the aggregated throughput of the whole network [59]. Each AP attempts to tune the physical parameters such as operating frequency[1] and transmission power in order to maximize the SINR and hence the throughput. In our work, we investigate the issue of maximizing the overall throughput of the network, defined as the summation of throughput of all cells, by finding the optimal frequency and transmission power allocation strategy. Also, due to the concern of scalability and computational complexity, we prefer a decentralized solution to the throughput maximization problem.

Unfortunately, the throughput maximization problem is challenging. For example, the frequency and power selected by one AP affects the SINR of other APs, and vice versa. Worse yet, if the APs belong to different regulation entities, the non-cooperative APs may only want to maximize their own cell's throughput rather than the overall one. Therefore, the throughput maximization problem is coupled and finding the optimum

[1] We will use *frequency* and *channel* interchangeably.

solution is not straightforward. Moreover, traditional site-planning methods in cellular networks are not feasible either. For example, the network administrator may want to add more APs when more users are joining the network or disable some APs where the associated users fail to pay the bill. The network topology is not static, although the changes take place slowly. Therefore, the demand for adaptability and light computation burden requires a decentralized solution for the throughput maximization problem.

In this work, we analyze the throughput maximization problem for both cooperative and non-cooperative scenarios. In the cooperative case, we model the interaction among all APs as an *identical interest game* and present a decentralized negotiation-based throughput maximizing algorithm for the joint frequency and power assignment. We show that this algorithm converges to the optimal frequency and power assignment strategy, which maximizes the overall throughput of the wireless mesh access network, with arbitrarily high probability. In the cases of non-cooperative APs, we prove the existence of Nash equilibria and show that the overall throughput performance is usually inferior to the cooperative cases. To bridge the performance gap, we propose a linear pricing scheme to combat with the selfish behaviors of non-cooperative APs.

The rest of this chapter is organized as follows. Section 4.2 outlines the system model we considered in the work. The cooperative wireless mesh access networks and the non-cooperative counterpart are investigated in Section 4.3 and Section 4.4, respectively. An extension of our model is discussed in Section 4.5 and the performance evaluation is provided in Section 4.6. Finally, Section 4.7 concludes this chapter.

4.2 System Model

In this work, we consider a wireless mesh access network illustrated in Figure 4-1. Each AP and corresponding clients form a cell. Without loss of generality, we assume that all the cells operate with IEEE 802.11b standard and the interference exclusively comes from the cells with same frequency. Furthermore, the distance between cells are sufficiently large in the sense that the accumulated interference experienced at the

receiver only affects the SINR value and not block the whole transmission. We assume that the channels are slow-varying additive white Gaussian noise (AWGN) channels. The channel gains of each pair of nodes are assumed to be constant over the time period of interest. As we are interested in the maximum achievable throughput, we consider the worst case where all APs are saturated. In other words, the APs always have packets to transmit and they can communicate with each other via the backbone mesh routers with negligible delay. Also, we assume that the APs are transmitters and clients are receivers due to the dominance of downlink traffic, as assumed[2] in [61] [62] and [63]. We only focus on the joint frequency and power allocation where the contention behavior is less relevant and thus omitted. Therefore, we can simplify our model as that all the APs are transmitting data to the associated clients consistently. We assume that each AP is capable of adjusting the operating frequency and power as well as acquiring the SINR values measured at the client by short ACK messages.

Let us first consider the simplest case where there is only one cell in the wireless mesh access network, i.e., a single WLAN. In the following two sections, we assume that the APs have pre-determined and fixed modulation and coding schemes. In other words, upon receiving the SINR value[3] measured by the client, denoted by γ, the AP tunes the physical parameters in order to maximize the *throughput*, which is defined as

$$R^*(\gamma) = \max_{R_i} R_i \times (1 - P_e(\gamma, R_i)) \tag{4–1}$$

where R_i is the raw data rate specified by the IEEE 802.11 standard and R^*, i.e., the throughput of this cell, is a non-decreasing function of received SINR γ. P_e is the error

[2] The dominance of the downlink traffic is verified by the experimental measurements in [60] as well.

[3] Although there is no interference in this case, we adopt SINR instead of SNR for notation consistency.

probability of the transmission channel, which is a function of SINR value providing the modulation and coding scheme [64]. Apparently, if there is only one cell in the mesh access network, the AP will boost the power as much as possible to increase the value of γ and thus the throughput is maximized.

We now consider the cases where N cells coexist in the wireless mesh access network. Let p_i and f_i denote the power and frequency for the i-th AP, respectively. We use $\mathbf{p} = [p_1, p_2, \cdots, p_N]$ and $\mathbf{f} = [f_1, f_2, \cdots, f_N]$ to represent the power and frequency assignment vector for all N APs. Therefore, for each cell i, the value of SINR[4] , i.e., γ_i, is a function of $(\mathbf{p}, \mathbf{f})$. The throughput of one cell depends not only on the power level and frequency of itself, but also those of other APs in the network. Therefore, the throughput maximization problem is coupled and by no means straightforward.

In the following two sections, we will discuss the scenarios where the APs are cooperative and non-cooperative, respectively, under the assumption that the modulation and coding schemes of APs are pre-loaded and fixed. In Section 4.5, we will extend our analysis by considering the scenario where the APs are capable of adaptive coding and modulation. The performance evaluation of all scenarios are provided by simulations in Section 4.6.

4.3 Cooperative Access Networks

In this section, we consider the scenarios where all APs in the wireless mesh access network are cooperative. The transmission power of APs are quantized into discrete power levels for simplicity. From the system point of view, we want to find a joint frequency and power level assignment such that the overall throughput in the whole

[4] Throughout the chapter, the term *SINR of the cell* represents the average SINR among all the clients in the cell, which can be obtained by a moving average of the reported SINR value.

network is maximized. Our objective function can be written as

$$U_{network}(\mathbf{p}, \mathbf{f}) = \sum_{i=1}^{N} R_i^*(\gamma_i) = \sum_{i=1}^{N} R_i^*(\mathbf{p}, \mathbf{f}) \tag{4–2}$$

where R_i^* is defined in (4–1).

However, finding the optimal frequency and power assignment which maximizes (4–2) is non-trivial. The interdependency makes the problem coupled and difficult to solve by traditional optimization methods [65]. A combination of $(\mathbf{p}, \mathbf{f})$ is named a *profile* and a naive approach to solve the problem is to investigate all profiles exhaustively. However, this is impossible in practice. For example, in a medium-size wireless mesh access network with 20 APs where each has 3 frequency channels and 10 power levels, the search space is $(3 \times 10)^{20}$ profiles! Obviously, the centralized algorithms are not favorable in the wireless mesh access network due to the scalability concern. Next, we will introduce a decentralized negotiation-based throughput maximization algorithm, from a game-theoretical perspective.

4.3.1 Cooperative Throughput Maximization Game

The APs in the wireless mesh access networks are considered as *players*, i.e., *decision makers* of the game. We model the interaction among APs as a *Cooperative Throughput Maximization Game (CTMG)*, where each player has an identical objective function U_i, as

$$U_i(\mathbf{p}, \mathbf{f}) = U_{network}(\mathbf{p}, \mathbf{f}) = \sum_{j=1}^{N} R_j^*(\mathbf{p}, \mathbf{f}) \ , \forall i. \tag{4–3}$$

For each player i, all possible frequency and power level pairs form a *strategy space* Φ_i which has a size of $c \times l$, where c is the number of frequency channels available and l is the number of feasible power levels. Define

$$\Omega = \Phi_1 \times \Phi_2 \times \cdots \times \Phi_N. \tag{4–4}$$

Then, the N players autonomously negotiate about the joint frequency-power profile in Ω in order to find the optimal profile which maximizes (4–3). However, due to the

interdependency among N players caused by mutual interference, one question of interest is that whether this negotiation will eventually meet an agreement, a.k.a., a Nash equilibrium. The importance of Nash equilibria lies in that a possible steady state of the system is guaranteed. If the game has no Nash equilibrium, the negotiation process never stops and oscillates in an everlasting fashion. In addition, we are concerning about what the performance of the steady states would be, if exist, in terms of overall throughput of the whole network. We provide answers to these questions in the following.

Lemma 3. *The CTMG is a* potential game*.*

A potential game is defined as a game where there exists a *potential function* P such that

$$P(a', a_{-i}) - P(a'', a_{-i}) = U_i(a', a_{-i}) - U_i(a'', a_{-i}) \; \forall i, a', a'' \tag{4–5}$$

where U_i is the utility function for player i and a', a'' are two arbitrary strategies in Φ_i. More specifically, we have $a' = [p_i', f_i']$ and $a'' = [p_i'', f_i'']$. The notation of a_{-i} denotes the vector of choices made by all players *other than* i. Potential games have been broadly applied in modeling the interactions in communication networks [66]. The popularity is on account of the nice properties of potential games, such as

- Potential games have at least one Nash equilibrium.
- All Nash equilibria are the maximizers of the potential function, either locally or globally.
- There are several learning schemes available which are guaranteed to converge to a Nash equilibrium, such as *better response* and *best response* [67] [68].

For detailed description about potential games, readers are referred to [67] and [69], which investigate the potential game theory in engineering context.

We observe that in the cooperative case, each player has the same utility function as in (4–3), which is the overall throughput of the network. Apparently, one potential

function of the game is the common utility function itself, i.e.,

$$P = U_1 = U_2 = \cdots = U_N. \tag{4–6}$$

In fact, the games where all players share the same utility function are called *identical interest games* [70], which is a special case of potential games and hence all the properties of potential games can be applied directly.

In the literature, both best response and better response are popular learning mechanisms that have been utilized in potential games [71–73]. At each step of the best response approach, one of the players investigates its strategy space and chooses the one with maximum utility value. This updating procedure is carried out sequentially. The primary drawback of the best response is the computational complexity, which grows linearly with the cardinality of the strategy space. An improvement of the best response is the so-called better response, where at each step, the player updates as long as the randomly selected strategy yields a better performance. The dramatically reduced computation is the tradeoff with the convergence speed. Both the best response and the better response dynamics are guaranteed to converge to a Nash equilibrium in potential games [66]. However, there may be multiple Nash equilibria in a potential game and the performance of different equilibria may vary dramatically. Therefore, although the best response and the better response could guarantee the convergence, they may reach an undesirable Nash equilibrium with inferior performance.

Figure 4-2. An illustrative example of multiple Nash equilibria

Let us consider an illustrative example in Figure 4-2. There are four labeled APs in the network. A and B are close to each other, and so are C and D. Without loss of

generality, we assume that the APs have the same power and only adjust the operating frequencies in an order of $A \rightarrow B \rightarrow C \rightarrow D$ to avoid the interference. The adaptation continues with the best response mechanism until a Nash equilibrium is reached. Suppose that there are two frequency channels available, say 1 and 2. First, A randomly selects one channel, say 1. B will pick 2. Next, C has the chance to update. Since C is closer to B than A, channel 1 will be selected. Finally, D will choose channel 2. By inspection, we claim that profile $1-2-2-1$ is a Nash equilibrium since no player is willing to update its strategy unilaterally. Meanwhile, we observe that another profile $1-2-1-2$ is also a Nash equilibrium. Obviously, the second Nash equilibrium generates much less interference than the first Nash equilibrium and hence yields superior performance in terms of overall throughput. However, the best response only leads to the less desirable Nash equilibrium.

In fact, the existence of multiple Nash equilibria is observed in [71] by simulations. However, the authors fail to specify which one would be the steady state of their game due to the limitation of the best response, even in a statistical fashion. Recall that the Nash equilibria are the maximizers of the potential function in potential games, converging to an inferior Nash equilibrium analogously indicates being trapped at a local optimum of the potential function. However, it is the global optimum, i.e., the optimal Nash equilibrium, that is the desirable steady state which we are yearning for.

Next, we introduce a negotiation-based throughput maximization algorithm (NETMA) which can converge to the optimal Nash equilibrium with arbitrarily high probability.

4.3.2 NETMA- Negotiation-Based Throughput Maximization Algorithm

We assume that the APs are homogeneous and each has a unique ID for routing purpose. Each AP maintains two variables D_{pre} and D_{cur}. The AP has the knowledge of its current throughput and records it in D_{cur}. Whenever there is a change of throughput

caused by exterior interference[5] , the AP sets $D_{pre} = D_{cur}$ and resets D_{cur} with the newly measured throughput. When the wireless mesh access network enters the *negotiation phase*[6] , NETMA is executed. The detailed procedure of NETMA is provided as follows.

NETMA:

- **Initialization:** For each AP, a pair of frequency and power level is randomly selected. Set $D_{pre} = D_{cur}$, the current throughput.
- **Repeat:**
  1. Randomly choose one of the AP, say k, as the updating one, i.e., each AP updates with probability $1/N$.
  2. For the updating AP k:
     (a) Randomly chooses a pair of frequency and power level, say f' and p', from the strategy space Φ_k. Then the AP computes the current throughput with f' and p' and records it into D_{cur}.
     (b) Broadcasts a short notifying message which contains its unique ID_k to all the other APs in the mesh access network.
  3. For each AP other than k, say j:
     (a) If the γ_j value changes, records the previous throughput into D_{pre} and the current throughput into D_{cur}. Remains unchanged otherwise.
     (b) Upon receiving the notifying message, a three-value vector of $[D_{pre}, D_{cur}, ID_j]$ is sent back to the k-th AP.
  4. After receiving all the three-value vectors by counting the identifiers ID_j, the k-th AP computes the sum throughput before and after f' and p' are selected, which are denoted by P_{pre} and P_{cur}.

[5] We assume the channel is slow-varying and the change of throughput for a single cell is due to the mutual interference only.

[6] To reduce the negotiation overhead, a negotiation phase can be initiated by the network administrator after a new contracted user joins or a current user terminates the service, or on a daily basis.

5. For a *smoothing factor* $\tau > 0$, the k-th AP keeps f' and p' with probability

$$\frac{e^{P_{cur}/\tau}}{e^{P_{cur}/\tau} + e^{P_{pre}/\tau}} = \frac{1}{1 + e^{(P_{pre} - P_{cur})/\tau}} \tag{4–7}$$

6. The k-th AP broadcasts another short notifying message, which indicates the end of updating process and a specific number δ, to all the other APs.

– **Until:** The stopping criteria Γ is met.

Note that in step 6, the specific format of δ depends on the predefined stopping criterion Γ. For example,

- If the stopping criterion is the maximum number of negotiation steps, δ is a counter which adds one after each updating process.
- If the stopping criterion is that no AP has updated for a certain number of steps, δ is a binary number where 1 means updating.
- If the stopping criterion is that the difference between sum throughput obtained in consecutive steps are less than a predefined threshold ϵ, δ is the calculated sum throughput after each updating process.

We can have other stopping criteria Γs and corresponding formats of δ as well.

The NETMA algorithm is inspired by the work in [74], where a similar algorithm was first introduced in the context of stream control in MIMO interference networks. The distinguishing feature of this type of negotiation algorithms, from the better response and the best response, is the randomness deliberately introduced on the decision making in step 5. The rationale can be illustrated in Figure 4-2 intuitively. If there is no randomness in decision making , i.e., $\tau = 0$, the four APs may get trapped at a low efficiency Nash equilibrium $1 - 2 - 2 - 1$. However, with the randomness caused by nonzero τ, they may reach an intermediate state $1 - 2 - 2 - 2$ and arrive at the optimum Nash equilibrium $1 - 2 - 1 - 2$ eventually. Moreover, the updating rule in step 5 also implies that if f' and p' yield a better performance, i.e., $P_{pre} - P_{cur} < 0$, the k-th AP will keep them with high probability. Otherwise, it will change with high probability.

The steady state behavior of NETMA is characterized in the following theorem.

Theorem 4.1. *NETMA converges to the optimal Nash equilibrium in CTMG with arbitrarily high probability.*

Proof. The proof of Theorem 4.1 follows similar lines of the proof in [74] and [75].

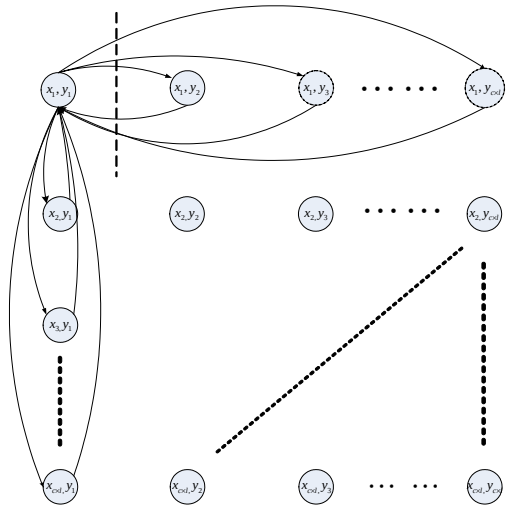

Figure 4-3. Markovian chain of NETMA with two players

First, we observe that the joint frequency-power negotiation generates an N-dimensional Markovian chain. Figure 4-3 illustrates the Markovian chain introduced by NETMA with two players, say A and B. Let x and y be the choices for each player , where $x \in \Phi_A$ and $y \in \Phi_B$. In other words, player A can choose a frequency-power pair from $[x_1, \cdots, x_{c\times l}]$ and player B can choose from $[y_1, \cdots, y_{c\times l}]$. Note that at an arbitrary time instant, only one of the players can update. In Figure 4-3, for example, state (x_1, y_1) can only transit to a state either in the same row or the same column, not anywhere else. This is true for every state in the Markovian chain. Let $S_{i,j}$ denote the state of (x_i, y_i). We have

$$Pr(S_{m,n}|S_{i,j}) = \begin{cases} \frac{e^{P(S_{m,n})/\tau}}{2\times c\times l\times(e^{P(S_{m,n})/\tau}+e^{P(S_{i,j})/\tau})}, \\ \text{if } m = i \text{ or } n = j \\ 0, \\ \text{otherwise.} \end{cases} \tag{4–8}$$

where τ is the smoothing factor in step 5 of NETMA and $P(S_{i,j})$ is the value of the potential function, i.e., (4–21), at the state of $S_{i,j}$.

Let us derive the stationary distribution Pr^* for each state. We examine the balanced equations. Writing the balance equations [76] at the dashed line, we obtain

$$\sum_{k=2}^{c\times l} Pr^*(S_{1,1}) \times Pr(S_{1,k}|S_{1,1}) = \sum_{k=2}^{c\times l} Pr^*(S_{1,k}) \times Pr(S_{1,1}|S_{1,k}). \tag{4–9}$$

By substituting (4–9) with (4–8), we have

$$\begin{aligned} & \textstyle\sum_{k=2}^{c\times l} Pr^*(S_{1,1}) \times \frac{e^{P(S_{1,k})/\tau}}{e^{P(S_{1,1})/\tau}+e^{P(S_{1,k})/\tau}} \\ = \; & \textstyle\sum_{k=2}^{c\times l} Pr^*(S_{1,k}) \times \frac{e^{P(S_{1,1})/\tau}}{e^{P(S_{1,1})/\tau}+e^{P(S_{1,k})/\tau}}. \end{aligned} \tag{4–10}$$

Observing the symmetry of equation (4–10) as well as the Markovian chain, we note that the set of equations in (4–10) are all balanced if for arbitrary state $\tilde{S}$ in the strategy space Ω, the stationary distribution is

$$Pr^*(\tilde{S}) = \mathcal{K} e^{P(\tilde{S})/\tau} \tag{4–11}$$

where $\mathcal{K}$ is a constant. By applying the probability conservation law [77] [76], we obtain the stationary distribution for the Markovian chain as

$$Pr^*(\tilde{S}) = \frac{e^{P(\tilde{S})/\tau}}{\sum_{S_i\in\Omega} e^{P(S_i)/\tau}} \tag{4–12}$$

for arbitrary state $\tilde{S} \in \Omega$.

In addition, we observe that the Markovian chain is irreducible and aperiodic. Therefore, the stationary distribution given in (4–12) is valid and unique.

Let S^* be the optimal state which yields the maximum value of potential function P, i.e.,

$$S^* = \text{argmax}_{S_i\in\Omega} P(S_i). \tag{4–13}$$

From (4–12), we have

$$\lim_{\tau \to 0} Pr^*(S^*) = 1 \tag{4–14}$$

which substantiates that NETMA converges to the optimal state in probability.

Finally, the analogous analysis can be straightforwardly extended to an N-dimensional Markovian chain and thus completes the proof.

In NETMA, there is no central computational unit required. The joint frequency-power assignment is achieved by negotiations among cooperative APs and the maximum overall throughput is achieved with arbitrarily high probability. The autonomous behavior and decentralized implementation make NETMA suitable for large scale wireless mesh access networks. Moreover, NETMA has fast adaptability for the topology change of the wireless mesh access networks. NETMA does not depend on any rate adaption algorithms, nor on any underlying MAC protocols. In our simulation in Section 4.6, we use IEEE 802.11b as the MAC layer protocol. However, it can be easily extended to arbitrary MAC protocol with multi-rate multi-channel capability, such as IEEE 802.11a. In addition, even with the existence of exterior interference source, such as coexisting WLANs, NETMA works properly as well since the objective of NETMA is to maximize the overall throughput of the network in the current wireless environments. The tradeoff between algorithmic performance and convergence speed is controlled by parameter τ in step 5, where large τ represents extensive space search with slow convergence. On the contrary, small τ represents limited space search with fast convergence. Note that the smoothing factor τ here is analogous to the concept of *temperature* in simulated annealing [78]. Therefore, it is advisable that at the beginning period of the negotiation, the value of τ is set with a large number and keeps deceasing as the negotiation iterates. We choose $\tau = 10/k^2$ in our simulations, where k denotes the negotiation step.

In step 1, we require that each AP updates with a probability of $1/N$. For example, we can utilize a random token mechanism where each updating AP randomly selects an AP as the next updating AP, i.e., passing the token. Note that in NETMA, even an

erroneous operation happens, for example, two APs update at the same time in our case, it only prolongs the convergence time for NETMA yet does not affect the final output of NETMA. This is because that such an error, as verified in [72] via extensive simulations, has no influence on the statistically monotonic-increasing tendency of the potential function.

4.4 Non-Cooperative Access Networks

In the previous section, we discuss the scenarios where all APs in the wireless mesh access network are cooperative, and the overall throughput is maximized by negotiations among autonomous APs using the NETMA mechanism. However, cooperation is not always attainable. Although the functionality of relaying packets for each other can be achieved by incentive mechanisms such as [79], the adjustable parameters inside each cell cannot be enforced and effectively controlled. The N APs may belong to distinct self-interested users and they care about exclusively their own throughput rather than the overall aggregated throughput. In other words, the utility function of each selfish user is

$$U_i = R_i^*(\gamma_i) \tag{4–15}$$

where R_i^* is the throughput of the i-th cell, defined in (4–1). Analogous to CTMG, we can formulate the interaction among N selfish APs as a *Non-cooperative Throughput Maximizing Game (NTMG)* where each AP is attempting to find the frequency-power pair which maximizes its own SINR value as well as the corresponding throughput. As in the cooperative case, each player's utility function depends on the frequency and power of itself as well as those of others. However, NTMG is no longer an identical interest game.

Lemma 4. *In NTMG, all the APs will transmit with the maximal power at the Nash equilibrium, if exists.*

Proof. The proof of Lemma 4 is straightforward. For a single player, we have

$$\gamma_i = \frac{p_i g_{ii}}{\sum_{k \in \mathcal{F}_i(f_i)} p_k g_{ki} + N_i}. \tag{4–16}$$

where g_{ij} is the channel gain from cell i's transmitter to j's receiver and N_i is the Gaussian noise at the i's receiver. $\mathcal{F}_i(f_i)$ denotes the set of cells which operate at the same frequency f_i other than cell i. Note that given other players' strategies, γ_i is a monotonic increasing function of p_i and so is U_i. Assume at a Nash equilibrium of NTMG, the k-th AP has a power level of p_k satisfying $0 \leq p_k < p_{max}$, where p_{max} denotes the maximum power defined by MAC layer. The k-th AP is inclined to increase its power p_k in order to yield a higher value of U_i, which contradicts the definition of Nash equilibrium. Thus, at the Nash equilibrium of NTMG, if exists, all the APs will operate at the same power level, i.e., p_{max}.

Based on Lemma 4, the NTMG can be viewed as a simplified game where each player has the same power and only adjusts the frequency to minimize the interference. Moreover, according to (4–15) (4–16) and the assumption of uniform environment, the NTMG is equivalent to the following simplified game where each player has the utility function[7] as

$$U_i = -(\sum_{k \in \mathcal{F}_i(f_i)} p_{max} g_{ki} + N_i) \tag{4–17}$$

and U_i is a function of frequency assignment vector $\mathbf{f}$ exclusively.

As in the cooperative case, the frequency selection among N players is mutually dependent. The question arises that whether this frequency adjusting dynamic converges, or equivalently, whether NTMG has a Nash equilibrium. We provide the answer of this question in the following theorem.

[7] The negative sign comes from the convention that utility functions are the ones to be maximized.

Theorem 4.2. *There exists at least one Nash equilibrium in NTMG.*

Proof. Let us first consider the simplified game. For each player, the utility function is given as

$$U_i = -(\sum_{k \in \mathcal{F}_i(f_i)} p_k g_{ki} + N_i) \tag{4–18}$$

$$= -(\sum_{k \neq i, k \in N} p_k g_{ki} \times \delta(f_i - f_k) + N_i) \tag{4–19}$$

where

$$\delta(k) = \begin{cases} 1, & \text{if } k = 0 \\ 0, & \text{otherwise.} \end{cases} \tag{4–20}$$

We conjecture that one of the feasible potential functions is

$$P = -\frac{1}{2} \times \sum_{i \in N} \sum_{k \in \mathcal{F}_i(f_i)} p_k g_{ki}. \tag{4–21}$$

The verification is as follows.

$$\begin{aligned} 2P &= -\sum_{i \in N} \sum_{k \in \mathcal{F}_i(f_i)} p_k g_{ki} \\ &= -\left\{ \sum_{k \in \mathcal{F}_i(f_i)} p_k g_{ki} + \sum_{j \neq i, j \in N} \sum_{k \in \mathcal{F}_j(f_j)} p_k g_{kj} \right\} \\ &= -\left\{ \sum_{k \in \mathcal{F}_i(f_i)} p_k g_{ki} + \sum_{j \neq i, j \in N} \{ p_i g_{ij} \delta(f_i - f_j) \right. \\ &\quad \left. + \sum_{k \in \mathcal{F}_j(f_j), k \neq i} p_k g_{kj} \} \right\} \\ &= -\left\{ \sum_{k \neq i, k \in N} p_k g_{ki} \delta(f_k - f_i) \right. \\ &\quad + \sum_{j \neq i, j \in N} p_i g_{ij} \delta(f_i - f_j) \\ &\quad \left. + \sum_{j \neq i, j \in N} \sum_{k \in \mathcal{F}_j(f_j), k \neq i} p_k g_{kj} \right\}. \end{aligned} \tag{4–22}$$

Note that

$$p_k g_{ki} \delta(f_k - f_i) = p_i g_{ik} \delta(f_i - f_k) \tag{4–23}$$

for any pair of i, k. We have

$$P = -\left\{ \sum_{k \neq i, k \in N} p_k g_{ki} \delta(f_k - f_i) + \frac{1}{2} \times Q(-i) \right\} \tag{4–24}$$

where

$$Q(-i) = \sum_{j \neq i, j \in N} \sum_{k \in \mathcal{F}_i(f_i), k \neq i} p_k g_{kj} \tag{4–25}$$

and $Q(-i)$ is independent of f_i. Therefore, for arbitrary two frequencies a' and a'' of player i, we have

$$Q_{a'}(-i) = Q_{a''}(-i) \tag{4–26}$$

and

$$\begin{aligned} & P(a', a_{-i}) - P(a'', a_{-i}) \\ = \quad & \left\{ \sum_{k \in \mathcal{F}_i(a')} p_k g_{ki} + \tfrac{1}{2} \times Q_{a'}(-i) \right\} \\ & - \left\{ \sum_{k \in \mathcal{F}_i(a'')} p_k g_{ki} + \tfrac{1}{2} \times Q_{a''}(-i) \right\} \\ = \quad & U_i(a', a_{-i}) - U_i(a'', a_{-i}). \end{aligned} \tag{4–27}$$

Therefore, according to the definition in (4–5), the simplified game is a potential game and has at least one Nash equilibrium. Thus, the existence of Nash equilibrium in NTMG is obtained from the equivalence derived from Lemma 4.

As shown in Lemma 4, at the equilibrium, the non-cooperative APs will always transmit at the maximum power level. This seem to be the best choice for each one of the APs. However, it is usually not a favorable strategy from a social-welfare point of view. To bridge the performance gap, we propose a *linear pricing* scheme to combat with the selfish behaviors, i.e., the players are forced to pay a *tax* proportional to the utilized resources. For example, we could impose a price to all selfish APs for the power

they utilize. Hence for each AP, the utility function becomes

$$U_i = R_i^*(\gamma_i) - \lambda_p^i p_i \tag{4–28}$$

where λ_p^i represents the *power utilization price* specific for the i-th AP and p_i is its transmission power. Therefore, the more power AP uses, the more tax it has to pay. By imposing power prices properly, a more desirable equilibrium may be induced, from a social-welfare point of view. We define the corresponding game as a Non-cooperative Throughput Maximization Game with Pricing (NTMGP).

Let us first investigate the impact of prices on the behaviors of players. If $\lambda_p^i = 0$, where no price is imposed, the i-th AP will transmit at the maximum power and causes extra interference to other APs. However, if we impose an unbearably high price, say $\lambda_i^p = \infty$, the AP would rather not to transmit at all. Based on these observations, we propose a heuristic linear pricing scheme to improve the overall throughput in non-cooperative wireless mesh access networks.

To enforce the scheme, we introduce a *pricing dictator unit* (PDU) into the network which determines the prices for all APs and informs them timely. In addition, we assume that the PDU has the monitoring capability and is aware of the operating frequencies of each cell. There are two prices charged by the PDU for each non-cooperative AP. Besides the power utilizing price λ_p^i, a *frequency switching price* λ_f^i is imposed on the i-th AP whenever it changes the operating frequency. The price setting process is described as follows.

Price setting process:

Phase I:

- The PDU sets $\lambda_f^1 = \cdots \lambda_f^N = 0$ and $\lambda_p^1 = \cdots \lambda_p^N = 0$ and all APs play NTMG until converges, i.e., a Nash equilibrium is reached.
- The PDU collects the current throughput information from each cell, denoted by M_i, where i is the index of the cell.

Phase II:

- The PDU sets $\lambda_f^1 = \cdots \lambda_f^N = \infty$.
- For each AP indexed by $i = 1, \cdots, N$:

  1. The PDU sets $\lambda_p^i = \infty$ for the i-th AP and let the APs play the NTMGP. Upon convergence, the PDU collects the overall throughput, say V_i, in the current price setting.
  2. Calculate the power utilizing price for the i-th AP as

$$\tilde{\lambda}_p^i = \frac{V_i - \sum_{j=1, j\neq i}^{N} M_j}{p_{max}} \tag{4–29}$$

  3. Reset $\lambda_p^i = 0$.

Output:

- Power utilizing price vector $\tilde{\lambda}_{\mathrm{p}} = [\tilde{\lambda}_p^1, \cdots, \tilde{\lambda}_p^N]$
- Frequency switching price vector $\tilde{\lambda}_{\mathrm{f}} = [\infty, \cdots, \infty]$

In the price setting process above, the PDU imposes zero prices for all APs initially. As a consequence, all APs will transmit with p_{max} at the equilibrium, as shown in Lemma 4. Upon convergence, the PDU fixes the frequency switching price to infinity which discourages the non-cooperative APs from switching channels thereafter. In (4–29), $\sum_{j=1, j\neq i}^{N} M_j$ is the sum throughput for all cells other than i, when the i-th AP transmits with the maximal power due to the zero power price. Similarly, V_i is the sum throughput of other cells when the i-th AP is silent due to the unaffordable power price. Therefore, in (4–29), the power utilization price charged for the i-th AP, a.k.a., $\tilde{\lambda}_p^i$, can be viewed as a compensation to the impact it causes on the overall throughput of other cells. The more power it utilizes, the more severe it affects the other players and thus the more it pays, as illustrated in (4–28). Hence, by imposing taxes deliberately, the selfish behaviors of non-cooperative APs are effectively discouraged and a more desirable equilibrium can be induced, in term of overall throughput of the whole network. The proof of existence of Nash equilibrium in NTMGP is straightforward. Note that the utility

function of (4–28) is quasi-concave with respect to power. The existence of pure strategy Nash equilibrium follows directly from the results of [80]. We will present the detailed performance evaluation of CTMG, NTMG and NTMGP in Section 4.6.

4.5 An Extension to Adaptive Coding and Modulation Capable Devices

So far, we have assumed that the throughput of a cell is given in the form of (4–1), which is not a continuous function. To be precise, in both Section 4.3 and Section 4.4, we are confined to the traditional IEEE 802.11 family devices where the modulation and coding schemes are pre-determined and fixed. For example, Table 4-1 provides a mapping between SINR values and corresponding rates [81], the feasible data transmission rate is a discrete set and is usually much less than the theoretical channel capacity. We name such devices as *legacy IEEE 802.11 devices*.

Table 4-1. Data rates v.s. SINR thresholds with maximum BER = 10^{-5}

Rate(Mbps)	Minimum SINR (dB)
1	-2.92
2	1.59
5.5	5.98
11	6.99

However, thanks to the advance of coding techniques, the maximum data transmission rate can be largely closed to the theoretical Shannon capacity in AWGN channels [82]. Note that achieving this requires variable-rate transmissions by matching to the instantaneous SINR, which can be implemented in practice through adaptive coding and modulation (ACM) techniques [83]. This motivates us to extend our results to ACM-capable devices. More specifically, we are considering more advanced and powerful APs which attempt to tune the frequency and power in order to maximize

$$C_i(\gamma_i) = W_i \log_2(1 + \gamma_i) \tag{4–30}$$

where C_i is the Shannon capacity of the i-th cell, and W_i is the bandwidth. Note that in this scenario, the maximum achievable transmission rate, as denoted by the Shannon capacity, is a continuous variable with respect to γ_i, rather than discrete, as exemplified in Table 4-1. It is worth noting that the only difference in this scenario is the alternative objective function of each AP. Therefore, all the results we have obtained so far are extendable[8] to this special scenario with merely a change of the objective function.

Furthermore, due to the continuity of the objective function in (4–30), the aforementioned heuristic pricing scheme in Section 4.4 can be improved. Without loss of generality, we assume that all the cells have unity bandwidth. Restated, we assume that the PDU is a centralized device which knows the channel environment sufficiently by greedy acquiring. In addition, the PDU is assumed to have monitoring capability and is aware of the operating frequency of each cell. The tailored pricing scheme for this ACM-capable scenario is described as follows.

- First, the PDU sets $\lambda_f^1 = \cdots \lambda_f^N = 0$ and $\lambda_p^1 = \cdots \lambda_p^N = 0$ and all APs play selfishly, until a Nash equilibrium is achieved.
- The PDU sets $\lambda_f^1 = \cdots \lambda_f^N = \infty$.
- For each AP indexed by $i = 1, \cdots, N$, the PDU sets

[8] More specifically, in the cooperative case, we replace (4–2) with $U_{network}(\mathbf{p}, \mathbf{f}) = \sum_{i=1}^{N} C_i(\gamma_i)$ whereas in the non-cooperative case, (4–15) and (4–28) are replaced by $U_i = C_i(\gamma_i)$ and $U_i = C_i(\gamma_i) - \lambda_p^i p_i$, respectively.

$$
\begin{aligned}
\lambda_p^i &= |\sum_{k\in\mathcal{F}_i} \frac{\partial C_k}{\partial p_i}| \\
&= |\sum_{k\in\mathcal{F}_i} -\frac{p_k \times g_{kk} \times g_{ik}}{\ln 2 \times (1+\gamma_k) \times (\sum_{j\in\mathcal{F}_k} p_j \times g_{jk} + N_k)^2}| \\
&= \sum_{k\in\mathcal{F}_i} \frac{p_k \times g_{kk} \times g_{ik}}{\ln 2 \times (1+\gamma_i) \times (\frac{p_k \times g_{kk}}{\gamma_k})^2} \\
&= \sum_{k\in\mathcal{F}_i} \frac{g_{ik} \times \gamma_k^2}{\ln 2 \times (1+\gamma_k) \times p_k \times g_{kk}}.
\end{aligned} \tag{4–31}
$$

Then the PDU informs each AP the corresponding prices, i.e., $\lambda_f^i = \infty$ and λ_p^i calculated in (4–31).

Note that the major difference in this pricing scheme lies in (4–31), where the λ_p^i charged for the i-th AP is the *Pigouvian price* levied to discourage its reckless power increase.

After obtaining the prices imposed by the PDU, each AP fixes the operating frequency and calculates the optimum power p_i^*, which maximizes $U_i = C_i - p_i\lambda_p^i$, according to the following steps.

$$
\frac{\partial U_i}{\partial p_i} = \frac{\partial C_i}{\partial p_i} - \lambda_p^i \tag{4–32}
$$

where

$$
\frac{\partial C_i}{\partial p_i} = \frac{g_{ii}}{\ln 2 \times (\sum_{k\in\mathcal{F}_i} p_k \times g_{ki} + N_i) \times (1+\gamma_i)}. \tag{4–33}
$$

By setting (4–32) equal to zero, we have

$$
p_i^* = \left[\frac{1}{\ln 2 \times \lambda_p^i} - \frac{\sum_{k\in\mathcal{F}_i} p_k \times g_{ki} + N_i}{g_{ii}}\right]_{p_{min}}^{p_{max}}. \tag{4–34}
$$

where $[x]_a^b$ denotes $\max\{\min\{b, x\}, a\}$ and p_{max}, p_{min} represent the maximum and minimum power of the device, respectively. Note that $\sum_{k\in\mathcal{F}_i} p_k \times g_{ki} + N_i$ can be easily measured when the i-th AP sets its transmission power to zero. Therefore, finding the

optimum power of each AP requires only local information and can be implemented in a distributed fashion.

In (4–31), we observe that the prices imposed on APs depend on the power vector $\mathbf{p}$, and vice versa. Therefore, after each AP optimizes its power according to (4–34), the PDU measures the new value of power, adjusts the price following (4–31), and then announces the new price again. The pricing setting process in (4–31) and the utility maximization process in (4–34) are executed in an iterative manner, until convergence. The whole pricing scheme is summarized as follows.

Pricing Scheme:

1. The PDU initially sets zero prices. As a consequence, all APs will converge at a Nash equilibrium with maximum power.
2. The PDU sets infinity for the frequency switching price which prevents the whole network from unstable frequency oscillations.
3. The PDU sets and announces the power prices for each AP according to (4–31).
4. Informed by the PDU, each AP optimizes its transmission power following (4–34).
5. Go back to step 3 until the iteration converges.

The performance evaluation of this tailored pricing scheme is illustrated in the next section.

4.6 Performance Evaluation

4.6.1 Legacy IEEE 802.11 Devices

In this subsection, we first investigate the performance of NETMA, NTMG and NTMGP with legacy devices, i.e., the scenarios we considered in Section 4.3 and Section 4.4. We assume the wireless mesh access network has N homogeneous APs. The other simulation parameters are summarized as follows.

- Each AP has a maximum power $p_{max} = 100mW$ and a minimum power $p_{min} = 10mW$ and 10 different power levels as $[10mW, 20mW, \cdots, 100mW]$.
- The noise experienced at each receiver is assumed identical and has a power of $2mW$.

- All APs use IEEE 802.11b standard as the MAC protocol. In other words, each AP has four feasible data rate, $1, 2, 5.5, 11$ Mbps and 3 non-overlapping channels, i.e., $c = 3$.
- Without loss of generality, we assume that the received power is inversely proportional to the square of the Euclidian distance.
- The smoothing factor τ decreases as $\tau = 10/k^2$, where k is the negotiation step.
- The stopping criteria for NETMA and NTMG are the maximum number of iterations, denoted by ω.

For the sake of simplicity, we utilize a table-driven rate adaption algorithm provided in Table 4-1. Note that our results can also be applied to arbitrary propagation models, rate adaptation algorithms and underlying multi-channel multi-rate MAC protocols.

4.6.1.1 Example of small networks

We first consider a small wireless mesh access network with 5 APs, i.e., $N = 5$. All APs are randomly located in a square of 10-by-10 area. The global optimum solution is obtained by enumerating all feasible strategies, i.e., $(3 \times 10)^5$ profiles, as the performance benchmark. We first investigate the cooperative scenario where NETMA mechanism is applied. Next, the non-cooperative scenario is considered and each AP operates at the maximum power and adjusts the frequency only. The stopping criteria for both NETMA and NTMG are the maximum number of iterations where $\omega = 200$. The performance comparison is shown in Figure 4-4.

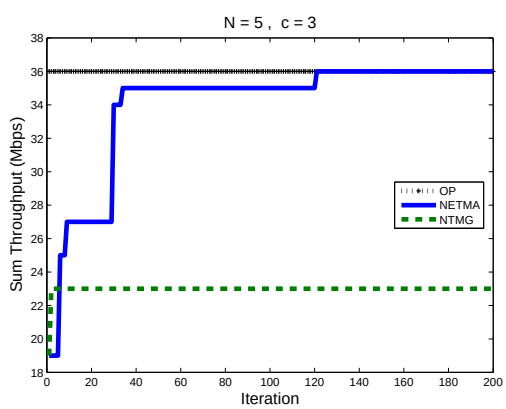

Figure 4-4. Performance evaluation of the wireless mesh access network with N = 5 and c = 3

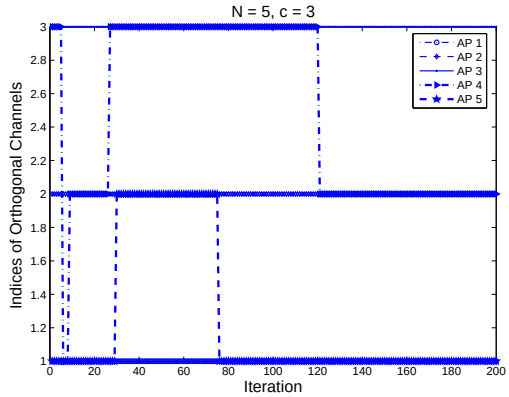

Figure 4-5. The trajectory of frequency negotiations in NETMA when N = 5 and c = 3

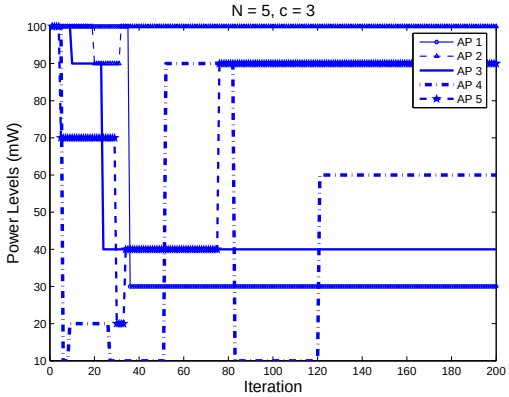

Figure 4-6. The trajectory of power negotiations in NETMA when N = 5 and c = 3

As indicated by the *OP* curve, the global optimum obtained by enumeration approach functions as the upper bound of the overall throughput. In Figure 4-4, we observe that NETMA gradually catches up with the global optimum as negotiations go. As expected, the non-cooperative APs yield remarkably inferior performance in terms of overall throughput, depicted by the *NTMG* curve. The inefficiency is due to the selfish behavior that APs transmit at the maximum power and are regardless of the interference. The existence of Nash equilibrium in both CTMG and NTMG are substantiated by the convergence of curves in Figure 4-4. Figure 4-5 and Figure 4-6 depict the trajectories of frequency negotiations and power level negotiations in NETMA, respectively. At the initialization, each AP randomly picks a frequency and a power level

and negotiates with each other following NETMA mechanism, until the optimum Nash equilibrium is achieved. Note that when the frequency vector and power vector converge in Figure 4-5 and Figure 4-6, the corresponding overall throughput obtained by NETMA catches the global optimum in Figure 4-4 simultaneously.

4.6.1.2 Example of large networks

We now consider a large wireless mesh access network with 20 APs. The enumeration approach is no longer feasible in this scenario due to the enormous strategy space. The 20 APs are randomly scattered in a d-by-d square, where the *side length* d is a tunable parameter in simulations. We investigate both cooperative and non-cooperative cases represented by *NETMA* and *NTMG* curves, where the maximum number of iterations is set to $\omega = 1000$. Figure 4-7 pictorially depicts the performance inefficiency of NTMG caused by the non-cooperative APs which transmit at the maximum power. The average throughput per AP is calculated by averaging the results of 50 simulations, for each value of the side length d. In Figure 4-7, it is worth noting that as the side length d gets bigger, the performance gap between NETMA and NTMG reduces. The reason is that when the area is large, the impact of mutual interference is less severe and so is the performance deterioration. However, when the network is crowded, i.e., d is small, the selfish behaviors are remarkably devastating.

To alleviate the throughput degradation by the non-cooperative APs, we implement the linear pricing scheme introduced in Section 4.4. The throughput improvement is illustrated as *NTMGP* in Figure 4-7. It is noticeable that by utilizing the proposed pricing scheme, the efficiency of Nash equilibrium is dramatically enhanced, especially for crowded networks. Therefore, the selfish incentives of the non-cooperative APs have been effectively suppressed.

4.6.2 ACM-Capable Devices

In this subsection, we investigate the performance of our model with ACM-capable devices. Since the major difference lies in the improved pricing scheme tailored for this

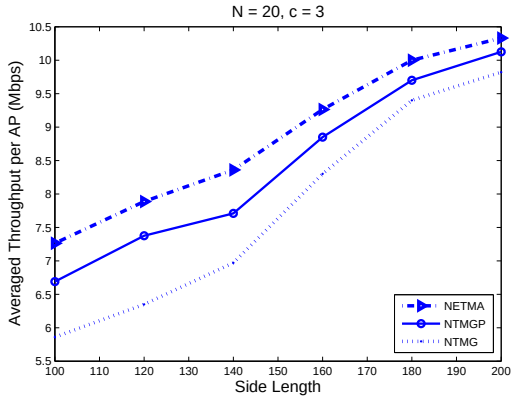

Figure 4-7. Performance evaluation of the wireless mesh access network with N = 20 and c = 3

specific scenario, we will only provide the performance evaluation of the tailored pricing scheme, i.e., NTMGP, in order to avoid duplicate results. We consider a populated network where 30 APs are randomly scattered in an $100m$-by-$100m$ square, i.e., $N = 30$. All other simulation parameters are the same as in the previous subsection except that the power is a continuous variable in this scenario. We first investigate the performance in terms of overall achievable rate of the network when no pricing scheme is applied, as a performance benchmark. Afterwards, the tailored pricing scheme is implemented to improve the equilibrium efficiency, a.k.a., the overall performance at the equilibrium. As shown in Figure 4-8, the overall achievable rate of the network is dramatically improved by the pricing scheme. The PDU adapts the announced price for each AP according to the optimum power, which is calculated by the previous announced price, in an iterative fashion. The aggregated achievable rate converges as the price setting iteration goes, as depicted by Figure 4-8.

Figure 4-9 shows the trajectories of the power utilization prices for each AP. The counterpart of actual utilized power is illustrated in Figure 4-10, where the curves start at p_{max} and evolve with the announced price in Figure 4-9.

As observed in Figure 4-8, to achieve a better performance, the price setting process needs to be executed iteratively, comparing with the “one shot” heuristic

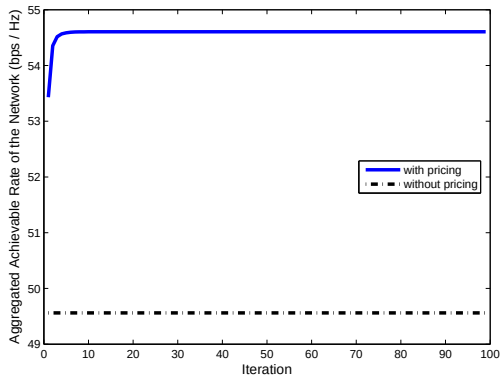

Figure 4-8. Performance evaluation of the wireless mesh access network with/without the pricing scheme

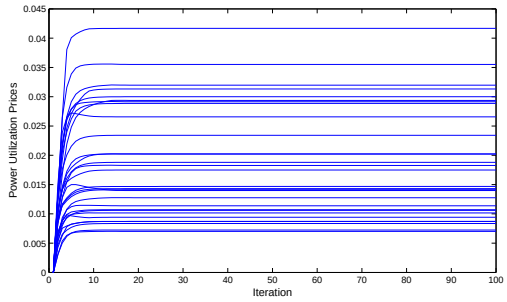

Figure 4-9. The trajectories of power utilization prices of each ACM-capable AP

pricing scheme proposed for legacy devices. Therefore, the further improvement of the equilibrium efficiency is achieved as a tradeoff of communication overheads. However, it is worth noting that even at the first iteration, where the prices are determined by p_{max}, the induced equilibrium yields remarkable superior performance than the case where no pricing scheme is applied.

4.7 Conclusions

In this chapter, we investigate the throughput maximization problem in wireless mesh networks. The problem is coupled due to the mutual interference and hence challenging. We first consider a cooperative case where all APs collaborate with each other in order to maximize the overall throughput of the network. A negotiation-based throughput maximization algorithm, a.k.a., NETMA, is introduced. We prove that

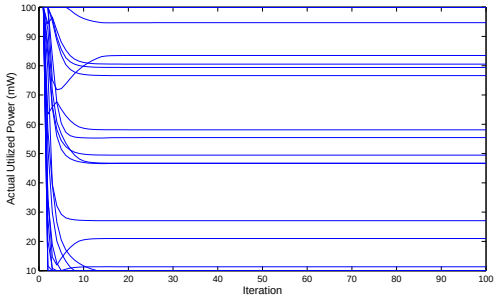

Figure 4-10. The trajectories of actual power utilized by each ACM-capable AP

NETMA converges to the optimum solution with arbitrarily high probability. For the non-cooperative scenarios, we show the existence and the inefficiency of Nash equilibria due to the selfish behaviors. To bridge the performance gap, we propose a pricing scheme which tremendously improves the performance in terms of overall throughput. The analytical results are verified by simulations. In addition, we extend our model and analytical results to the scenarios where more advanced APs are utilized, i.e., the devices with the adaptive coding and modulation capability. In this scenario, we propose a tailored pricing scheme which remarkably improves the overall performance in an iterative fashion.

CHAPTER 5
CROSS LAYER INTERACTIONS IN WIRELESS SENSOR NETWORKS

5.1 Introduction

Wireless sensor networks have attracted significant attention in both industrial and academic communities in the past few years, especially with the advances in low-power circuit design and small size energy supplies which significantly reduce the cost of deploying large scale wireless sensor networks. The sensor networks can sense and measure the physical environment, e.g., temperature, speed, sound, radiation and the movement of the object etc. In addition, wireless sensor networks have become an important solution for military applications such as information gathering and intrusion detections. Other implementations of the wireless sensor networks include the healthcare body sensor networks, vehicular-to-roadside communication networks, multimedia sensor networks and underwater communication networks. For more discussions on the wireless sensor networks, refer to the survey papers such as [84] and [85].

Since the sensor nodes in the network are usually placed in hostile environments, wireless transmissions among sensor nodes are strongly preferred. In addition, due to the restrained size of wireless sensor nodes, the computational capability of a single node is limited. Therefore, the measured information is usually transmitted to a remote data processing center (DPC) for further data analysis. Furthermore, due to the unreliable wireless links, multiple data sinks may exist in the network which collect the measured data and transmit the packets to the DPC node securely and reliably, possibly through the Internet.

Before the wide deployment of wireless sensor networks, a systematic understanding on the performance of the multi-hop wireless sensor networks is desired. However, finding a suitable and accurate analytical model for wireless sensor networks is particularly challenging. First, the time varying channel conditions among wireless links

significantly complicate the analysis for the network performance in terms of throughput and experienced delay, even in an average sense [1, 86, 87]. Secondly, due to the unpredictability of the behavior of the monitored object, the exogenous traffic arrival to the network, i.e., the number of newly generated packets, is a stochastic process. Therefore, to ensure the stability of the network, i.e., to keep the queues in the network constantly finite, the analytical model of wireless sensor networks should comprise a rate admission control mechanism which can dynamically adjust the number of admitted packets into the network. Thirdly, due to the hostile wireless communication links, a dynamic routing scheme should be included in the analytical model. Moreover, the model should capture the complex issue of wireless link scheduling which is significantly challenging due to the mutual interference of wireless transmissions. Lastly, in order to fully explore the network resource and to mitigate the network congestion, an appropriate analytical network model should be able to dynamically deliver packets through multiple data sinks and thus an automatic load balancing solution can be achieved.

In the existing literature, most of the proposed models for wireless sensor networks rely on the fluid model [6], where a flow is characterized by a source node and a specific destination node, e.g., [3, 4, 6, 7]. However, this model is not applicable to the cases where the generated packets can be delivered to *any* of the sink nodes, i.e., the destination node is one of the sinks and is selected dynamically. Moreover, this fluid model neglects the actual queue interactions within the wireless sensor network. In this work, to study the cross layer interactions of the multi-hop wireless sensor networks, we propose a *constrained queueing model* where a packet needs to wait for service in a data queue. More specifically, we investigate the joint rate admission control, dynamic routing, adaptive link scheduling and automatic load balancing solution to the wireless sensor network through a set of interconnected queues. Due to the wireless interference and the underlying scheduling constraints, at a particular time slot, only a subset

of queues can be scheduled for transmissions simultaneously. To demonstrate the effectiveness of the proposed constrained queueing model, we investigate the stochastic network utility maximization (SNUM) problem in multi-hop wireless sensor networks. Based on the proposed queueing model, we develop an adaptive network resource allocation (ANRA) scheme which is a cross layer solution to the SNUM problem and yields a $(1-\epsilon)$ near-optimal solution to the global optimum network utility where $\epsilon > 0$ can be arbitrarily small. The proposed ANRA scheme consists of multiple layer components such as joint rate admission control, traffic splitting, dynamic routing as well as adaptive link scheduling. In addition, the ANRA scheme is essentially an online algorithm which only requires the instantaneous information of the current time slot and hence significantly reduces the computational complexity.

The rest of the chapter is organized as follows. Section 5.2 briefly summarizes the related work in the literature. The constrained queueing model for the cross layer interactions of wireless sensor networks is proposed in Section 5.3. The stochastic network utility maximization problem of the wireless sensor network is investigated in Section 5.4, where a cross layer solution, a.k.a., the ANRA scheme is developed. The performance analysis of the ANRA scheme is provided in Section 5.5. An example which demonstrates the effectiveness of the ANRA scheme is given in Section 5.6 and Section 5.7 concludes this chapter.

5.2 Related Work

To capture the cross layer interactions of multi-hop wireless sensor networks, several analytical models have been proposed in the literature. For example, in [3–7, 88], the multi-hop network resource allocation problem has been studied through a fluid model. Each flow, or session, is characterized by a source and a destination node where single path routing or multi-path routing schemes are implemented. Most of the work rely on the dual optimization framework which decomposes the complex cross layer interactions into separate sub-layer problems by introducing dual variables. For example,

the flow injection rate, controlled by the source node of the flow, is calculated by solving an optimization problem with the knowledge of the dual variables, a.k.a., shadow prices [6, 7], of all the links that are utilized. However, there are several drawbacks for the fluid based model. First, to calculate the optimum flow injection rate, the information along all paths should be collected in order to implement the rate admission control mechanism. In a dynamic environment such as wireless sensor networks, this process of information collection may take a significant amount of time which inevitably prolongs the network delay. Secondly, the optimization based solutions usually pursue fixed operating points which are hardly optimal in dynamic wireless settings with stochastic traffic arrivals and time varying channel conditions. Thirdly, the fluid model usually assumes that the changes of the flow injection rates are "perceived" by all the nodes along its paths instantaneously. The actual queue dynamics and interactions are neglected.

In contrast, following the seminal paper of [12], many solutions have been focused on the queueing model for studying the complex interactions of communication networks. Neely et.al. extend the results of [12] into wireless networks with time varying channel conditions. For a more complete survey of this area, refer to [17]. The key component of the queue based solutions in these papers is the MaxWeight scheduling algorithm [12, 14]. Intuitively, at a time slot, the network picks the set of queues which (1) can be active simultaneously and (2) have the maximum overall weight. It is well-known that the MaxWeight algorithm is throughput-optimal in the sense that any arrival rate vector that can be supported by the network can be stabilized under the MaxWeight scheduling algorithm. In addition, the MaxWeight algorithm is an online policy which requires only the information about current queue sizes and channel conditions. However, one notorious drawback of the MaxWeight algorithm is the delay performance. The reason is that in order to achieve the throughput-optimality, the MaxWeight algorithm explores a dynamic routing solution where long paths are utilized even under a light traffic load. This phenomenon is substantiated via simulations

by [89]. In [89], the authors propose a variant of the MaxWeight algorithm where the average number of hops of transmissions is minimized. Therefore, when the traffic is light, the proposed solution provides a much lower delay than the traditional MaxWeight algorithm. However, as a tradeoff, the induced network capacity region in [89] is noticeably smaller than that of the original MaxWeight algorithm. Consequently, it is difficult to provide a minimum rate guarantee on all the sessions in the network. Our work is inspired by [89]. With respect to [89], however, our work innovates in the following ways. First, different from [89], we focus on a heavy-loaded wireless sensor network. Therefore, our solution incorporates a rate admission control mechanism which is not considered in [89]. Secondly, rather than minimizing the overall number of hops, we maximize the overall network utility which can also ensure the fairness among competitive traffic sessions. Thirdly, we specifically provide a minimum average rate guarantee for every session to ensure the QoS requirement. Fourthly, instead of a single destination scenario as considered in [89], we extend the model to cases where multiple data sink nodes are available. Each source node can deliver the packets to any of the sinks. Moreover, the dynamic routing and the issue of automatic load balancing is realized by the network on the fly. Finally, while [89] treats different sessions equally when minimizing the overall number of hops, our model prioritizes all the sessions with different QoS requirements. Therefore, a more flexible solution with service differentiations can be achieved. We will present the constrained queueing model in the next section.

5.3 A Constrained Queueing Model for Wireless Sensor Networks

5.3.1 Network Model

We consider a multi-hop wireless sensor network represented by a directed graph $\mathcal{G} = \{N, L\}$ where N and L denote the set of vertices and the set of links, respectively. We will use the notation of $|A|$ to represent the cardinality of set A, e.g., the number of nodes in the network is $|N|$ and $|L|$ is the number of links. The time is slotted as

$t = 0, 1, \cdots$ and at a particular time slot t, the instantaneous channel data rate of link $(m, n) \in L$ is denoted by $\mu_{m,n}(t)$. In other words, link (m, n) can transmit a number of $\mu_{m,n}(t)$ packets during time slot t. Note that the value of $\mu_{m,n}(t)$ is a random variable. Denote $\boldsymbol{\mu}(t)$ as the *network link rate vector* at time slot t. In this work, we assume that $\boldsymbol{\mu}(t)$ remains constant within one time slot but is subject to changes at time slot boundaries. The value of $\boldsymbol{\mu}(t)$ is assumed to be evolving following an irreducible and aperiodic Markovian chain with arbitrarily large yet finite number of states. However, the steady state distributions are unknown to the network.

At time slot t, the network selects a feasible *link schedule*, denoted by $I(t) = \{I_1(t), I_2(t), \cdots, I_{|L|}(t)\}$ where $I_l(t) = 1$ if link l is selected to be active and $I_l(t) = 0$ otherwise. The set of all feasible link schedules is denoted by $\Omega(t)$ which is determined by the underlying scheduling constraints such as interference models and duplex constraints. Therefore, selecting an interference-free link schedule in the network graph $\mathcal{G}$ is equivalent to the process of attaining an independent set in the associated conflict graph $\tilde{\mathcal{G}}$, where the vertices are the links in $\mathcal{G}$ and a link exists in $\tilde{\mathcal{G}}$ if the two original links in $\mathcal{G}$ cannot transmit simultaneously.

5.3.2 Traffic Model

There are a number of $|S|$ *source nodes* in the wireless sensor network which consistently monitor the surroundings and inject exogenous traffic to the network. The generated packets need to be delivered to the remote data processing center (DPC) in a multi-hop fashion. To simplify analysis, we assume that each source node is associated uniquely with a *session*. The set of source nodes is denoted by $S = \{n_1^0, n_2^0, \cdots, n_{|S|}^0\}$ where $n_s^0, s = 1, \cdots, |S|$ is the source node of session s. It is worth noting that the following analysis can be extended straightforwardly to the scenarios where each source node may generate multiple sessions.

There are $|D|$ number of *sinks* in the network which are connected to the remote data processing center via the Internet. In other words, the sink nodes can be

viewed as the gateways of the wireless sensor network. Denote the set of sinks as $D = \{d_1, d_2, \cdots, d_{|D|}\}$. In this work, we consider a general scenario where the data packets from a source node can be delivered to the DPC via *any* of the sink node in D. Therefore, different from the existing literature such as [3, 88, 89], the source nodes do not specify the particular destination node for the generated packets. The selection of the destination node is achieved by the network via dynamic routing schemes. The network topology considered in this work is illustrated in Figure 5-1.

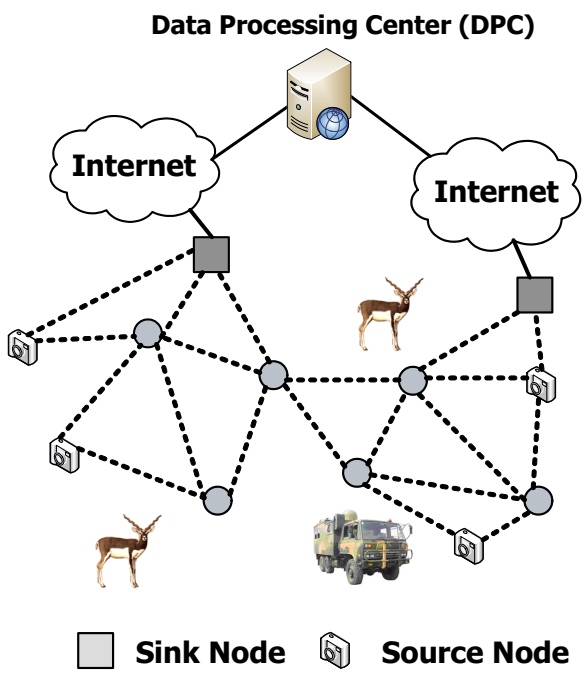

Figure 5-1. Topology of wireless sensor networks

For a particular node in the network, say node n, we denote ϕ_n^d as the number of minimum hops from node n to the d-th data sink in set D. Define

$$\widetilde{\phi_n} = \min_d(\phi_n^d), d = 1, \cdots, |D| \tag{5–1}$$

as the minimum value of ϕ_n^d for node n, i.e., the minimum number of hops from node n to *a* sink node in set D. We assume that node n is aware of the value of $\widetilde{\phi_n}$ as well as those values of the neighboring nodes, which are attainable via precalculations by traditional routing mechanisms such as Dijkstra's algorithm.

At time slot t, the exogenous arrival of session s, i.e., the number of new packets[1] generated by the source node of session s, is denoted by $A_s(t)$. We assume that there is an upper bound for the number of new packets within one time slot, i.e., $A_s(t) \leq A_{\max}, \forall s, t$. For ease of exposition, we assume that $A_s(t)$ is i.i.d. over time slots with an average rate of λ_s. However, the data rates from multiple source nodes can be arbitrarily correlated. For example, if the wireless sensor network is deployed for monitoring purpose, it is very likely that a movement of the object will trigger several concurrent updates of the nearby sensors.

Denote the vector $\boldsymbol{\lambda} = \{\lambda_1, \cdots, \lambda_{|S|}\}$ as the *network arrival rate vector*. The network capacity region Λ is thus defined as all the *feasible*[2] network arrival vectors that can be supported by the network via certain policies, including those with the knowledge of futuristic traffic arrivals and channel rate conditions. In this work, we consider a heavy-loaded traffic scenario where the network arrival vector $\boldsymbol{\lambda}$ is outside of the network capacity region. Therefore, in order to achieve the network stability, a rate admission control mechanism is implemented at the source nodes. More specifically, at time slot t, we only admit a number of $X_s(t)$ packets into the network from the source node of session s, i.e., n_s^0. Apparently, we have

$$X_s(t) \leq A_s(t), \forall s, t. \tag{5–2}$$

In addition, we assume that each session has a continuous, concave and differentiable utility function, denoted by $U_s(X_s(t))$, which reflects the degree of satisfaction by

[1] We assume that the packets have a fixed length. For scenarios with variable packet lengths, the unit of data transmissions can be changed to bits per slot and the following analysis still holds.

[2] Note that additional constraints may be imposed. For example, the constraints on the minimum average rate and the maximum average power expenditure can be enforced. For more discussions, please refer to [17].

transmitting $X_s(t)$ number of packets. It is worth noting that by selecting proper utility functions, the fairness among competitive sessions can be achieved. For example, if $U_s(X_s(t)) = \log(X_s(t))$, a *proportional fairness* among multiple sessions can be enforced [4, 10, 11].

5.3.3 Queue Management

For each node n in the network, there are $|N| - \widetilde{\phi_n}$ number of queues that are maintained and updated. The queues are denoted by $Q_{n,h}$, where $h = \widetilde{\phi_n}, \cdots, |N| - 1$. Note that $|N| - 1$ is the maximum number of hops for a loop-free routing path in the network. The packets in the queue of $Q_{n,h}$ are guaranteed to reach one of the sink nodes in set D within h hops, as will be shown in Section 5.4. It is interesting to observe that for a newly generated packet by session s, the source node, i.e., n_s^0, can place it in any of the queues of $Q_{n_s^0,h}$, where $h = \widetilde{\phi_{n_s^0}}, \cdots, |N| - 1$, for further transmission. That is to say, consecutive packets from the source node n_s^0 may traverse through different number of hops before reaching a destination sink node in set D. Therefore, when a new packet is generated, the source node needs to make a decision on which queue the packet should be placed, namely, traffic splitting decision. In addition, the decision should be made promptly on an online basis with low computational complexity.

With a slight abuse of notation, we use $Q_{n,h}$ to denote the queue itself and $Q_{n,h}(t)$ to represent the number of queue backlogs[3] in time slot t. For a single queue, say $Q_{n,h}$, it is stable if [13, 14]

$$\lim_{B\to\infty} g(B) \to 0 \tag{5–3}$$

where

$$g(B) = \limsup_{T\to\infty} \frac{1}{T} \sum_{t=0}^{T-1} \Pr(Q_{n,h}(t) > B).$$

The network is stable if all the individual queues in the network are stable.

[3] In the unit of packets.

For a link $(n, j) \in L$, we require that the packets from $Q_{n,h}$ can be only transmitted to $Q_{j,h-1}$, if exists. Therefore, the queue updating dynamic for $Q_{n,h}$ is given by

$$Q_{n,h}(t+1) \leq \left[Q_{n,h}(t) - \sum_{(n,j)\in L} u_{n,j}^{n,h}(t) \right]^{+} + \sum_{(m,n)\in L} u_{m,n}^{m,h+1}(t) + \sum_{s} X_s^h(t)\delta_{n=n_s^0} \tag{5–4}$$

where $[A]^+$ denotes $\max(A, 0)$ and $u_{n,j}^{n,h}(t)$ represents the allocated data rate for the transmissions of $Q_{n,h} \to Q_{j,h-1}$ on link (n, j), at time slot t, and

$$\sum_{h=\widetilde{\phi_n}}^{N-1} u_{n,j}^{n,h}(t) = u_{n,j}(t)$$

where $u_{n,j}(t) = \mu_{n,j}(t)$ if $I_{n,j}(t) = 1$, i.e., link (n, j) is scheduled to be active during time slot t, and $u_{n,j}(t) = 0$ otherwise. The notation of $X_s^h(t)$ denotes the number of packets that are admitted to the network for session s and are stored in queue $Q_{n,h}$ for future transmissions. The indicator function $\delta_A = 1$ if event A is true and $\delta_A = 0$ otherwise. Note that the inequality in (5–4) incorporates the scenarios where the transmitter of a particular link has less packets in the queue than the allocated data rate. We assume that during one time slot, the numbers of packets that a single queue can transmit and receive are upper bounded. Mathematically speaking, we have

$$\sum_{(m,n)\in L} u_{m,n}^{m,h+1}(t) \leq u_{in}, \forall n, h, t, \tag{5–5}$$

and

$$\sum_{(n,j)\in L} u_{n,j}^{n,h}(t) \leq u_{out}, \forall n, h, t. \tag{5–6}$$

5.3.4 Session-Specific Requirements

In this work, we consider a scenario where each session has a specific rate requirement α_s. Therefore, to ensure the minimum average rate, we need to find a policy

that

$$\lim_{T\to\infty} \frac{1}{T} \sum_{t=0}^{T-1} X_s(t) \geq \alpha_s, \forall s. \tag{5–7}$$

In addition, we assume that each session in the network has an average hop requirement β_s. More specifically, define

$$M_s(t) = \sum_{h=\widetilde{\phi_{n_s^0}}}^{|N|-1} h X_s^h(t) \tag{5–8}$$

where

$$\sum_{h=\widetilde{\phi_{n_s^0}}}^{|N|-1} X_s^h(t) = X_s(t), \forall s, t.$$

We require that for each session s,

$$\lim_{T\to\infty} \frac{1}{T} \sum_{t=0}^{T-1} M_s(t) \leq \beta_s, \forall s. \tag{5–9}$$

Note that the average hop for a particular session s is related to the average delay experienced and the average energy consumed for the packet transmissions of session s. Therefore, by assigning different values of α_s and β_s, a prioritized solution among multiple competitive sessions can be achieved for the network resource allocation problem.

5.4 Stochastic Network Utility Maximization in Wireless Sensor Networks

In the previous section, we propose a constrained queueing model to investigate the performance of multi-hop wireless sensor networks. The model consists of several important issues from different layers, including the rate admission control problem, the dynamic routing problem as well as the challenge of adaptive link scheduling. To better understand the proposed constrained queueing model, in this section, we will examine the stochastic network utility maximization problem (SNUM) in multi-hop wireless sensor networks. As a cross layer solution, an Adaptive Network Resource Allocation (ANRA) scheme is proposed to solve the SNUM problem jointly. The proposed ANRA scheme is an online algorithm in nature which provably achieves an asymptotically optimal average

overall network utility. In other words, the average network utility induced by the ANRA scheme is $(1-\epsilon)$ of the optimum solution where $\epsilon > 0$ is a positive number that can be arbitrarily small, with a tradeoff with the average delay experienced in the network.

5.4.1 Problem Formulation

Recall that every session s possesses a utility function $U_s(X_s(t))$ which is continuous, concave and differentiable. Without loss of generality, in the rest of this chapter, we will assume that $U_s(X_s(t)) = \log(X_s(t))$. Therefore, in light of the stochastic traffic arrival as well as the time varying channel conditions, our objective is to develop a policy which maximizes

Stochastic Network Utility Maximization (SNUM) Problem

$$\sum_s E(U_s(X_s(t))) \tag{5–10}$$

s.t.

- The network remains stable.
- The average rate requirements of all $|S|$ sessions, denoted by $\boldsymbol{\alpha} = \{\alpha_1, \cdots, \alpha_{|S|}\}$, are satisfied.
- The average hop requirements of all $|S|$ sessions, denoted by $\boldsymbol{\beta} = \{\beta_1, \cdots, \beta_{|S|}\}$, are satisfied.

Note that if the underlying statistical characteristics of the stochastic traffic arrivals and the time varying channel conditions are known, the SNUM problem is inherently a standard optimization problem and thus is easy to solve. However, due to the unawareness of the steady state distributions, the SNUM problem is remarkably challenging. In addition, in wireless sensor networks, dynamic algorithmic solutions with low computational complexity are strongly desired. In the following, we propose an ANRA scheme to solve the SNUM problem asymptotically. The ANRA scheme is a cross layer solution which consists of joint rate admission control, traffic splitting,

dynamic routing as well as adaptive link scheduling components. Moreover, the ANRA algorithm can achieve an automatic load balancing solution by utilizing different sink nodes corresponding to the variations of the network conditions. The ANRA algorithm is an online algorithm in nature which requires only the state information of the current time slot. We show that the ANRA algorithm achieves a $(1-\epsilon)$ optimal solution where ϵ can be arbitrarily small. Therefore, the proposed ANRA algorithm is of particular interest for dynamic wireless sensor networks with time varying environments.

5.4.2 The ANRA Cross Layer Algorithm

Before presenting the proposed ANRA scheme, we introduce the concept of virtual queues [16, 17, 34] to facilitate our analysis. Specifically, for each session s, we maintain a virtual queue Y_s, which is initially empty, and the queue updating dynamic is defined as

$$Y_s(t+1) = [Y_s(t) - X_s(t)]^+ + \alpha_s, \forall s, t. \tag{5–11}$$

Similarly, we define another virtual queue for every session s, denoted by Z_s, and the queue dynamic is given by

$$Z_s(t+1) = [Z_s(t) - \beta_s]^+ + M_s(t), \forall s, t, \tag{5–12}$$

where $M_s(t)$ is defined in (5–8). Note that the virtual queues are software based counters which are easy to maintain. For example, the source node of each session can calculate the values of virtual queues $Y_s(t)$ and $Z_s(t)$ and update the values accordingly following (5–11) and (5–12). In addition, we introduce a positive parameter J which is tunable as a system parameter. The impact of J on the algorithm performance will be discussed shortly. The proposed ANRA cross layer algorithm is given as follows.

ADAPTIVE NETWORK RESOURCE ALLOCATION (ANRA) SCHEME:

- **Joint Rate Admission Control and Traffic Splitting (at time t):**

For each source node, say n_s^0, there are a number of queues, i.e., $Q_{n_s^0,h}$, $h = \widetilde{\phi_{n_s^0}}, \cdots, |N|-1$. Find the value of h which minimizes

$$Z_s(t)h + Q_{n_s^0,h}(t) \tag{5–13}$$

where ties are broken arbitrarily. Denote the optimum value of h as h^*. The source node n_s^0 admits a number of new packets as

$$X_s(t) = \min\left(\widetilde{X_s(t)}, A_s(t)\right) \tag{5–14}$$

where

$$\widetilde{X_s(t)} = \left[\frac{J}{2\left(Z_s(t)h^* + Q_{n_s^0,h^*}(t)\right) - 2Y_s(t)}\right]^+. \tag{5–15}$$

For traffic splitting, the source node n_s^0 will deposit all $X_s(t)$ packets in $Q_{n_s^0,h^*}$.

- **Joint Dynamic Routing and Link Scheduling (at time t):**
  For each link $(m,n) \in L$, define a link weight denoted by $W_{m,n}(t)$, which is calculated as

$$W_{m,n}(t) = \left[\max_{h=\widetilde{\phi_m},\cdots,|N|-1}\left(Q_{m,h}(t) - Q_{n,h-1}(t)\right)\right]^+. \tag{5–16}$$

  Note that if $Q_{n,h-1}$ does not exist, the transmissions from queue $Q_{m,h}$ to $Q_{n,h-1}$ are prohibited. At time slot t, the network selects an interference-free link schedule $I(t)$ which solves

$$\max_{I(t)\in\Omega(t)} \mu_{m,n}(t)W_{m,n}(t). \tag{5–17}$$

  If link (m,n) is active, i.e., $I_{m,n}(t) = 1$, the queue of $Q_{m,\bar{h}}$ is selected for transmissions where

$$\bar{h} = \text{argmax}_{h=\widetilde{\phi_m},\cdots,|N|-1}\left(Q_{m,h}(t) - Q_{n,h-1}(t)\right). \tag{5–18}$$

END

Note that (5–17) is similar to the original MaxWeight algorithm, introduced in [12] and generalized in [13, 14, 34]. The dynamic routing and link scheduling are addressed jointly by solving (5–17), which requires centralized computation. However, following [12], many work have been focused on the distributed solutions of (5–17). Although the distributed computation issue is not the focus of this work, we emphasize that our proposed ANRA scheme can be approximated well by existing distributed solutions such as [36–38, 41, 42, 45, 46, 48].

For the packets placed at queue $Q_{n_s^0,h}$, at most h hops of transmissions are needed in order to reach one of the sink nodes in set D. This can be verified straightforwardly due to the requirement that a transmission from $Q_{m,h}$ to $Q_{n,h-1}$ can occur if and only if $h-1 \geq \widetilde{\phi_n}$. Moreover, the joint rate admission control and the optimum traffic splitting components of ANRA can be implemented by the source node in a distributed fashion. Note that in order to calculate the instantaneous admitted rate, the source node of session s needs only to know the local queue backlog information. Moreover, the decision of traffic splitting requires only local queue information as well. Therefore, at every time slot, the joint rate admission control and traffic splitting decision can be made on an online basis in accordance to the time varying conditions of local queues. Furthermore, we will show that this simple adaptive strategy does not incur any loss of optimality. The achieved network utility induced by the ANRA scheme can be pushed arbitrarily close to the optimum solution. Next, we will characterize the global optimum utility in the network and provide the main performance results of the proposed ANRA scheme.

5.4.3 Performance of the ANRA Scheme

In this section, we first characterize the global optimum solution of the SNUM problem in (5–10). Define U^* as the global maximum network utility that any scheme can achieve, i.e., the optimum solution of (5–10). In order to achieve U^*, it is naturally to consider more complicated policies such as those with the knowledge of futuristic arrivals and channel conditions. However, in the following theorem, we show that, somewhat surprisingly, the global optimum solution of the SNUM problem can be achieved by certain stationary policies, i.e., the responsive action is chosen regardless of the current queue sizes in the network and the time slot that the decision is made. Recall that we have assumed that for each session, $A_s(t)$ is i.i.d. over time slots. Denote $\mathbf{A}(t)$ as the vector of instantaneous arrival rates of all sessions, at time slot t. Let $\mathcal{A}$ be the set of all possible value of $\mathbf{A}(t)$. Note that for every element in $\mathcal{A}$, i.e.,

$\mathcal{A}_a, a = 1, \cdots, |\mathcal{A}|$, we have $0 \preceq \mathcal{A}_a \preceq A_{\max}$ where $\preceq$ denotes the element-wise comparison. We use π_a to represent the steady state distribution of $\mathcal{A}_a$.

Theorem 5.1. *If the constraints in the SNUM problem are satisfied, the maximum network utility, denoted by U^*, can be achieved by a class of stationary randomized policies. Mathematically, the value of U^* is the solution of the following optimization problem, with the auxiliary variables p_a^k and R_a^k, as*

$$\max \sum_a \pi_a \sum_s U_s(\sum_{k=1}^{|S|+1} p_a^k R_a^k) \tag{5–19}$$

s.t.

- *The constraints in (5–10) are satisfied.*
- $0 \preceq R_a^k \preceq \mathcal{A}_a$.
- $p_a^k \geq 0, \forall a, k$.
- $\sum_{k=1}^{|S|+1} p_a^k = 1, \forall a$.

Proof. We prove Theorem 5.1 by showing that for arbitrary policy which satisfies the constraints in the SNUM problem, the overall network utility is at most U^*, which is the optimum utility attained by a class of stationary randomized policies. In other words, we need to show that

$$U^P = \limsup_{T\to\infty} \frac{1}{T} \sum_{t=0}^{T-1} \left(\sum_s U_s(X_s(t)) \right) \leq U^* \tag{5–20}$$

where U^P is the average network utility under a policy P.

For each state in $\mathcal{A}$, say $\mathcal{A}_a$, define R_a as the set of nonnegative rate vectors that are element-wise smaller than $\mathcal{A}_a$. Define $\mathcal{CR}_a$ as the convex hull of set R_a. Therefore, any point in $\mathcal{CR}_a$ can be considered as a feasible network admitted rate vector given that the current arrival rate vector is $\mathcal{A}_a$. Note that every point in $\mathcal{CR}_a$ is a vector with a dimension of $|S|$-by-1. Therefore, it can be represented by a convex combination of at most $|S| + 1$ points, denoted by $R_a^k, k = 1, \cdots, |S| + 1$, according to Caratheodory's theorem. In light of this, we first consider a time interval from 0 to $T - 1$. Denote $N_a(T)$

as the set of time slots that $\mathbf{A}(t) = \mathcal{A}_a$. Therefore, we can rewrite (5–20) as

$$U^P = \limsup_{T\to\infty} \sum_a \frac{|N_a(T)|}{T} \sum_s U_s \left(\sum_{k=1}^{|S|+1} p_a^k R_a^k \right).$$

Due to the stationary assumption, we have

$$U^P = \sum_a \pi_a \sum_s \limsup_{T\to\infty} U_s \left(\sum_{k=1}^{|S|+1} p_a^k R_a^k \right).$$

Note that we also assume that the utility function is continuous and bounded. Therefore, the compactness of the utility functions is assured. Next, we focus on a subsequence of time durations, denoted by $T_i, i = 1, \cdots, \infty$. Denote

$$U_{net}^P(T_i) = \sum_a \pi_a \sum_s U_s \left(\sum_{k=1}^{|S|+1} p_a^k(T_i) R_a^k \right).$$

It is straightforward to verify that

$$U^P = \limsup_{i\to\infty} U_{net}^P(T_i).$$

Due to the compactness of the utility functions, following Bolzano-Weierstrass theorem [90], we claim that there exists a subsequence of $T_i, i = 1, \cdots, \infty$, such that

$$\lim_{i\to\infty} U_s \left(\sum_{k=1}^{|S|+1} p_a^k(T_i) R_a^k \right) \to \widetilde{U_s^a}.$$

Denote $\widetilde{p_a^k}$ as the values which generate $\widetilde{U_s^a}$, i.e.,

$$\widetilde{U_s^a} = U_s \left(\sum_{k=1}^{|S|+1} \widetilde{p_a^k} R_a^k \right).$$

We have

$$U^P = \limsup_{i\to\infty} U_{net}(T_i) = \sum_a \pi_a \sum_s U_s \left(\sum_{k=1}^{|S|+1} \widetilde{p_a^k} R_a^k \right).$$

According to the definition of U^* in (5–19), we conclude that $U^P \leq U^*$.

Intuitively, Theorem 5.1 indicates that the global maximum network utility can be achieved by certain randomized stationary policies. However, to calculate U^*, the stationary policy needs to know the steady state distributions which are difficult to obtain in practice. In light of this, we propose an adaptive network resource allocation scheme, namely, ANRA, which is an online solution and does not require such statistical information as a priori. For notation succinctness, denote

$$U^A(t) = \sum_s E\left(U_s(X_s(t))\right)$$

as the expected network utility induced by the ANRA scheme. The performance of the ANRA algorithm, with a parameter J, is given as the following theorem.

Theorem 5.2. *For a given system parameter J, we have*

$$\liminf_{T\to\infty} \frac{1}{T}\sum_{t=0}^{T-1} U^A(t) \geq U^* - \frac{\bar{B}}{J} \tag{5–21}$$

where $\bar{B}$ is a constant and is given by

$$\begin{aligned}\bar{B} &= |N|(|N|-1)\left((u_{out})^2 + (u_{in} + A_{\max})^2\right) \\ &+ \sum_s \left((\alpha_s)^2 + (\beta_s)^2\right) + |S|(A_{\max})^2\left((|N|-1)^4 + 1\right).\end{aligned}$$

In addition, the constraints in the SNUM problem, i.e., (5–10), are satisfied simultaneously.

Proof. The proof of Theorem 5.2 is deferred to Section 5.5.

It is worth noting that if we let $J \to \infty$, the performance induced by the ANRA algorithm can be arbitrarily close to the global optimum solution U^*. However, as a tradeoff, a larger value of J also yields a longer average queue size in the network. According to Little's Law, a larger queue size corresponds to a longer average delay experienced in the network. Therefore, by selecting the value of J properly, a tradeoff

between the network optimality and the average delay in the network can be achieved. We will discuss more about this issue in the next section.

5.5 Performance Analysis

In this section, we provide a proof to Theorem 5.2 in the previous section. Recall that in (5–11) and (5–12), we introduce two virtual queues, i.e., $Y_s(t)$ and $Z_s(t)$ for each session s. Therefore, the average rate and the average hop requirements from all sessions are converted into the stability requirements for the virtual queues. For example, the virtual queue update of $Y_s(t)$ is given by (5–11). If the virtual queue Y_s is stable, the average arrival rate should be less than the average departure rate of the queue, i.e.,

$$\alpha_s \leq \lim_{T\to\infty} \frac{1}{T} \sum_{t=0}^{T-1} X_s(t),$$

which is exactly the minimum average rate requirement imposed by session s. By the same token, the average hop requirement of session s is converted to the stability problem of the virtual queue Z_s. Define $\overline{\boldsymbol{Q}}(t) = (\boldsymbol{Q}(t), \boldsymbol{Y}(t), \boldsymbol{Z}(t))$, namely, all the data queues and the virtual queues in the network. Our objective is to find a policy which stabilizes the network with respect to $\overline{\boldsymbol{Q}}$ while maximizing the overall network utility.

We first take the square of (5–4) and have

$$\begin{aligned}
&\Big(Q_{n,h}(t+1)\Big)^2 \leq \Big(Q_{n,h}(t)\Big)^2 \\
&+ \left(\sum_{(n,j)\in L} u_{n,j}^{n,h}(t)\right)^2 + \left(\sum_{(m,n)\in L} u_{m,n}^{m,h+1}(t) + \sum_s X_s^h(t)\delta_{n=n_s^0}\right)^2 \\
&-2Q_{n,h}(t)\left(\sum_{(n,j)\in L} u_{n,j}^{n,h}(t) - \sum_{(m,n)\in L} u_{m,n}^{m,h+1}(t) - \sum_s X_s^h(t)\delta_{n=n_s^0}\right).
\end{aligned}$$

Since we assume that each node generates at most one session, we have

$$\sum_s X_s^h(t)\delta_{n=n_s^0} \leq A_{\max}, \forall t, n.$$

Note that if we allow that a node can initiate multiple sessions, we have

$$\sum_s X_s^h(t)\delta_{n=n_s^0} \leq |S|A_{\max}, \forall t, n$$

where $|S|$ is the number of sessions in the network.

In light of (5–5) and (5–6), we have

$$\begin{aligned} &\Big(Q_{n,h}(t+1)\Big)^2 - \Big(Q_{n,h}(t)\Big)^2 \leq \Big(u_{out}\Big)^2 + \Big(u_{in} + A_{\max}\Big)^2 \\ - \;& 2Q_{n,h}(t)\left(\sum_{(n,j)\in L} u_{n,j}^{n,h}(t) - \sum_{(m,n)\in L} u_{m,n}^{m,h+1}(t) - \sum_s X_s^h(t)\delta_{n=n_s^0}\right). \end{aligned} \tag{5–22}$$

We next sum (5–22) over all the data queues in the network, i.e., $Q_{n,h}$, and have

$$\begin{aligned} &\sum_{n,h}\Big(Q_{n,h}(t+1)\Big)^2 - \sum_{n,h}\Big(Q_{n,h}(t)\Big)^2 \leq B_1 \\ - \;& 2Q_{n,h}(t)\left(\sum_{(n,j)\in L} u_{n,j}^{n,h}(t) - \sum_{(m,n)\in L} u_{m,n}^{m,h+1}(t) - \sum_s X_s^h(t)\delta_{n=n_s^0}\right) \end{aligned} \tag{5–23}$$

where

$$B_1 = |N|(|N|-1)\Big((u_{out})^2 + (u_{in} + A_{\max})^2\Big).$$

Note that $M_s(t)$, defined in (5–8), satisfies

$$M_s(t) \leq (|N|-1)^2 A_{\max}.$$

Next, we take the square of (5–11) and (5–12) and thus have

$$\Big(Y_s(t+1)\Big)^2 \leq \Big(Y_s(t)\Big)^2 + \Big(X_s(t)\Big)^2 + (\alpha_s)^2 - 2Y_s(t)\Big(X_s(t) - \alpha_s\Big)$$

and

$$\Big(Z_s(t+1)\Big)^2 \leq \Big(Z_s(t)\Big)^2 + \Big(M_s(t)\Big)^2 + (\beta_s)^2 - 2Z_s(t)\Big(\beta_s - M_s(t)\Big).$$

Similarly, we sum over all the sessions and have

$$\sum_s \Big(Y_s(t+1)\Big)^2 - \sum_s \Big(Y_s(t)\Big)^2 \leq B_2 - 2\sum_s Y_s(t)\Big(X_s(t) - \alpha_s\Big)$$

where

$$B_2 = |S|(A_{\max})^2 + \sum_s (\alpha_s)^2.$$

Also, we obtain

$$\sum_s \Big(Z_s(t+1)\Big)^2 - \sum_s \Big(Z_s(t)\Big)^2 \leq B_3 - 2\sum_s Z_s(t)\Big(\beta_s - M_s(t)\Big)$$

where

$$B_3 = \sum_s (\beta_s)^2 + |S|\left(|N|-1\right)^4 (A_{\max})^2.$$

Define the system-wide Lyapunov function as

$$L(\overline{\mathbf{Q}}(t)) = \sum_{n,h} \Big(Q_{n,h}(t)\Big)^2 + \sum_s \Big(Y_s(t)\Big)^2 + \sum_s \Big(Z_s(t)\Big)^2.$$

Next, we define the Lyapunov drift [14] of the system as

$$\Delta = E\left(L(\overline{\mathbf{Q}}(t+1)) - L(\overline{\mathbf{Q}}(t)) \mid \overline{\mathbf{Q}}(t)\right). \tag{5–24}$$

Define

$$\bar{B} = B_1 + B_2 + B_3,$$

we have

$$\begin{aligned}
\Delta \;\leq\; & \bar{B} - 2\sum_{n,h} Q_{n,h}(t) E\left(\sum_{(n,j)\in L} u_{n,j}^{n,h}(t) - \sum_{(m,n)\in L} u_{m,n}^{m,h}(t) - \sum_s X_s^h(t)\delta_{n=n_s^0}\Big|\overline{\mathbf{Q}}(t)\right) \\
- \;& 2E\left(\sum_s Y_s(t)(X_s(t)-\alpha_s)\Big|\overline{\mathbf{Q}}(t)\right) - 2E\left(\sum_s Z_s(t)(\beta_s - M_s(t))\Big|\overline{\mathbf{Q}}(t)\right).
\end{aligned}$$

Next, we subtract both sides by $JE\Big(\sum_s U_s(X_s(t))|\overline{\mathbf{Q}}(t)\Big)$ and have

$$\begin{aligned}
&\Delta - JE\left(\sum_s U_s(X_s(t))\Big|\overline{\mathbf{Q}}(t)\right) \leq \bar{B} \\
- \;& 2\sum_{n,h} Q_{n,h}(t) E\left(\sum_{(n,j)\in L} u_{n,j}^{n,h}(t) - \sum_{(m,n)\in L} u_{m,n}^{m,h+1}(t)\Big|\overline{\mathbf{Q}}(t)\right) \\
+ \;& 2E\left(\sum_s\sum_h Q_{n_s^0,h}(t) X_s^h(t)\Big|\overline{\mathbf{Q}}(t)\right) - 2E\left(\sum_s Y_s(t)X_s(t)\Big|\overline{\mathbf{Q}}(t)\right) + 2\sum_s Y_s(t)\alpha_s \\
+ \;& 2E\left(\sum_s Z_s(t)M_s(t)\Big|\overline{\mathbf{Q}}(t)\right) - 2\sum_s Z_s(t)\beta_s - JE\left(\sum_s U_s(X_s(t))\Big|\overline{\mathbf{Q}}(t)\right). \qquad (5\text{–}25)
\end{aligned}$$

We rewrite the R.H.S. of (5–25) as

$$\begin{aligned}
&\text{R.H.S.} = \bar{B} + 2\sum_s Y_s(t)\alpha_s - 2\sum_s Z_s(t)\beta_s \\
- \;& 2\sum_{n,h} Q_{n,h}(t) E\left(\sum_{(n,j)\in L} u_{n,j}^{n,h}(t) - \sum_{(m,n)\in L} u_{m,n}^{m,h+1}(t)\Big|\overline{\mathbf{Q}}(t)\right) \\
- \;& E\left(\sum_s 2Y_s(t)X_s(t) - \sum_s 2Z_s(t)M_s(t) - \sum_s\sum_h 2Q_{n_s^0,h}(t)X_s^h(t) + J\sum_s U_s(X_s(t))\Big|\overline{\mathbf{Q}}(t)\right).
\end{aligned}$$

We observe that the dynamic routing and scheduling component of the ANRA scheme is actually maximizing

$$\sum_{n,h} Q_{n,h}(t) E\left(\sum_{(n,j)\in L} u_{n,j}^{n,h}(t) - \sum_{(m,n)\in L} u_{m,n}^{m,h+1}(t)\Big|\overline{\mathbf{Q}}(t)\right). \qquad (5\text{–}26)$$

In addition, the joint rate admission control and traffic splitting component of the ANRA scheme is essentially maximizing

$$E\left(\sum_s 2Y_s(t)X_s(t) - \sum_s 2Z_s(t)M_s(t) - \sum_s\sum_h 2Q_{n_s^0,h}(t)X_s^h(t) + J\sum_s U_s(X_s(t))\Big|\overline{\mathbf{Q}}(t)\right) \qquad (5\text{–}27)$$

with the constraints of

$$\sum_h X_s^h(t) = X_s(t), \forall s, t. \qquad (5\text{–}28)$$

To see this, we can decompose (5–27) to show that each session s only maximizes

$$JU_s\left(X_s(t)\right) + 2Y_s(t)X_s(t) - 2Z_s(t)\sum_h hX_s^h(t) - \sum_h 2Q_{n_s^0,h}(t)X_s^h(t). \tag{5–29}$$

Therefore, the proposed ANRA algorithm indeed minimizes the R.H.S. of (5–25) over all policies.

Consider a reduced network capacity region, denoted by Λ_ϵ, parameterized by $\epsilon > 0$, as

$$\{\boldsymbol{\lambda} | \lambda_{n,h} + \epsilon \in \Lambda\} \tag{5–30}$$

where Λ is the original network capacity region and

$$\lambda_{n,h} = \lim_{T\to\infty} \frac{1}{T}\sum_{t=0}^{T-1}\sum_s X_s^h(t)\delta_{n=n_s^0}. \tag{5–31}$$

Define U_ϵ^* as the global optimum network utility achieved in the reduced capacity region. Apparently, we have $\lim_{\epsilon\to 0} U_\epsilon^* \to U^*$. In addition, denote $X_{s,\epsilon}^{h*}(0)$, $X_{s,\epsilon}^{h*}(1)$, $\cdots$, $X_{s,\epsilon}^{h*}(t), \cdots$ as the optimum rate sequence which yields U_ϵ^*. Define $\bar{X}_s^\epsilon$ as the average of the optimum rate sequence of session s, in the reduced capacity region. It is straightforward to verify that $\bar{X}_s^\epsilon + \epsilon$ is in the original network capacity region Λ. Therefore, following a similar analysis as in [13–15, 91], we claim that there exists a randomized policy, denoted by R, which generates

$$E\left(\sum_{(n,j)\in L} u_{n,j}^{n,h}(t) - \sum_{(m,n)\in L} u_{m,n}^{m,h+1}(t)\right) \geq X_{s,\epsilon}^{h*} + \epsilon \tag{5–32}$$

if n is one of the source nodes and

$$E\left(\sum_{(n,j)\in L} u_{n,j}^{n,h}(t) - \sum_{(m,n)\in L} u_{m,n}^{m,h+1}(t)\right) \geq \epsilon \tag{5–33}$$

for other nodes. Furthermore, policy R ensures

$$E\left(\sum_h X_{s,\epsilon}^{h*}(t) \geq \alpha_c + \epsilon\right)$$

and

$$E\left(M^*_{s,\epsilon}(t)+\epsilon \leq \beta_s\right)$$

where $M^*_{s,\epsilon}(t)$ is generated by $X^{h*}_{s,\epsilon}(t)$. Due to the fact that the proposed ANRA scheme minimizes the R.H.S. of (5–25) overall all policies, including R, we have

$$\begin{aligned}
&\Delta - JE\left(\sum_s U_s(X_s(t))\Big|\overline{\mathbf{Q}}(t)\right)\\
&\leq \bar{B} - 2\epsilon\left(\sum_{n,h} Q_{n,h}(t)+\sum_s Y_s(t)+\sum_s Z_s(t)\right) - JE\left(\sum_s U_s(\sum_h X^{h*}_{s,\epsilon}(t)+\epsilon)\Big|\overline{\mathbf{Q}}(t)\right).
\end{aligned}$$

We next take the expectation with respect to $\overline{\mathbf{Q}}(t)$ and obtain

$$\begin{aligned}
&L(\overline{\mathbf{Q}}(t+1)) - L(\overline{\mathbf{Q}}(t)) - JE\left(\sum_s U_s(X_s(t))\right)\\
&\leq \bar{B} - 2\epsilon E\left(\sum_{n,h} Q_{n,h}(t)+\sum_s Y_s(t)+\sum_s Z_s(t)\right)\\
&-JE\left(\sum_s U_s(\sum_h X^{h*}_{s,\epsilon}(t)+\epsilon)\right).
\end{aligned} \tag{5–34}$$

We sum over time slots $0,\cdots,T-1$ and have

$$L(\overline{\mathbf{Q}}(T)) - L(\overline{\mathbf{Q}}(0)) - \sum_{t=0}^{T-1} JE\left(\sum_s U_s(X_s(t))\right) \leq T\bar{B} - \sum_{t=0}^{T-1} JE\left(\sum_s U_s(\sum_h X^{h*}_{s,\epsilon}(t)+\epsilon)\right) \tag{5–35}$$

since

$$E\left(\sum_{n,h} Q_{n,h}(t)+\sum_s Y_s(t)+\sum_s Z_s(t)\right)$$

is always nonnegative. Next, we divide the both sides of (5–35) by T and rearrange terms to have

$$\frac{1}{T}\sum_{t=0}^{T-1} JE\left(\sum_s U_s(X_s(t))\right) \geq \frac{1}{T}\sum_{t=0}^{T-1} JE\left(\sum_s U_s(\sum_h X^{h*}_{s,\epsilon}(t)+\epsilon)\right) - \bar{B} - \frac{L(\overline{\mathbf{Q}}(0))}{T}$$

where the nonnegativity of the Lyapunov function is utilized. Since we assume that the initial queue backlogs in the system are finite and the virtual queues are initially empty,

taking $\epsilon \to 0$ and $\liminf_{T\to\infty}$ yields the performance result of the ANRA algorithm stated in Theorem 5.2.

We next show that the constraints of the SNUM problem are also satisfied. To illustrate this, we show that the queues in the network, including real data queues and virtual queues, are stable. Based on (5–34), we sum over time slots $0, \cdots, T-1$ and have

$$\sum_{t=0}^{T-1} 2\epsilon E\left(\sum_{n,h} Q_{n,h}(t) + \sum_{s} Y_s(t) + \sum_{s} Z_s(t)\right) \leq L(\overline{\mathbf{Q}}(0)) + \sum_{t=0}^{T-1} JE\left(\sum_{s} U_s(X_s(t))\right) + T\bar{B}. \tag{5–36}$$

Due to $X_s(t) \leq A_{\max}$ and the assumptions on the utility function, we claim that $U_s(t)$ is upper bounded and denote the maximum utility within one time slot as $U_{\max}$, i.e.,

$$U_s(t) \leq U_{\max}, \forall s, t. \tag{5–37}$$

Divide the both sides of (5–36) by T and we have

$$\frac{1}{T}\sum_{t=0}^{T-1} 2\epsilon E\left(\sum_{n,h} Q_{n,h}(t) + \sum_{s} Y_s(t) + \sum_{s} Z_s(t)\right) \leq \frac{L(\overline{\mathbf{Q}}(0))}{T} + J|S|U_{\max} + \bar{B}.$$

By taking $\limsup_{T\to\infty}$, we have

$$\limsup_{T\to\infty} \frac{1}{T}\sum_{t=0}^{T-1} E\left(\sum_{n,h} Q_{n,h}(t) + \sum_{s} Y_s(t) + \sum_{s} Z_s(t)\right) \leq \frac{J|S|U_{\max} + \bar{B}}{2\epsilon}. \tag{5–38}$$

Note that the above analysis holds for any feasible value of ϵ. Denote φ as the maximum value of ϵ such that Λ_φ is not empty. Finally, we conclude that

$$\limsup_{T\to\infty} \frac{1}{T}\sum_{t=0}^{T-1} E\left(\sum_{n,h} Q_{n,h}(t) + \sum_{s} Y_s(t) + \sum_{s} Z_s(t)\right) \leq \frac{J|S|U_{\max} + \bar{B}}{2\varphi} < \infty. \tag{5–39}$$

The stability of the network follows immediately from Markov's Inequality and thus completes the proof.

It is worth noting that as shown in (5–39), a large value of J induces a longer average queue size in the network. Therefore, a tradeoff between the algorithm

performance of the ANRA scheme and the average delay experienced in the network can be controlled effectively by tuning the value of J.

5.6 Case Study

In this section, we demonstrate the effectiveness of the ANRA algorithm numerically through a simple network shown in Figure 5-2. We stress that, however, this exemplifying study case reproduces all the challenging problems involved in the complex cross layer interactions in time varying environments, such as stochastic traffic arrivals, random channel conditions and dynamic routing and scheduling etc. As shown in Figure 5-2, the source nodes in the network are node A and B whereas the destination sink nodes are denoted by E and F.

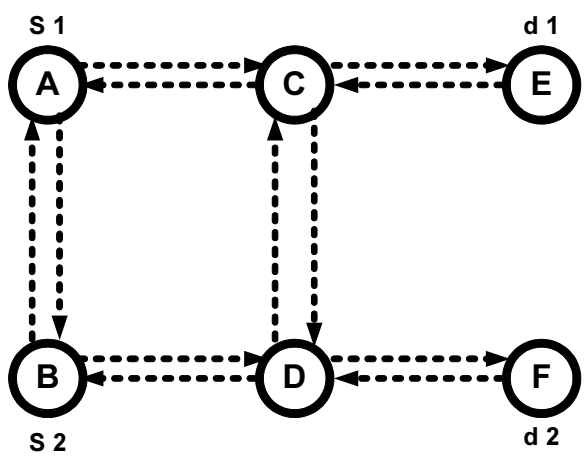

Figure 5-2. Example network topology

There are six nodes and twelve links in the network. Therefore, node A and B each maintains four queues, from hop 2 to hop 5, and node C and D each maintains five queues, from hop 1 to hop 5, in the buffer. At each time slot, a wireless link is assumed to have three equally possible data rates[4] , 2, 8 and 16. The traffic arrivals are i.i.d. with three equally possible states, i.e., 0, 10 and 20. The minimum rate requirements of the

[4] Note that the unit of data transmissions is packet per slot.

two sessions are 5 and 8 and the average hop requirements of the sessions are 30 and 10. Without loss of generality, we assume that at a given time slot, two links with a common node cannot be active simultaneously. For example, if link $A \rightarrow B$ is active, link $B \rightarrow A$, $A \rightarrow C$, $C \rightarrow A$, $B \rightarrow D$ and $D \rightarrow B$ cannot be selected.

Figure 5-3 depicts the average network utility achieved by the ANRA scheme for different values of J where each experiment is executed for 50000 time slots. We can observe from Figure 5-3 that the overall network utility rises as the value of J increases. However, the speed of utility improvement decreases and the achieved network utility converges to the global optimum utility U^* gradually. To demonstrate the tradeoff of different values of J, in Figure 5-4, we show the average queue size in the network for $J = 20$, 50, 200, 500, 1000, 2000, 5000, 10000 and 20000. We can see that, as expected, the average queue size increases as the value of J gets larger. Note that the average queue size is related to the average delay in the network. Therefore, a tradeoff between the network optimality and the average experienced delay can be achieved by tuning the value of J.

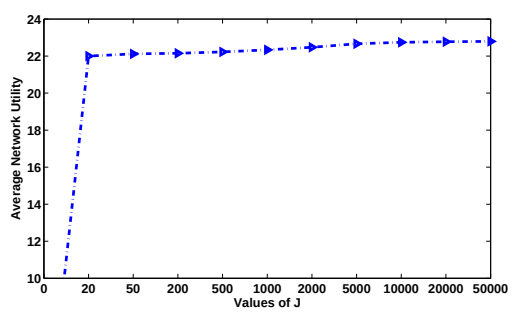

Figure 5-3. Average network utility achieved by ANRA for different values of J

In Figure 5-5, we illustrate the sample trajectories of the admitted rates of two sessions with $J = 5000$, for the first 50 time slots. We can observe that each session admits different amount of packets into the network adaptively following the time varying conditions of the network. In addition, we depict the trajectories of the four virtual queues with the same settings, in Figure 5-6, for the first 100 time slots. By comparing

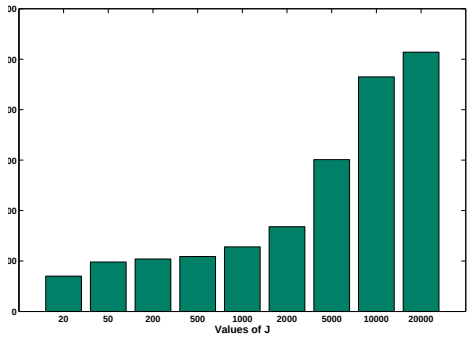

Figure 5-4. Average network queue size by ANRA for different values of J

Figure 5-5 and Figure 5-6 jointly, we can observe that for the minimum rate virtual queue, say Y_1, whenever there is the tendency that the virtual queue is accumulating, as depicted in Figure 5-6, the corresponding admitted rate by session 1 increases in Figure 5-5. By the definition of the virtual queue, a larger backlog of Y_1 indicates that the average departure rate of the virtual queue, i.e., the average admitted rate, is insufficient. Therefore, the source node of session 1 will attempt to increase the admitted rate and thus the backlog of the virtual queue will decrease accordingly where the stability of the virtual queue can be assured.

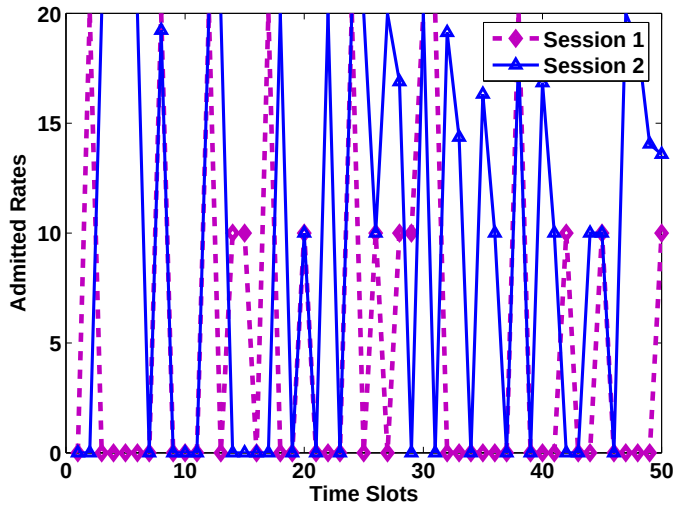

Figure 5-5. Sample trajectories of the admitted rates of two sessions for $J = 5000$

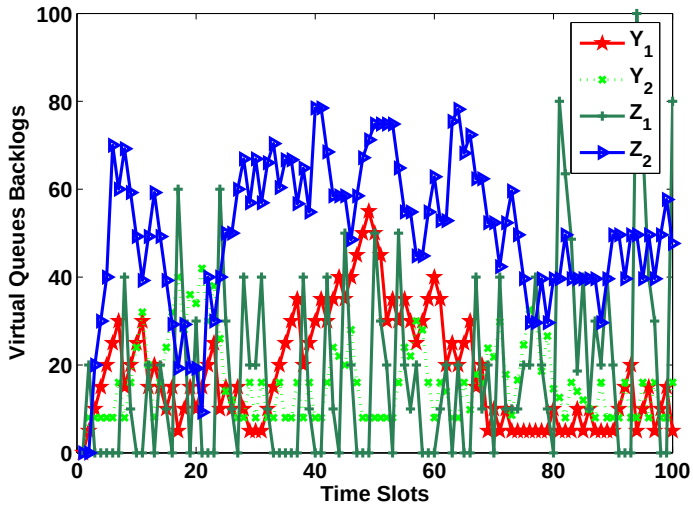

Figure 5-6. Sample trajectories of the virtual queues for $J = 5000$

In Figure 5-7, the traffic splitting decisions of the two source nodes, i.e., the hop selections of the source nodes, are illustrated. We can observe that both source nodes incline to utilize the queues with the smaller number of hops. The queues with longer hops, e.g., $h = 3$ or 4, are used only when the queue backlogs in the queues with smaller hops are overwhelmed. In addition, we can see that on average, session 2 utilizes a smaller number of average hops than session 1. Recall that session 2 has a much more stringent constraint on the average number of hops than session 1, i.e., 10 v.s. 30. Therefore, the source node of session 2, i.e., n_2^0, inclines to deposit more packets on the queues with smaller hop counts. As a consequence, by assigning different values of rate and hop requirements, a service differentiation solution can be achieved by the ANRA scheme among multiple competitive sessions in the network. In addition, a near-optimal network utility can be attained simultaneously.

5.7 Conclusions and Future Work

In this chapter, we propose a constrained queueing model to capture the cross layer interactions in multi-hop wireless sensor networks. Our model consists of components from multiple layers such as rate admission control, dynamic routing and wireless link scheduling. Based on the proposed model, we investigate the stochastic network

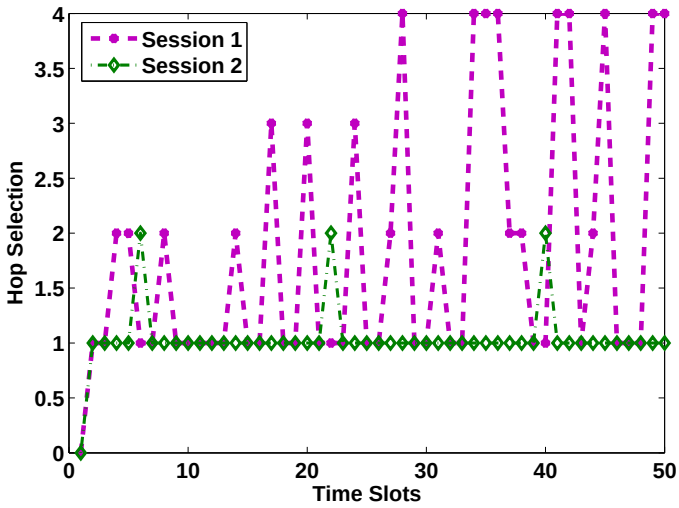

Figure 5-7. Sample trajectories of the hop selections for $J = 5000$

utility maximization problem in wireless sensor networks. As a cross layer solution, an adaptive network resource allocation scheme, a.k.a., ANRA algorithm, is proposed. The ANRA algorithm is an online mechanism which yields an overall network utility that can be pushed arbitrarily close to the global optimum solution.

As a future work, energy-aware distributed scheduling algorithms are to be studied and evaluated. In addition, the extension of our model to wireless sensor networks with network coding seems interesting and needs further investigation.

CHAPTER 6
THRESHOLD OPTIMIZATION FOR RATE ADAPTATION ALGORITHMS IN IEEE 802.11 WLANS

6.1 Introduction

IEEE 802.11 WLAN has become the dominating technology for indoor wireless Internet access. While the original IEEE 802.11 DSSS only provides two physical data rates (1 Mbps and 2 Mbps), the current IEEE standard provides several available data rates based on different modulation and coding schemes. For example, IEEE 802.11b supports 1 Mbps, 2 Mbps, 5.5 Mbps and 11 Mbps and IEEE 802.11g provides 12 physical data rates up to 54 Mbps. In order to maximize the network throughput, IEEE 802.11 devices, i.e., stations, need to adaptively change the data rate to combat with the time-varying channel environments. For instance, when the channel is good, a high data rate which usually requires higher SNR can be utilized. On the contrary, a low data rate which is error-resilient might be favorable for a bad channel. The operation of dynamically selecting data rates in IEEE 802.11 WLANs is called *rate adaptation* in general.

The implementation of rate adaptation algorithms is not specified by the IEEE 802.11 standard. This intentional omission flourishes the studies on this active area where a variety of rate adaptation algorithms have been proposed [92–108]. The common challenge of rate adaptation algorithms is how to match the unknown channel condition optimally such that the network throughput is maximized. According to the methods of estimating channel conditions, rate adaptation algorithms can be divided into two major categories. The first one is called *closed-loop* rate adaptation. Most schemes in this approach enable the receiver to measure the channel quality and sends back this information explicitly to the transmitter for rate adaptation. For example, the receiver records the SNR or RSSI value of the received packet and sends this information back to the transmitter via CTS or ACK packet. Consequently, the transmitter estimates the channel condition based on the feedback signal and adjusts the data rate accordingly.

By utilizing additional feedback mechanisms, the close-loop rate adaptation algorithms can achieve a better performance than the open-loop counterpart. However, in practice, the close-loop rate adaptation algorithms are rarely used in commercial IEEE 802.11 devices. This is because that the extra feedback information needs to be conveyed reliably and hence an inevitable modification on the current IEEE 802.11 standard is needed. This non-compatibility hinders the close-loop rate adaptation algorithms from practical implementations in current off-the-shelf IEEE 802.11 products.

The second category of rate adaptation algorithms, which is predominantly adopted by the vendors, is labeled as *open-loop* algorithms. The widely utilized Auto Rate Fallback algorithm, a.k.a., ARF, falls into this category. As many other open-loop rate adaptation algorithms, ARF adjusts the date rate solely based on the IEEE 802.11 ACK packets. For example, in Enterasys RoamAbout IEEE 802.11 card [109], two consecutive frame transmission failures, indicated by not receiving ACKs promptly, induces a rate downshift, while ten consecutive successful frame transmissions triggers a rate upshift [110]. Most commercialized IEEE products follow this up/down scheme [95, 96]. In this chapter, we focus on the open-loop rate adaptation algorithms due to the practical merits. More specifically, we consider a threshold-based rate adaptation algorithm which works as follows. If there are θ_u consecutive successful transmissions, the data rate is upgraded to the next level. On the other hand, if θ_d consecutive transmissions failed, a rate downshift is triggered. Since ARF is merely a special case of this threshold-based rate adaptation algorithm, our analysis can be applied to ARF and its variants as well.

As a tradeoff with simplicity, there are several challenges existing for the threshold-based rate adaptation algorithm. First, due to the trial-and-error based up/down mechanism, it inherently lacks the capability of capturing short dynamics of the channel variations [96]. To tackle this issue, Qiao *et.al.* propose a fast responsive rate adaptation solution in [92]. By introducing a measure of “delay factor”, the responsiveness of the

threshold-based rate adaptation algorithm can be guaranteed. The second challenge of the threshold-based rate adaptation algorithm is the indifference to collision-induced failures and noise-induced failures. It is worth noting that in a multiuser WLAN, an ACK timeout can be ascribed to either an MAC layer collision, or an erroneous channel. However, the threshold-based rate adaptation algorithm is unable to distinguish them effectively. Therefore, excessive collisions may introduce unnecessary rate degradations which significantly deteriorate the system performance. Attributing the actual reason of a transmission failure, or a packet loss, is named *loss diagnosis* [111] and has attracted tremendous attention from the community. For example, Choi *et.al.* [112] propose an algorithmic solution, which is specific to the threshold-based rate adaptation algorithm, to mitigate the collision effect in multiuser IEEE 802.11 WLANs. Therefore, the performance deterioration by the "indifference to collisions" can be compensated effectively.

While the first two challenges of the threshold-based rate adaptation algorithm have been tackled effectively, the third major obstacle, namely, the optimal selection of the up/down thresholds, remains as an open problem. A systematic treatment on how to select the values of θ_u and θ_d in the threshold-based rate adaptation algorithm is lacking in the literature, although several heuristic solutions are proposed [93, 94].

The contribution of this work is twofold. First, we analytically investigate the behavior of the threshold-based rate adaptation algorithm from a reverse engineering perspective. In other words, we answer the essential yet unresolved question, i.e., *"What is the threshold-based rate adaptation algorithm actually optimizing?"*, by unveiling the implicit objective function. As a result, several intuitive observations of the threshold-based rate adaptation algorithm can be explained straightforwardly by inspecting this objective function. Therefore, our reverse engineering model provides an alternative means to understand the threshold-based rate adaptation algorithm. Our work is a complement to the recent trend of reverse engineering studies on existing

heuristics-based networking protocols, such as TCP (transport layer) [4, 113, 114], BGP (network layer) [115] and random access MAC protocol (data link layer) [116]. To the best of our knowledge, this is the first work of studying threshold-based rate adaptation algorithms from a reverse engineering perspective. Our results explicitly show that the values of θ_u and θ_d play an important role in the objective function and thus the network performance hinges largely on the selection of the up/down thresholds. In light of this, we propose a threshold optimization algorithm which dynamically tunes the up/down thresholds of the threshold-based rate adaptation algorithm and provably converges to the stochastic optimum solution in arbitrary stationary random environments. We show that the optimal selection of the thresholds significantly enhances the system's performance.

The rest of chapter is organized as follows. Section 6.2 briefly overviews the state-of-the-art rate adaptation algorithms in the literature. The reverse engineering model of the threshold-based rate adaptation algorithm is derived in Section 6.3. In Section 6.4, the threshold optimization algorithm is proposed. The performance evaluations are provided in Section 6.5 and Section 6.6 concludes this chapter.

6.2 Related Work

RBAR [103] proposes an SNR-based close-loop rate adaptation algorithm where the rate decision relies on the feedback signal from the receiver. Specifically, the receiver estimates the channel condition and determines a proper rate via the RTS/CTS exchange. While consistently outperforms the open-loop rate adaptation algorithms such as ARF, RBAR is incompatible with the current IEEE 802.11 standard by altering the CTS frames [96]. In [105], a hybrid rate adaptation algorithm with SNR-based measurements is proposed, where the measured SNR is utilized to bound the range of feasible settings and thus shortens the response time to channel variations. [97] is another example of the close-loop rate adaptation algorithms which attempts to improve the throughput by predicting the channel coherence time, which is nevertheless difficult

in practice. Chen *et.al.* introduce a probabilistic-based rate adaptation for IEEE 802.11 WLANs. In [100], a rate-adaptive acknowledgement based rate adaptation algorithm is introduced. The basic idea is that by varying the ACK transmission rate, the appropriate rate information is conveyed to the transmitter. Wang and Helmy [108] propose a traffic-aware rate adaptation algorithm which explicitly relates the background traffic to the rate selection problem. However, aforementioned solutions either rely on altering the frame structures, or do not conform to the *de facto* IEEE 802.11 standard in commercial usage[1] . CHARM [101] avoids the overhead of RTS/CTS by leveraging the channel reciprocity. However, modifications on the IEEE 802.11 standardized frame structures, e.g., beacons and probe signals, are still needed.

In light of the complexity and the incompatibility of the close-loop rate adaptation algorithms, alternative open-loop rate adaptation algorithms are proposed. Although usually providing inferior performance than the close-loop solutions, open-loop algorithms soon become the predominant technique in commercial IEEE 802.11 devices due to the simplicity and the compatibility. The most popular open-loop rate adaptation algorithm is the ARF protocol proposed by Ad and Leo [104] where a rate upshift is triggered by ten consecutive successful transmission while two consecutive failures induce a rate downshift. SampleRate [102] is another widely adopted open-loop rate adaptation algorithm which performs arguably the best in static settings [96]. However, as pointed out by [96], SampleRate suffers from significant packet losses in fast changing channels. ONOE [106] is a credit-based mechanism included in MadWiFi drivers. The credit is determined by the number of successful transmissions, erroneous transmissions and retransmissions jointly. However, it is pointed in [98] that ONOE is less sensitive to individual packet failure and behaves over-conservatively.

[1] For example, they largely rely on the RTS/CTS signaling mechanism which is hardly used in practice.

As mentioned previously, one of the drawbacks of the simple open-loop rate adaptation algorithms is the inability to discriminate the collision-induced losses and the noise-induced losses. While several collision-aware rate adaptations are available in the literature [95, 96, 99, 107], they base on the close-loop solutions which utilize either RTS/CTS signaling or modifications on the standard. In [110], [112], Choi *et.al.* propose a collision mitigation algorithm for open-loop ARF algorithm based on a Markovian modeling. However, the channel conditions are assumed to be constant in their work. In this work, on the contrary, we particularly focus on the threshold optimization to combat with fast channel fluctuations rather than collisions. Therefore, in tandem with [110, 112], our work provide a solution to jointly mitigate the channel fluctuations and the multiuser collisions. For example, the up/down thresholds, i.e., θ_u and θ_d can be first calculated by our threshold optimization algorithm in Section 6.4. Next, they are subjected to further adjustments following [112] to mitigate the collision effects.

6.3 Reverse Engineering for the Threshold-Based Rate Adaptation Algorithm

We consider a station in a multi-rate IEEE 802.11 WLAN. There are N stations in the WLAN where each station, say i, has a transmission probability of p_i. Note that the equivalence of the p-persistent model and the IEEE 802.11 binary exponential backoff CSMA/CA model has been extensively studied in [116] and [117]. Throughout this work, we assume that the transmission probability of each station is fixed. The interaction of the data rate and the transmission probability remains as future research. Without loss of generality, we assume that the stations have a same transmission probability of p.

In this work, we focus on the widely deployed open loop threshold-based rate adaptation algorithm. Not surprisingly, the speed of channel variations has a great impact on the performance of the rate adaptation algorithm. While the original intention of the threshold-based rate adaptation algorithm is to maximize the average throughput, a natural question arises that whether this is indeed the case. In this section, to better understand the impact of θ_u and θ_d on the performance of the threshold-based rate

adaptation algorithm, we investigate the threshold-based rate adaptation algorithm via a reverse engineering approach. We assume that the RTS/CTS signals are turned off. In a time slot, say t, we denote the channel state[2] as $s(t)$ and denote the successful transmission probability, given the current transmission rate $r(t)$ and the channel condition $s(t)$, as

$$P_S\left(s(t), r(t)\right) = p(1-p)^{N-1}\left(1 - e(s(t), r(t))\right) \tag{6–1}$$

where e denotes the frame error rate (FER) and is given by

$$e(s(t), r(t)) = 1 - (1 - P_e(s(t), r(t)))^L \tag{6–2}$$

and $P_e(s(t), r(t))$ is the bit error rate (BER) which is determined by the current data rate, i.e., modulation scheme, and the current channel condition. L is the frame length of the packet. Similarly, we define $P_F(s(t), r(t)) = 1 - P_S(s(t), r(t))$ as the transmission failure probability at time t. It is worth noting that both P_S and P_F are functions of the current data rate $r(t)$ as well as the instantaneous channel condition $s(t)$, which is random. Particularly, we assume that the threshold-based rate adaptation algorithm will increase the data rate by an amount of δ if there are θ_u consecutive successful transmissions and decrease it by δ if there are θ_d consecutive failures. Denote $u = \theta_u - 1$ and $d = \theta_d - 1$ for notation succinctness. We define a binary indicator function $\zeta(t)$ where $\zeta(t) = 1$ means that the transmission at time slot t is successful and $\zeta(t) = 0$ otherwise. Mathematically, the updating rule of the threshold-based rate adaptation algorithm can be written as

[2] Note that the number of feasible channel states can be potentially infinite.

$$
\begin{aligned}
r(t+1) &= (r(t)+\delta)\Gamma_{\zeta(t)=1}\Gamma_{\zeta(t-1)=1}\cdots\Gamma_{\zeta(t-u)=1} \\
&\quad +(r(t)-\delta)\Gamma_{\zeta(t)=0}\Gamma_{\zeta(t-1)=0}\cdots\Gamma_{\zeta(t-d)=0} \\
&\quad +r(t)\Gamma_{o.w.}
\end{aligned} \tag{6–3}
$$

where

$$
\Gamma_x = \begin{cases} 1, & \text{if event x is true} \\ 0, & \text{if event x is false.} \end{cases} \tag{6–4}
$$

For example, $\Gamma_{\zeta(t)=1} = 1$ if the transmission at time t is successful and $\Gamma_{\zeta(t)=1} = 0$ otherwise. The symbol of $o.w.$ denotes the event that neither θ_u consecutive successful nor θ_d consecutive failed transmissions happened. For simplicity, we assume that the maximum allowable data rate is sufficiently large and the minimum data rate is zero, i.e., not transmitting. Define

$$
\mathbf{h}(t) = [r(t), r(t-1), \cdots, r(1), e(s(t), r(t)), \cdots, e(s(1), r(1))] \tag{6–5}
$$

as the *history vector*. In addition, we define

$$
Z(t+1) = \mathcal{E}\left\{r(t+1)|\mathbf{h}(t)\right\} \tag{6–6}
$$

where $\mathcal{E}$ is the expectation operator.

Condition:

(C.1) The channel states between two consecutive successful transmissions or two consecutive failed transmissions are independent random variables.

We emphasize that the restrictive condition (C.1) is not our general assumption in this work. If (C.1) is satisfied, however, the derivation of the reverse engineering analysis can be presented in a more concise form, as will be shown shortly.

First, we obtain

$$\begin{aligned}
&\mathcal{E}\left\{\Gamma_{\zeta(t)=1}\Gamma_{\zeta(t-1)=1}\cdots\Gamma_{\zeta(t-u)=1}|\mathbf{h}(t)\right\} \\
&= \Pr\left\{\Gamma_{\zeta(t)=1}=1,\Gamma_{\zeta(t-1)=1}=1,\cdots,\Gamma_{\zeta(t-u)=1}=1|\mathbf{h}(t)\right\}
\end{aligned} \tag{6–7}$$

If condition (C.1) is satisfied, (6–7) can be further decomposed as

$$\begin{aligned}
&\mathcal{E}\left\{\Gamma_{\zeta(t)=1}\Gamma_{\zeta(t-1)=1}\cdots\Gamma_{\zeta(t-u)=1}|\mathbf{h}(t)\right\} \\
= \;& \Pr\left\{\Gamma_{\zeta(t)=1}=1|\mathbf{h}(t)\right\}\times\Pr\left\{\Gamma_{\zeta(t-1)=1}=1|\mathbf{h}(t)\right\} \\
&\cdots\times\Pr\left\{\Gamma_{\zeta(t-u)=1}=1|\mathbf{h}(t)\right\} \\
= \;& \prod_{k=0}^{u}P_S(s(t-k),r(t-k))
\end{aligned} \tag{6–8}$$

Similarly, we have

$$\begin{aligned}
&\mathcal{E}\left\{\Gamma_{\zeta(t)=0}\Gamma_{\zeta(t-1)=0}\cdots\Gamma_{\zeta(t-d)=0}|\mathbf{h}(t)\right\} \\
&= \Pr\left\{\Gamma_{\zeta(t)=0}=1,\Gamma_{\zeta(t-1)=0}=1,\cdots,\Gamma_{\zeta(t-u)=0}=1|\mathbf{h}(t)\right\}
\end{aligned} \tag{6–9}$$

If (C.1) is assumed to be valid, we can obtain

$$\begin{aligned}
&\mathcal{E}\left\{\Gamma_{\zeta(t)=0}\Gamma_{\zeta(t-1)=0}\cdots\Gamma_{\zeta(t-d)=0}|\mathbf{h}(t)\right\} \\
&= \prod_{k=0}^{d}(1-P_S(s(t-k),r(t-k))
\end{aligned} \tag{6–10}$$

For notation succinctness, we will temporarily assume that (C.1) is satisfied. The condition will be relaxed after the implicit objective function is revealed. Therefore, we

can write (6–6) as

$$
\begin{aligned}
& Z(t+1) = \mathcal{E}\left\{r(t+1)|\mathbf{h}(t)\right\} \\
= \; & (r(t)+\delta)\prod_{k=0}^{u} P_S(s(t-k), r(t-k)) \\
& +(r(t)-\delta)\prod_{k=0}^{d}(1-P_S(s(t-k), r(t-k)) \\
& +r(t)\left(1-\prod_{k=0}^{u} P_S(s(t-k), r(t-k))\right. \\
& \left.-\prod_{k=0}^{d}(1-P_S(s(t-k), r(t-k))\right) \\
= \; & r(t)+\delta\left(\prod_{k=0}^{u} P_S(s(t-k), r(t-k))\right. \\
& \left.-\prod_{k=0}^{d}(1-P_S(s(t-k), r(t-k))\right)
\end{aligned} \tag{6–11}
$$

Let us revisit (6–3), which can be rewritten as

$$
\begin{aligned}
r(t+1) \; = \; & r(t)+\delta\left(\frac{1}{\delta}\times\left(\,(r(t)+\delta)\Gamma_{\zeta(t)=1}\cdots\Gamma_{\zeta(t-u)=1}\right.\right. \\
& +(r(t)-\delta)\Gamma_{\zeta(t)=0}\Gamma_{\zeta(t-1)=0}\cdots\Gamma_{\zeta(t-d)=0} \\
& \left.\left.+r(t)\Gamma_{o.w.}-r(t)\;\right)\right) \\
= \; & r(t)+\delta\xi(t)
\end{aligned} \tag{6–12}
$$

where

$$
\begin{aligned}
\xi(t) \; = \; & \frac{1}{\delta}\times\left\{\;(r(t)+\delta)\Gamma_{\zeta(t)=1}\Gamma_{\zeta(t-1)=1}\cdots\Gamma_{\zeta(t-u)=1}\right. \\
+ \; & (r(t)-\delta)\Gamma_{\zeta(t)=0}\Gamma_{\zeta(t-1)=0}\cdots\Gamma_{\zeta(t-d)=0} \\
+ \; & \left.r(t)\Gamma_{o.w.}-r(t)\;\right\}.
\end{aligned} \tag{6–13}
$$

It should be noted that

$$\begin{aligned}\mathcal{E}\{\xi(t)|\mathbf{h}(t)\} &= \prod_{k=0}^{u} P_S(s(t-k), r(t-k)) \\ &- \prod_{k=0}^{d}(1 - P_S(s(t-k), r(t-k)). \end{aligned} \tag{6–14}$$

Therefore, we observe that (6–12) is a form of stochastic approximation with respect to (6–11). Next, we present the reverse engineering theorem for the threshold-based rate adaptation algorithm.

Theorem 6.1. *The threshold-based rate adaptation algorithm of (6–3) is a stochastic approximation which solves an implicit objective function $U(t)$, with a constant stepsize of δ, where $U(t)$ is in the form of*

$$\begin{aligned}U(t) &= r(t)\left\{\prod_{k=0}^{u} P_S(s(t-k), r(t-k))\right. \\ &\left. - \prod_{k=0}^{d}(1 - P_S(s(t-k), r(t-k))\ \right\} + \mathcal{K} \end{aligned} \tag{6–15}$$

if condition (C.1) is satisfied and $\mathcal{K}$ is a constant with respect to rate $r(t)$.

Proof. Theorem 1 follows directly from the previous analysis. Note that the threshold-based rate adaptation algorithm can be written as

$$r(t+1) = r(t) + \delta\xi(t) \tag{6–16}$$

where $\xi(t)$ is the stochastic gradient and satisfies

$$\mathcal{E}\{\xi(t)|\mathbf{h}(t)\} = \frac{\partial U}{\partial r(t)}\,|_{\mathrm{h}(t)} \tag{6–17}$$

Hence Theorem 1 holds.

If condition (C.1) does not hold, we can replace

$$\prod_{k=0}^{u} P_S(s(t-k), r(t-k))$$

and

$$\prod_{k=0}^{d}(1 - P_S(s(t-k), r(t-k))$$

in (6–15) with

$$\Pr\{\Gamma_{\zeta(t)=1}, \cdots, \Gamma_{\zeta(t-u)=1}|\mathbf{h}(t)\} \tag{6–18}$$

and

$$\Pr\{\Gamma_{\zeta(t)=0}, \cdots, \Gamma_{\zeta(t-d)=0}|\mathbf{h}(t)\} \tag{6–19}$$

respectively and the theorem remains valid.

It is worth noting that the objective function $U(t)$ is a time-varying function which is determined by the data rate as well as the channel conditions of the past τ time slots where $\tau = \max(\theta_u, \theta_d)$. Note that the data rate within the last τ time slots always remains unchanged. However, the channel fluctuations affect the successful transmission probability P_S and thus alter the objective function $U(t)$.

The partial derivative of the objective of $U(t)$ given $\mathbf{h}(t)$, i.e.,

$$\widetilde{\xi(t)} = \prod_{k=0}^{u} P_S(s(t-k), r(t-k)) - \prod_{k=0}^{d}(1 - P_S(s(t-k), r(t-k)) \tag{6–20}$$

is also time-varying. If the probability that the last θ_u transmissions are all successful is greater than the probability that the last θ_d transmissions are all failures, the station tends to increase the data rate and vice versa. The speed of rate increasing or deceasing is determined by the difference of these two probabilities. In other words, the partial derivative in (6–20) could be either positive or negative which corresponds to a rate upshift or a rate downshift. The absolute value of the instantaneous derivative determines the speed of rate changing.

A direct computation of the partial derivative in (6–20) is challenging, if not impossible, due to the uncertainty induced by the unpredictable stochastic channel. Therefore, the threshold-based rate adaptation algorithm, described in (6–3), utilizes

an alternative stochastic approximation approach with the unbiased estimation of $\widetilde{\xi(t)}$, i.e., $\xi(t)$ in (6–13), which significantly reduces the computational complexity since only local information based on ACKs is required. This nature of simplicity and practicability facilitates the popularity of the threshold-based rate adaptation algorithm and its variants such as ARF.

To achieve a better understanding of (6–15), let us consider the following extreme cases from a reverse engineering standpoint.

- $(u = 0, d = 0) \Rightarrow (\theta_u = \theta_d = 1)$: In this case, the threshold-based rate adaptation algorithm increases the data rate if the current transmission is successful and decreases otherwise. From (6–15), we can observe that this aggressive algorithm merely compares the successful probability with the failure probability of the current time slot and expects that the next time slot will remain the current channel condition.

- $(u = +\infty, d = 0) \Rightarrow (\theta_u = +\infty, \theta_d = 1)$: From (6–15), we can see that the derivative is always negative since the first part of (6–20) is zero. Therefore, the threshold-based rate adaptation will keep decreasing data rate until the minimum data rate is reached, i.e., zero, which is consistent with the intuition.

- $(u = 0, d = +\infty) \Rightarrow (\theta_u = 1, \theta_d = +\infty)$: In this scenario, the second part of (6–20) is always zero and thus the algorithm will keep upgrading data rate until the maximum data rate is achieved.

- $(u = +\infty, d = +\infty) \Rightarrow (\theta_u = \infty, \theta_d = +\infty)$: The derivative of (6–20) is always zero and hence the data rate never changes.

Hence, by inspecting (6–15) and (6–20) directly, we provide an alternative means to understand the behavior of the threshold-based rate adaptation algorithm. In (6–3), we have assumed a constant stepsize δ while in current off-the-shelf IEEE 802.11 devices, a discrete set of data rates are provided. However, continuous rate adaptation can be achieved by controlling the transmission power jointly or deploying Adaptive-Coding-and-Modulation (ACM) capable devices. Therefore, our reverse engineering model, while fits in continuous rate scenarios, provides an approximate model for discrete rate adaptation scenarios. We believe that the reverse engineering result in this work provides a first step towards a comprehensive understanding on the

good-yet-simple rate adaptation algorithm designs. In addition, based on the unveiled implicit objective function of (6–15), the interactions of rate adaptations among multiple IEEE 802.11 stations can be investigated in a game theoretical framework.

It is immediate to observe from (6–15) and (6–20) that the selection of θ_u and θ_d has significant impact on the performance of the rate adaptation algorithm. Ideally, the rate adaptation algorithm attempts to find the data rate which maximizes the expected throughput in the next time slot, i.e.,

$$r' = \text{argmax}_r r \times P_S(s(t+1), r). \tag{6–21}$$

Define

$$V = r \times P_S(s(t+1), r). \tag{6–22}$$

Therefore, if we can estimate the value of $\frac{\partial V}{\partial r}$ and relate it by

$$\widetilde{\xi(t)} \to \frac{\partial V}{\partial r}, \tag{6–23}$$

then the threshold-based rate adaptation algorithm is indeed optimizing the expected throughput via the stochastic approximation approach. However, to achieve a derivative estimation of a general non-Markovian system is non-trivial [118] [119]. Moreover, if the channel appears totally random, e.g., non-stationary and fast fading, there exists no effective optimization-based solution unless certain level of knowledge on the channel randomness is available. Therefore, in the next section, we will consider a stationary random channel environment. Nevertheless, the stochastic channel can be slow-varying or fast-varying following arbitrary probabilistic distributions. We propose a threshold optimization algorithm which provably converges to the stochastic optimum values of θ_u and θ_d and the overall performance of the network is remarkably enhanced.

6.4 Threshold Optimization Algorithm

In this section, we model the stochastic channel as a stationary random process denoted by $s(t)$. It is worth noting that if the channel is quasi-static, i.e., $s(t)$ is a

piecewise constant function, the probing-based rate adaptation algorithms, e.g., SampleRate [102], can achieve good performance. It is interesting to observe that even in a quasi-static environment, for different channel conditions, the optimal values of θ_u and θ_d may be different. One feasible way to find the optimum values of θ_u and θ_d with different channel conditions, in a quasi-static environment, is the sample-path based policy iteration approach introduced in [120] and [121], based on the Markovian model of the threshold-based rate adaptation algorithm proposed in [110].

However, it is arguable that the channel environment is stochastic and time-varying in nature. Therefore, it is not unusual that the channel condition has already changed before the optimization algorithm has reached a steady state solution. The algorithm will be thereby consistently chasing after a moving object and thus the thresholds are always chosen suboptimally. This is more severe in a fast fading stochastic environment. In light of this, we alternatively pursue *the stochastic optimum values* of the thresholds in a time-varying and potentially fast changing channel environment. That is to say, we attempt to find the set of values for θ_u and θ_d which maximize the *expected* system performance with respect to the random channel. Before elaborating further, we briefly outline the learning automata techniques based on which our threshold optimization algorithm is proposed.

6.4.1 Learning Automata

Learning automata techniques are first introduced in the control community where in many scenarios, the system is time-varying and stochastic in nature. Therefore, stochastic learning approaches are desired to address the stochastic control problem in random systems. The basic idea of learning automata techniques can be described as follows. We consider a stochastic environment and a set of finite actions available for the decision maker. Each selected action induces an output from the random environment. However, due to the stochastic nature, the outputs for a given input may be different at different time instances. Based on observations, a learning automata algorithm is

expected to find an action which is the stochastic optimum solution in the sense that the expected system's objective is maximized.

At each decision instance, the decision maker selects one of the actions according to a probability vector. The selected action is fed to the stochastic environment as the input and a random output is attained. The gist of learning automata techniques lies in the provable convergence to the ϵ-optimal solution, as will be defined later, in arbitrary stationary random environment. Thanks to the practicality and applicability, learning automata techniques have been broadly studied in various aspects of the communication and networking literature such as [122][123] [124] [125]. In this work, we propose a learning automata based threshold optimization algorithm which finds the stochastic optimum values of the up/down thresholds efficiently in any stationary yet potentially fast-varying random channel environment. The detailed implementations are introduced next.

6.4.2 Achieving the Stochastic Optimal Thresholds

We consider an IEEE 802.11 station as the decision maker which adjusts the values of θ_u and θ_d. Without loss of generality, we assume that the maximum value of θ_u and θ_d are m_u and m_d, i.e., the feasible set of θ_u is $\mathcal{A}_u = \{1, \cdots, m_u\}$ and that of θ_d is given by $\mathcal{A}_d = \{1, \cdots, m_d\}$. The station maintains two probability vectors P_u and P_d for $\mathcal{A}_u$ and $\mathcal{A}_d$, respectively. The k-th element in P_u, i.e., P_u^k, denotes the probability that θ_u is set to k. P_d^k is defined analogously. Simply put, at each decision instance, the threshold optimization algorithm randomly determines the values of θ_u and θ_d according to P_u and P_d. Next, the probability vectors, i.e., P_u and P_d, are updated and the iteration continues until convergence, i.e., $P_u^{m^*} = 1$ and $P_d^{n^*} = 1$ where m^* and n^* denote the stochastic optimal values of θ_u and θ_d, respectively.

Define a time series denoted by $\mathbf{t} = [t_0, t_1, \cdots]$ where t_0 denotes the starting time and other elements represent the exact time instances when the data rate is changed.

Denote

$$T(j) = [t_{j-1}, t_j],\ j = 1, 2, \cdots$$

as the j-th *time period*, or *time duration*. It is worth noting that within a particular time period, say j, the value of the data rate, the values of thresholds, i.e., θ_u and θ_d , are all fixed numbers. We denote these period-dependent parameters as[3] $r(j)$, $\theta_u(j)$ and $\theta_d(j)$. With this observation, we utilize the time series $\mathbf{t}$ as the time series of decision instances. More specifically, for example, at time t_j, a rate change is triggered either by $\theta_u(j)$ consecutive successful transmissions or $\theta_d(j)$ consecutive failed transmissions. In tandem with the data rate up/down shift, new values of the thresholds, i.e., $\theta_u(j+1)$ and $\theta_d(j+1)$ are determined by the threshold optimization algorithm according to the probability vectors P_u and P_d.

Besides P_u and P_d, we introduce additional vectors for $\mathcal{A}_u$ and $\mathcal{A}_d$, namely, the counting vectors C_u, C_d, the surplus vectors S_u, S_d, the estimation vectors D_u, D_d and the comparison vectors Z_u, Z_d. The definitions of parameters of the algorithm are provided as follows.

Algorithm:

Parameters[4] :

- P_u (P_d): The probability vector for θ_u (θ_d) over $\mathcal{A}_u$ ($\mathcal{A}_d$).
- m_u (m_d): The maximum value of θ_u (θ_d), or equivalently, the cardinality of $\mathcal{A}_u$ ($\mathcal{A}_d$).
- C_u (C_d): The counting vector of θ_u (θ_d) where the k-th element, i.e., C_u^k (C_d^k), denotes the times that k has been selected as the value of θ_u (θ_d).
- S_u (S_d): The surplus vector of θ_u (θ_d) where the k-th element, i.e., S_u^k (S_d^k), denotes the accumulated throughput with $\theta_u = k$ ($\theta_d = k$).

[3] Note that with a slight abuse of notation, we use j to denote the j-th time duration.

[4] We present the analogous definitions in the parenthesis.

- D_u (D_d): The estimation vector of θ_u (θ_d) where the k-th element, i.e., D_u^k (D_d^k), is calculated by $D_u^k = \frac{S_u^k}{C_u^k}$ ($D_d^k = \frac{S_d^k}{C_d^k}$).

- R: The resolution parameter which is a positive integer and is tunable by the station.

- δ_u (δ_d): The stepsize parameter of θ_u (θ_d) and is given by $\delta_u = \frac{1}{m_u \times R}$ ($\delta_d = \frac{1}{m_d \times R}$).

- φ_u (φ_d): The perturbation vector of θ_u (θ_d) where the k-th element, i.e., φ_u^k (φ_d^k), is a zero mean random variable which is uniformly distributed in $[-\frac{\rho}{C_u^k(C_d^k)}, +\frac{\rho}{C_u^k(C_d^k)}]_{-1}^{+1}$ where ρ is a system parameter and is controllable by the station. The notation of $[a, b]_y^x$ represents $[\max(a, y), \min(b, x)]$.

- Z_u (Z_d): The comparison vector of θ_u (θ_d) where the k-th element, i.e., Z_u^k (Z_d^k), is given by $Z_u^k = D_u^k + \varphi_u^k$ ($Z_d^k = D_d^k + \varphi_d^k$).

- B: The predefined convergence threshold, e.g., 1, which is determined by the station.

- J: A running parameter which records the updated maximum achieved throughput during one time period.

At time t_0:

Initialization:

- The station sets $P_u = [p_1, \cdots, p_i, \cdots, p_{m_u}]$ where $p_i = \frac{1}{m_u}$ for all $1 \leq i \leq m_u$. Similarly, P_d is given by $[p_1, \cdots, p_i, \cdots, p_{m_d}]$ where $p_i = \frac{1}{m_d}$ for all $1 \leq i \leq m_d$.

- Initializes C_u, C_d, S_u, S_d, D_u and D_d to zeros.

- Randomly selects the values of $\theta_u(1)$ and $\theta_d(1)$, say m, n, according to $P_u(1)$ and $P_d(1)$.

- Transmits with $\theta_u = m$ and $\theta_d = n$ until $T(1)$ ends, i.e., a data rate change is triggered.

- Records the average throughput within $T(1)$ as J.

At time $t_j (j \geq 1)$:

Do:

- Records the average throughput during T_j as $O(j)$. If $O(j) > J$, sets $J = O(j)$ and remains J unchanged otherwise.

- Updates the m-th element in the surplus vector S_u and the n-th element in S_d by adding the measured normalized throughput of the last time period, as $S_u^m = S_u^m + \frac{O(j)}{J}$ and $S_d^n = S_d^n + \frac{O(j)}{J}$.

- Updates the counting vectors by adding one to the m-th counter in C_u and the n-th counter in C_d, as $C_u^m = C_u^m + 1$ and $C_d^n = C_d^n + 1$.

- Updates the m-th element in D_u and the n-th element in D_d by $D_u^m = \frac{S_u^m}{C_u^m}$ and $D_d^n = \frac{S_d^n}{C_d^n}$.

- For every element in Z_u and Z_d, updates $Z_u^k = D_u^k + \varphi_u^k,\ k = 1, \cdots, m_u$ and $Z_d^k = D_d^k + \varphi_d^k,\ k = 1, \cdots, m_d$.

- Finds the element in Z_u with the highest[5] value of $Z_u^k, k = 1, \cdots, m_u$, say, the $\tilde{m}$-th element in $\mathcal{A}_u$.

- Similarly, finds the element in Z_d which has the highest $Z_d^k, k = 1, \cdots, m_d$, say, the $\tilde{n}$-th element in $\mathcal{A}_d$.

- Updates the probability vectors of P_u and P_d as

$$\begin{aligned} P_u^k &= \max\left(P_u^k - \delta_u, 0\right) \text{ if } k \neq \tilde{m}, k = 1, \cdots, m_u \\ P_u^k &= 1 - \sum_{k \neq \tilde{m}} P_u^k \text{ if } k = \tilde{m} \end{aligned} \tag{6–24}$$

and

$$\begin{aligned} P_d^k &= \max\left(P_d^k - \delta_d, 0\right) \text{ if } k \neq \tilde{n}, k = 1, \cdots, m_d \\ P_d^k &= 1 - \sum_{k \neq \tilde{n}} P_d^k \text{ if } k = \tilde{n} \end{aligned} \tag{6–25}$$

where $\delta_u = \frac{1}{m_u \times R}$ and $\delta_d = \frac{1}{m_d \times R}$.

- With the updated probability vectors P_u and P_d, new values of θ_u and θ_d, i.e., $\theta_u(j+1)$ and $\theta_d(j+1)$, are selected.

– Starts the transmissions in $T(j+1)$ with $\theta_u(j+1)$ and $\theta_d(j+1)$.

Until:

- $\max(P_u) \geq B$ and $\max(P_d) \geq B$ where B is the predefined convergence threshold.

[5] Note that a tie can be easily broken by a random selection.

End

The proposed threshold optimization algorithm is similar to the *stochastic estimator learning automata* proposed in [126]. The key feature of this genre of learning automata is the randomness deliberately introduced by φ_u^k and φ_d^k. Note that although φ_u^k and φ_d^k are zero mean random variables, their variances are dependent on the values of C_u^k and C_d^k, respectively. Specifically, the variances approach to zeros with the increase of the number of times that the corresponding values of θ_u and θ_d are selected. As a consequence, the threshold optimization algorithm inclines to more reliable stochastic estimates and thus possesses a faster convergence behavior than other learning algorithms [126]. The values that have been selected less frequently still have the chance of being considered as optimal. However, the missing probability diminishes to zero along iterations. In the algorithm, the resolution parameter R controls the stepsize of probability adjustment in the algorithm. A smaller value of R produces a fine-grained probability adjustment yet unavoidably prolongs the convergence time. The convergence threshold B determines the stopping criteria of the algorithm. Therefore, a tradeoff between optimality and convergence rate can be adjusted by tuning the value of B.

The steady state behavior of the proposed threshold optimization algorithm is provided in the following theorem.

Theorem 6.2. *The proposed threshold optimization algorithm is* ϵ-optimal *for any stationary channel environment with arbitrary distribution. Mathematically, for any arbitrarily small* $\epsilon > 0$ *and* $\gamma > 0$*, there exists a* t' *satisfying*

$$\Pr\{|1 - P_u^{m^*}| < \epsilon\} > 1 - \gamma \; \forall t > t' \tag{6–26}$$

and

$$\Pr\{|1 - P_d^{n^*}| < \epsilon\} > 1 - \gamma \; \forall t > t' \tag{6–27}$$

where m^* *and* n^* *are the stochastic optimal values of* θ_u *and* θ_d*, respectively.*

The proof of Theorem 6.2 follows similar lines as in [126] and is omitted for brevity. For more discussions on the stochastic estimator algorithms, refer to [127] and [128]. In the next section, we will demonstrate the efficacy of our proposed threshold optimization algorithm via simulations.

6.5 Performance Evaluation

In this section, we evaluate the performance of the proposed threshold optimization algorithm with simulations. For comparisons, we first implement the heuristics-based threshold adjustment algorithms in [93] and [94]. In [93], the downshift threshold θ_d is fixed to 1 and the default value of θ_u is 10. After θ_u successful transmissions, a data upshift is triggered and if the first transmission after the rate upshift is successful, the algorithm assumes that the link quality is improving rapidly [93]. Consequently, θ_u is set to a small number, e.g., $\theta_u = 3$, in order to capture the fast improving channel. Otherwise, the algorithm assumes that the channel is changing slowly and thus a larger value of θ_u is desired, e.g., $\theta_u = 10$. We denote this threshold adaptation scheme as DLA in our simulations. Another well-known threshold adjusting scheme, namely, AARF, is proposed in [94]. Similarly, the rate downshift threshold is fixed to $\theta_d = 2$ empirically. However, for θ_u, a binary exponential backoff scheme is applied. If the first transmission after a rate upshift failed, the data rate is switched back to the previous rate and the value of θ_u is doubled with a maximum value of 50. The value of θ_u is reset to 10 whenever a rate downshift is triggered.

To simulate the indoor office environment for IEEE 802.11 WLANs, we simulate a Rayleigh fading channel environment. In other words, we assume a flat fading environment. However, it could be either a fast fading or slow fading channel. The Doppler spread (in Hz) corresponds to the channel fading speed where a large Doppler spread value represents a fast fading channel and a small Doppler spread indicates a slow-varying channel. It should be noted that the Doppler spread value describes the time dispersive nature of the wireless channel [129], which is inversely proportional to

the channel coherence time. More specifically, we relate the channel coherence time T_c and the Doppler spread value f_m as [129]

$$T_c = \frac{0.423}{f_m}. \tag{6–28}$$

Therefore, a larger Doppler spread value indicates a small channel coherence time which represents a fast fading scenario. We conduct the simulations under various channel fading conditions via different Doppler spread values. We consider the IEEE 802.11b PHY specification, i.e., the available data rates are 1 Mbps, 2 Mbps, 5.5 Mbps and 11 Mbps and the RTS/CTS signalling scheme is turned off. Since the objective of our proposed threshold optimization algorithm is to combat with the channel variation, the collision effect is omitted. Therefore, we consider a WLAN with one station consistently transmitting packets to the AP. However, note that [112] provides a complementary solution to mitigate the collision effect and thus our algorithms can work collectively as a joint solution. We emphasize that this simplification does not induce any loss of generality since although seemingly simple, it produces all the challenging problems involved in rate adaptation algorithms in a time-varying stochastic channel environment. The data traffic is generated using constant bit rate UDP traffic sources and the frame size is set to 1024 octets. The power of the transmitter and the power of thermal noise are set to 50 mW and 1 mW, respectively. The SNR-BER relation is given by Table 6-1 which is derived from [130].

We vary the Doppler spread value to simulate the various channel fading speeds. For each value of Doppler spread value, the simulation is executed for 1000 seconds and the average throughput of the following algorithms[6] , which are commonly based on the

[6] The performance comparison of ARF and other open-loop rate adaptation algorithms such as SampleRate and ONOE has been studied extensively in [96] and [98] for various channel conditions.

threshold-based up/down mechanism, are compared: (1), *OP* - the optimum throughput attained by assuming an oracle which foresees the variation of channel and adapts the data rate optimally. This curve is attained as a performance comparison benchmark; (2), *ARF* - the threshold-based rate adaptation algorithm with θ_u = 10 and θ_d = 2; (3), *DLA* - the dynamic threshold adjustment algorithm proposed in [93]; (4), *AARF* - the threshold adjustment algorithm proposed in [94]; (5), *TOA* - the threshold optimization algorithm proposed in this work. The algorithms are compared with each other in terms of the average system throughput (in Mbps). For TOA, without loss of generality, we assume that $m_u = m_d = 10$ and the resolution parameter R is 1. The convergence threshold B is 0.999 and ρ is 1. The performance curves of the aforementioned algorithms are plotted in Figure 6-1.

In Figure 6-1, we observe that except the OP curve, all other rate adaptation algorithms suffer from performance degradations with large Doppler spread values. Recall that a large Doppler spread value indicates a fast fading channel environment and hence the average throughput deteriorates due to the incompetency of capturing short channel fluctuations. Among which, ARF and AARF provide worst performance with a slight difference. DLA performs better due to the capability of switching between

Table 6-1. SNR v.s. BER for IEEE 802.11b data rates

SNR (dB)	BPSK (1Mbps)	QPSK (2Mbps)	CCK (5.5 Mbps)	CCK (11 Mbps)
1	$1.2E^{-5}$	$5E^{-3}$	$8E^{-2}$	$1E^{-1}$
2	$1E^{-6}$	$1.2E^{-3}$	$4E^{-2}$	$1E^{-1}$
3	$6E^{-8}$	$2.1E^{-4}$	$1.8E^{-2}$	$1E^{-1}$
4	$7E^{-9}$	$3E^{-5}$	$7E^{-3}$	$5E^{-2}$
5	$2.3E^{-10}$	$2.1E^{-6}$	$1.2E^{-3}$	$1.3E^{-2}$
6	$2.3E^{-10}$	$1.5E^{-7}$	$3E^{-4}$	$5.2E^{-3}$
7	$2.3E^{-10}$	$1E^{-8}$	$6E^{-5}$	$2E^{-3}$
8	$2.3E^{-10}$	$1.2E^{-9}$	$1.3E^{-5}$	$7E^{-4}$
9	$2.3E^{-10}$	$1.2E^{-9}$	$2.7E^{-6}$	$2.1E^{-4}$
10	$2.3E^{-10}$	$1.2E^{-9}$	$5E^{-7}$	$6E^{-5}$
$\vdots$	$\vdots$	$\vdots$	$\vdots$	$\vdots$

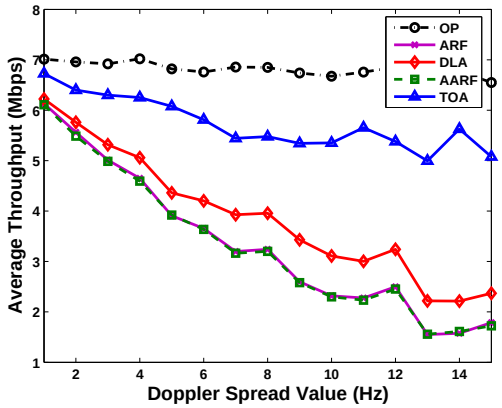

Figure 6-1. Average throughput v.s. Doppler spread values

the large value and the small value of θ_u for different channel conditions. Our proposed threshold optimization algorithm, as demonstrated in Figure 6-1, consistently outperforms other open-loop rate adaptation algorithms and bridges the performance gap with the OP curve. This superiority becomes remarkably significant in fast fading stochastic channel environments, i.e., scenarios with large Doppler spread values. While other algorithms are jeopardized by the unmature rate changes due to the uncertainty caused by the random and fast-varying channel environment, our proposed threshold optimization algorithm, based on the learning automata techniques, is able to find the stochastic optimum values of θ_u and θ_d which maximize the expected system performance. Therefore, our scheme is particularly suitable for fast changing yet statistically stationary random channel environments where other open-loop rate adaptation solutions usually provide unsatisfactory performance.

To illustrate the process of finding the stochastic optimum values of θ_u and θ_d, in Figure 6-2, we provide the trajectories of θ_u and θ_d in a sample simulation run with a fixed Doppler spread value of 10. It is observable that starting from the initial point, the threshold optimization algorithm adapts the values of θ_u and θ_d on the fly along with the rate changes. The algorithm soon finds the stochastic optimum values and θ_u and θ_d converge to the optimum solutions effectively. The evolutions of the probability vectors,

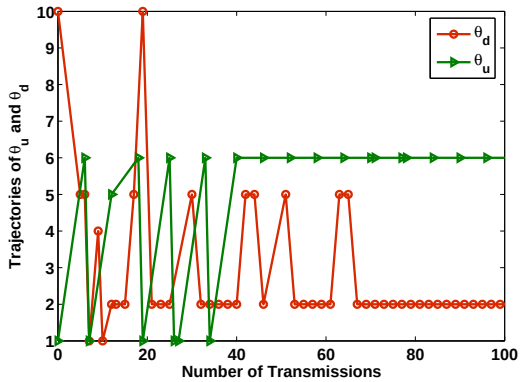

Figure 6-2. The trajectories of θ_u and θ_d in achieving the stochastic optimum values

i.e., P_u and P_d, are demonstrated in Figure 6-3 and Figure 6-4, respectively. Note that, in Figure 6-3, the sixth curve which represents the value of P_u^6 soon excels others and approaches to 1. Correspondingly, the value of θ_u converges to 6 rapidly as depicted in Figure 6-2. In Figure 6-4, the second curve approaches to unity gradually while others diminish to zeros. As a consequence, in Figure 6-2, the value of θ_d converges to the stochastic value, i.e., 2. In this sample run of simulation, the stochastic optimum values of θ_u and θ_d, which maximizes the expected throughput of the system, is given by θ_u = 6 and θ_d = 2. The proposed threshold optimization algorithm finds these values effectively and efficiently, while providing superior performance than other non-adaptive threshold-based rate adaptation algorithms, as demonstrated in Figure 6-1.

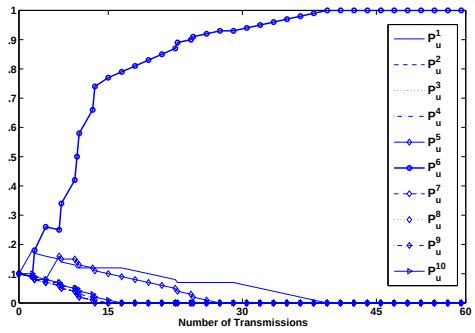

Figure 6-3. Evolution of the probability vector P_u

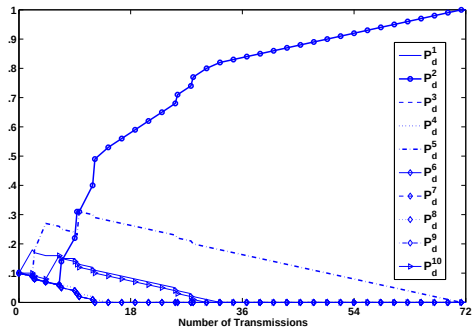

Figure 6-4. Evolution of the probability vector P_d

6.6 Conclusions and Future Work

In this chapter, we investigate the threshold-based rate adaptation algorithm which is predominantly utilized in practical IEEE 802.11 WLANs. Although widely deployed, the obscure objective function of this type of rate adaptation algorithms, commonly based on the heuristic up/down mechanism, is less comprehended. In this work, we study the threshold-based rate adaptation algorithm from a reverse engineering perspective. The implicit objective function, which the rate adaptation algorithm is maximizing, is unveiled. Our results provide, albeit approximate, an analytical model from which the threshold-based rate adaptation algorithm, such as ARF, can be better understood.

In addition, we propose a threshold optimization algorithm which dynamically adapts the up/down thresholds, based on the learning automata techniques. Our algorithm provably converges to the stochastic optimum solutions of the thresholds in arbitrary stationary yet potentially fast changing random channel environment. Therefore, by combining our work with the threshold adaptation scheme in [112], where the thresholds are adjusted to mitigate the collision effects, a joint collision and random channel fading resilient solution can be attained.

In this work, to emphasize on the impact of random channel variations, we restrict ourselves to the scenario where all stations have a fixed and known transmission probability p. The interaction of the transmission probabilities and the data rates seems

interesting and needs further investigation. Due to the competitive nature of channel access, a stochastic game formulation may be utilized.

CHAPTER 7
STOCHASTIC TRAFFIC ENGINEERING IN MULTI-HOP COGNITIVE WIRELESS MESH NETWORKS

7.1 Introduction

The past decade has witnessed the emergence of new wireless services in daily life. One of the promising techniques is the metropolitan wireless mesh networks (WMN), which are envisioned as a technology which advances towards the goal of ubiquitous network connection. Figure 7-1 illustrates an example of wireless mesh network. The wireless mesh network consists of edge routers, intermediate relay routers as well as the gateway node. Edge routers are the access points which provide the network access for the clients. The relay routers deliver the traffic aggregated at the edge routers to the gateway node, which is connected to the Internet, in a multi-hop fashion.

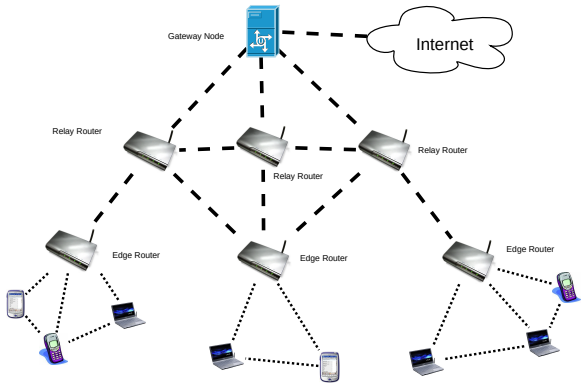

Figure 7-1. Architecture of wireless mesh networks

While the current deployed wireless mesh networks provide flexible and convenient services to the clients, the performance of a mesh network is still constrained by several limitations. The first barrier is due to the multi-hop nature of the wireless mesh network, where the nodes in geographic proximity generate severe mutual interference among each other and thus the network performance is devastated. To address this problem, several scheduling schemes have been proposed in the literature [131]. Recently, a novel coding-based scheme which may produce an interference-free wireless mesh

network, is proposed [132]. Another example of the interference-free network is the CDMA-based wireless mesh networks [133] where by assigning orthogonal codes for each link, the network throughput is remarkably improved.

The second hinderance for the network performance is the limited usable frequency resource. In current wireless mesh networks, the unlicensed ISM bands are most commonly adopted for backbone communications. Not surprisingly, the wireless mesh network is largely affected by all other devices in this ISM band, e.g., nearby WLANs and Bluetooth devices. Moreover, the limited bandwidth of the unlicensed band cannot satisfy the increasing demand for the bandwidth due to the evolving network applications. Ironically, as shown by a variety of empirical studies [134], the current allocated spectrum is drastically under-utilized. As a consequence, the urge to explore the unused whitespace of the spectrum, which can significantly enhance the performance of the wireless mesh networks, attracts tremendous attention in the community [135–139].

Cognitive radios are proposed as a viable solution to the frequency reuse problem [131]. The cognitive devices are capable of sensing the environment and adjusting the configuration parameters automatically. If the primary user, i.e., the legitimate user, is not using the primary band currently, the cognitive devices, namely, secondary users, will utilize this whitespace of the spectrum. Incorporating with the established interference-free techniques such as [132] and [18], the throughput of the wireless mesh network can be dramatically enhanced. The protocol design for cognitive wireless mesh networks (CWMN), or more generally, multi-hop cognitive radio networks, is an innovative and promising topic in the community [140] and has been less studied in the literature. In this work, we consider a cognitive wireless mesh network where the unlicensed band, e.g., ISM band, is utilized by the mesh routers for the backbone transmission. Moreover, each router is a cognitive device and hence is capable of

sensing and exploiting the unused primary bands for transmissions whenever the primary users are absent.

In this work, we investigate an important yet unexplored issue in the cognitive wireless mesh networks, namely, the stochastic traffic engineering problem. More specifically, we are particularly interested in how the traffic in the multi-hop cognitive radio networks should be steered, under the influence of random behaviors of primary users. It is worth noting that given a routing strategy, the corresponding network's performance, e.g., the average queueing delay encountered, is a random variable. The reason is that the available bandwidth for a particular link depends on the appearance of all the affecting primary users. If all the primary users are vacant, a link can utilize all available frequency trunks collectively by utilizing advanced physical layer techniques, e.g., OFDMA. However, if all the primary users are present, the only available frequency space is the unlicensed ISM band and thus the traffic on this link will experience longer delay than the previous case. In other words, the performance of a traffic engineering solution hinges intensely on the unpredictable random behaviors of the primary users. We emphasize that in multi-hop cognitive radio networks, this distinguishing feature of randomness, induced by the random behaviors of primary users, must be taken into account in protocol designs. Due to the location discrepancy, it is possible that some node is affected by many primary users while others are not. As a consequence, if we route the traffic via this particular node, the transmissions are more likely to be corrupted by the returns of the primary users. Apparently, a favorable solution is more inclined to steer the traffic from those "severely-affected area", to the paths which are less affected by the primary users. We will make this intuitive approach precise and rigorous in this work. To our best knowledge, this work is the first work on the traffic engineering problem in multi-hop cognitive radio networks, with a special focus on the impact of random behaviors from the primary users.

The rest of this chapter is organized as follows. The related work is reviewed in Section 7.2 and Section 7.3 provides the system model of our work. The stochastic traffic engineering problem with convexity is investigated in Section 7.4. In Section 7.5, we extend our framework to the non-convex stochastic traffic engineering problem. Performance evaluation is provided in Section 7.6, followed by concluding remarks in Section 7.7.

7.2 Related Work

Traditional traffic engineering (TE) algorithms are proposed as the solution to the traffic management of the network in a cost-efficient manner. Different from the traditional QoS routing, the traffic engineering solution not only guarantees a certain QoS level for each flow, but also optimizes a global performance metric over the whole network, by splitting the ingress traffic optimally among several available paths. The multi-path routing is usually supported by the Multi-Protocol Label Switching (MPLS) techniques where the explicit routing path for a packet is predetermined rather than being computed in a hop-by-hop fashion. For a pair of source and destination nodes, the set of available paths, a.k.a., label switched paths (LSP), are established and managed by signalling protocols such as RSVP-TE [141] and CR-LDP [142] or manually configuration. The traditional traffic engineering solution evolves to the stochastic traffic engineering (STE) solution when uncertainty exists in the network, e.g., the random returns of the primary users in our scenario. TE solutions require consistent route changes which are unfavorable in that the network will be overwhelmed by the oscillations induced by the unpredictable behaviors of the primary users. In light of this stability concern, STE solution alternatively pursues an optimum multi-path routing strategy such that the expected utility of the network is maximized. The stochastic traffic engineering with uncertainties are discussed in the literature such as in [143] and [144]. However, the previous works usually assume a probability distribution of the uncertainty, while in our scenario, the behaviors of the primary users are completely unpredictable

from the mesh network's point of view. Distinguishing from the previous works, we propose an algorithmic solution which requires no prior knowledge about the distribution of the uncertainty, in a stochastic network utility maximization framework. It is worth noting that our work differ from the traditional state-dependent traffic engineering solution as well. For example, in [145], a state dependent traffic engineering solution is proposed. However, the authors assume that the system state, i.e., the current value of uncertainty, is fully observable. In our approach, we do not assume that the ingress node has the perfect knowledge of the current appearance of the network. We will discuss this issue in detail in Section 7.4.

Recently, cognitive wireless mesh networks (CWMN) have attracted great attention in the literature. In [135], the channel assignment is discussed in a CWMN. In [136], a cluster-based cognitive wireless mesh network framework is proposed. The infrastructure-based cognitive network is discussed in [137] with a focus on the cooperative mobility and the channel selection schemes. The spectrum sensing and channel selection are jointly considered in a unified framework in [138]. In addition, the IEEE 802.16h is in the process of incorporating the cognitive radios into the WiMAX mesh networks [139]. However, none of the previous works considers the stochastic traffic engineering problem. Therefore, a systematic study of the impacts of the random returns from the primary users, on the network routing performance is lacking in the existing literature. In [146], the joint congestion control and traffic engineering problem is considered. He et.al. propose a distributed algorithm to balance the user's utility and the system's objective. However, the authors assume the environment is fixed and does not consider the randomness which is the distinguishing yet usually overlooked feature in cognitive radio networks. [147] and [148] discuss the routing issue in cognitive radio networks yet the impact of random returns of primary users is not investigated. Hou et.al. [149] [150] [151] [152] formulate the joint routing, power and subband allocation problem in cognitive radio networks as a mixed-integer programming. However, the

channels' bandwidths are assumed to be fixed, i.e., the random behaviors of primary users are still neglected. Our work is partially inspired by [153]. However, our work differs from theirs in three crucial aspects. First, by targeting the stochastic traffic engineering problem, our model differs from the joint power scheduling and rate control work in [154]. Secondly, in [153, 154], the authors only consider a single-path scenario while our work extends to a multi-path routing network where the network traffic can be steered. Thirdly and most importantly, [153, 154] require that the current system state is fully observable at the decision maker. To achieve this, the authors assume a centralized mechanism which knows all the channel states of all the links over the network. However, our work differs from [153, 154] significantly in that we do not require that the current system's state is known, which is of great practical interest since in multi-hop cognitive wireless mesh networks, the decision makers, i.e., the edge routers in our scenario, cannot be aware of the appearance of all primary users in the whole network as a priori. Moreover, our schemes enjoy a decentralized implementation, in contrast to centralized mechanisms in [153, 154], by utilizing the feedback signals and local information only. In our previous work of [20], we proposed a routing optimization scheme to combat with the randomness of instantaneous traffic in non-cognitive wireless mesh networks. With respect to [20], this work differs in the following ways. First, in the wireless mesh networks considered in [20], the capacity of each wireless link is assumed to be fixed, i.e., time-invariant. However, in cognitive wireless mesh networks, due to the unpredictable appearance of primary users, the bandwidth of each wireless link is random. Secondly, in [20], the quality of service (QoS) requirement is not considered. Nevertheless, in this chapter, we particularly address the QoS concern of each user, e.g., the expected accumulated delay on the paths cannot exceed a user-specific delay tolerance, as will be elaborated in Section 7.4. Thirdly and most importantly, the analysis in [20] was based upon the assumption that the users all have convex utility functions. In this work, we extend the techniques to address the scenarios

with non-convex utility functions. We will discuss the aforementioned issues further in the following sections.

7.3 System Model

We consider a multi-hop wireless mesh network illustrated in Figure 7-1 where an uplink traffic model is considered, i.e., all edge routers aggregate the traffic from clients and deliver to the gateway node via the intermediate relay routers. To ensure connectivity, we utilize the ISM 2.4G band as the underlying common channel for the wireless mesh network. In addition, each link can utilize the opportunistic channels, i.e., secondary bands to increase the link's achievable data rate whenever the primary user is vacant. We assume that there exists[1] $|\mathbb{M}|$ primary users. Each primary user possesses a licensed frequency channel and each mesh router is a cognitive node which has the capability of sensing the current wireless environment. We model the multi-hop cognitive wireless mesh network as a directional graph $\mathcal{G}$ where the vertices are the nodes. We also denote link (i, j) as link e, $e \in \mathbb{E}$ where $t(e) = i$ and $r(e) = j$ represent the transmitter and the receiver of link e.

We first consider a particular link denoted by (m, n). The instantaneous available frequency bands, at time t, for a node i is denoted by $I_i(t)$, which is determined by the current presence of the primary users. Besides the underlying ISM band, the communication between m and n can further utilize all secondary bands within $I_m(t) \bigcap I_n(t)$, if available. The current cognitive radio devices benefit largely from the software-defined radio (SDR) techniques with advanced coding/modulation capabilities. For example, by utilizing the multi-carrier modulation, e.g., OFDMA, a cognitive radio device can utilize all the disjoint available frequency band simultaneously [149, 150, 155–157]. At the transmitter, a software based radio combines waveforms for different sub-bands and thus transmit signal at these sub-bands simultaneously.

[1] The symbol of $|\mathbb{X}|$ represents the cardinality of the set $\mathbb{X}$.

While at the receiver, a software based radio decomposes the combined waveforms and thus receives signal at these sub-bands simultaneously [151, 152, 156, 157]. In this work, we assume a spectrum sensing scheme available that each node can sense the presence of the primary users in range, such as [131, 158], although the time of random returns cannot be predicted. A link will utilize all the available vacant bands and that the cognitive radios are full-duplex and can transmit at different bands concurrently [151, 152, 156, 157]. We further assume that some scheduling mechanism is in place or some physical layer mechanisms are utilized such that the nodes cannot interfere with each other during the transmissions. For example, in a multi-channel multi-radio wireless mesh network, the channels can be assigned properly that the transmissions do not interfere with the neighboring nodes [132, 159]. Other examples are the OFDMA/CDMA based wireless mesh networks [133, 160] where the interference among nodes can be eliminated by assigning orthogonal subcarriers/codes. We emphasize that this assumption is only for the sake of modeling simplicity and does not incur any loss of generality, as will be clarified shortly.

It is worth noting that the available bandwidth of each link in the cognitive wireless mesh network is a random variable. For example, at time instance t_1, node m has three secondary bands available, i.e., $I_m(t_1) = \{I_0, I_1, I_2, I_3\}$ and $I_n(t_1) = \{I_0, I_2, I_3, I_4, I_5\}$ due to the location discrepancy, where band 0 is the underlying unlicensed ISM band and $1, 2, 3, 4, 5$ are the licensed bands of primary users. The current bandwidth of link (m, n) is represented by $W_{m,n}(t_1) = BW_0 + BW_2 + BW_3$ where BW_i is the bandwidth of band i. At another time instance t_2, the primary user 2 returns and the bandwidth of link (m, n) becomes $W_{m,n}(t_2) = BW_0 + BW_3$. In other words, the bandwidth of links are random variables which are determined by the unpredictable appearance of the primary users. We model this randomness induced by the primary users as a stationary random process with arbitrary distribution. The system is assumed to be time-slotted. In each time slot n, the system state is assumed to be independent and is denoted by a state

vector $s = \{\delta_1, \cdots, \delta_{|\mathbb{M}|}\}, s \in \mathbb{S}$, where $\delta_i = 1$ denotes the absence of the i-th primary user and 0 otherwise. We denote the stationary probability distribution of state s as π_s. For the ease of exposition, we assume that the primary users are static. However, we emphasize that our model can be extended to mobile primary users scenarios straightforwardly. For example, if a primary user is moving following a Markovian walk model with well defined steady state distribution, the following analysis still applies. Without loss of generality, we express the link capacity in the form of CDMA-based networks, i.e., the capacity of a wireless link $e \in \mathbb{E}$, given the system state s, is denoted by c_e^s, which is given by [4, 161] $c_e^s = W_e^s \frac{1}{T} \log_2(1 + K\gamma_e^s)$, where W_e^s is the bandwidth of link e in state s and γ_e^s is the current SINR value of link e. The constant T is the symbol period and will be assumed to be one unit without loss of generality [4]. The constant $K = \frac{-\Phi_1}{log(\Phi_2 BER)}$ where Φ_1 and Φ_2 are constants depending on the modulation scheme and BER denotes the bit error rate. We will assume $K = 1$ in this work for simplicity [161]. Note that our network model can be incorporated into other types of networks such as MIMO, OFDM with TDMA or CSMA/CA based MAC protocols by modifying the form of the capacity accordingly, which represents the achievable data rate in general. For example, if we consider a scheduling-based MAC protocol where each link obtains a time share of the channel access, the achievable data rate is given by $c_e^s = \widetilde{c_e^s} \times \psi_e$ where ψ_e is the fraction of time that the link is active following the scheduling scheme and $\widetilde{c_e^s}$ is the nominal Shannon capacity of the link.

There are $|\mathbb{L}|$ unicast sessions in the network, denoted by set $\mathbb{L}$, where each session l has a traffic demand d_l. We associate each session with a unique user. Therefore, we will use *session l* and *user l* interchangeably. For each session $l \in \mathbb{L}$, we denote the source node and destination node as $S(l)$ and $D(l)$, respectively. Recall that we assume an uplink traffic model and thus all the source nodes are edge routers and the destination node is the gateway. Furthermore, to improve the reliability and

dependability, we allow multi-path routing schemes. We denote the available[2] set of acyclic paths from $S(l)$ to $D(l)$ by $\mathbb{P}_l$ and the k-th path is represented by P_l^k. We introduce a parameter r_l^k as the flow allocated in the k-th path of session l. The overall flow of user l, represented by x_l, is given as

$$x_l = \left[\sum_{k=1}^{|\mathbb{P}_l|} r_l^k \right]_0^{d_l} \tag{7–1}$$

where $[x]_a^b$ denotes $\max\{\min\{b, x\}, a\}$. Define an $|\mathbb{E}|$-by-$|\mathbb{P}_l|$ matrix $\mathbb{H}_l$ where the element $H_{e,k}^l = 1$ if link e is on the k-th path of $\mathbb{P}_l$ and 0 otherwise. Hence, $\mathbb{H} = \{\mathbb{H}_1, \cdots, \mathbb{H}_{|\mathbb{L}|}\}$ represents the network topology. Note that the traffic splitting and the source routing are executed on the source node $S(l)$.

For each link $e \in \mathbb{E}$, there is an associated cost function, denoted by $l_e^s(f_e, c_e^s)$ where f_e is the accumulated flow on link e. We assume the function l_e^s is an increasing, differentiable and convex function of f_e for a fixed c_e^s. For example, if we assume $l_e^s(f_e, c_e^s) = \frac{1}{c_e^s - f_e}$ when $c_e^s \geq f_e$, the cost essentially represents the delay for a unit flow on link e under the $M/M/1$ assumption. Note that in our scenario, even the accumulated flow f_e is fixed, the value of cost function is random due to the state-dependent variable c_e^s. From the network's perspective, the stochastic traffic engineering solution will distribute the aggregated flow among multiple paths optimally, in the sense that the overall network utility is maximized. In next section, we will formulate the stochastic traffic engineering problem in a stochastic network utility maximization framework [4] and provide a distributed solution which requires no priori information about the underlying probability distribution, i.e., π_s, of the system states.

[2] The available set of multiple paths can be obtained by signalling mechanisms such as RSVP-TE[141] or pre-configured manually. In this work, we assume a predetermined set of acyclic paths. The protocol design for acquiring such paths is beyond the scope of this work.

7.4 Stochastic Traffic Engineering with Convexity

7.4.1 Formulation

In the standard network utility maximization framework, each user has a utility function $U_l(x_l)$, which reflects the degree of satisfaction of user l by transmitting at a rate of x_l, e.g., $U_l(x_l) = \log(x_l)$. In this section, we assume the utility functions to be concave and differentiable. The non-convex utility functions are considered in Section 7.5. Note that the fairness issue can be embodied in the utility functions [4]. For example, in the seminal paper [113], the log-utility functions are adopted to achieve the proportional fairness among different flows.

Define a feasible stochastic traffic engineering solution as $\mathbf{r} = [\mathbf{r}_1, \cdots, \mathbf{r}_{|\mathbb{L}|}]$ where $\mathbf{r}_l \triangleq [r_l^1, \cdots, r_l^{|\mathbb{P}_l|}]$. We can formulate the stochastic traffic engineering problem as

$\underline{\mathcal{P}_1:}$

$$\max_{\mathbf{r}\geq 0} \sum_{l\in\mathbb{L}} U_l(\sum_{k\in\mathbb{P}_l} r_l^k)$$

s.t.

$$\sum_{k\in\mathbb{P}_l} r_l^k \leq d_l \ \forall l \in \mathbb{L} \tag{7–2}$$

$$\sum_{s\in\mathbb{S}} \pi_s \sum_{k\in\mathbb{P}_l} r_l^k \left(\sum_{e\in P_l^k} I_e^s(f_e, c_e^s) \right) \leq b_l \ \forall l \in \mathbb{L} \tag{7–3}$$

$$f_e \leq \sum_{s\in\mathbb{S}} \pi_s c_e^s \ \forall e \in \mathbb{E} \tag{7–4}$$

$$f_e = \sum_{l\in\mathbb{L}} \sum_{k\in\mathbb{P}_l} H_{e,k}^l r_l^k \ \forall e \in \mathbb{E} \tag{7–5}$$

$$c_e^s = W_e^s \frac{1}{T} \log_2(1 + K\gamma_e^s) \ \forall e \in \mathbb{E} \tag{7–6}$$

where $e \in P_l^k$ represents the links along the k-th path of user l. The variable in $\mathcal{P}_1$ is the vector of $\mathbf{r}$. The first set of constraints reflect that the overall data rates of all paths cannot exceed the traffic demand d_l. The second set of constraints indicate that for

each user l, the expected cost has to be no more than a predefined constraint b_l. The third set of constraints represent that the aggregated flow on link e cannot exceed the average link capacity. Apparently, if the underlying probability distribution of each state π_s is known as a priori, $\mathcal{P}_1$ is a deterministic convex optimization problem and thus easy to solve. However, in practice, the accurate measurement of probability distribution is a non-trivial task. In [20], we utilized a stochastic approximation based approach to circumvent the difficulty of estimating the probability distribution. In the following, we will extend this technique and develop a tailored distributed algorithm to address the issues of time-varying link capacities as well as the user-specific QoS requirements, which are of particular interest in multi-hop cognitive wireless mesh networks.

First, define the Lagrangian function of $\mathcal{P}_1$ as

$$
\begin{aligned}
& L(\mathbf{r}, \lambda, \mu, \mathbf{v}) \\
= & \sum_{l \in \mathbb{L}} U_l(\sum_{k \in \mathbb{P}_l} r_l^k) + \sum_{l \in \mathbb{L}} \lambda_l (d_l - \sum_{k \in \mathbb{P}_l} r_l^k) \\
& + \sum_{l \in \mathbb{L}} v_l \left(b_l - \sum_{s \in \mathbb{S}} \pi_s \sum_{k \in \mathbb{P}_l} r_l^k (\sum_{e \in P_l^k} l_e^s(f_e, c_e^s)) \right) \\
& - \sum_{e \in \mathbb{E}} \mu_e (f_e - \sum_{s \in \mathbb{S}} \pi_s c_e^s) \\
= & \sum_{l \in \mathbb{L}} \Bigg\{ U_l(\sum_{k \in \mathbb{P}_l} r_l^k) + \lambda_l (d_l - \sum_{k \in \mathbb{P}_l} r_l^k) + v_l b_l \\
& - v_l \sum_{s \in \mathbb{S}} \pi_s \sum_{k \in \mathbb{P}_l} r_l^k (\sum_{e \in P_l^k} l_e^s(f_e, c_e^s)) \Bigg\} \\
& - \sum_{e \in \mathbb{E}} \mu_e (f_e - \sum_{s \in \mathbb{S}} \pi_s c_e^s) \\
= & \sum_{s \in \mathbb{S}} \pi_s \Bigg\{ \sum_{l \in \mathbb{L}} \Bigg(U_l(\sum_{k \in \mathbb{P}_l} r_l^k) + \lambda_l (d_l - \sum_{k \in \mathbb{P}_l} r_l^k) + v_l b_l \\
& - \sum_{k \in \mathbb{P}_l} r_l^k (\sum_{e \in P_l^k} (v_l l_e^s(f_e, c_e^s) + \mu_e)) \Bigg) + \sum_{e \in \mathbb{E}} \mu_e c_e^s \Bigg\}
\end{aligned}
$$

Define

$$\begin{aligned}
&\mathcal{M}^s(\lambda, \mu, v) \\
&= \sup_{\mathbf{r} \geq 0} \Bigg\{ \sum_{l \in \mathbb{L}} \Bigg(U_l(\sum_{k \in \mathbb{P}_l} r_l^k) + \lambda_l(d_l - \sum_{k \in \mathbb{P}_l} r_l^k) + v_l b_l \\
&- \sum_{k \in \mathbb{P}_l} r_l^k (\sum_{e \in P_l^k} (v_l I_e^s(f_e, c_e^s) + \mu_e)) \Bigg) + \sum_{e \in \mathbb{E}} \mu_e c_e^s \Bigg\}
\end{aligned} \tag{7–7}$$

Let $\tilde{\mathbf{r}}$ be the optimum solution of (7–7). We will discuss how to obtain $\tilde{\mathbf{r}}$ shortly. The dual function of $\mathcal{P}_1$ is obtained by

$$g(\lambda, \mu, v) = \sum_{s \in \mathbb{S}} \pi_s \mathcal{M}^s(\lambda, \mu, v). \tag{7–8}$$

Thus, the dual problem of $\mathcal{P}_1$ is given by

$\underline{\mathcal{P}_2 :}$

$$\min_{\lambda, \mu, \mathbf{v} \geq 0} g(\lambda, \mu, \mathbf{v}). \tag{7–9}$$

7.4.2 Distributed Algorithmic Solution with the Stochastic Primal-Dual Approach

In this subsection, we propose a distributed algorithmic solution of $\mathcal{P}_1$, or equivalently $\mathcal{P}_2$, based on the stochastic primal-dual method. In order to reach the stochastic optimum solution, the dual variables λ, μ and $\mathbf{v}$ are updated according to the following dynamics

$$\lambda_l(n+1) = [\lambda_l(n) - \alpha_l(n)\zeta_l(n)]^+ \ \forall l \in \mathbb{L} \tag{7–10}$$

$$\mu_e(n+1) = [\mu_e(n) - \alpha_e(n)\xi_e(n)]^+ \ \forall e \in \mathbb{E} \tag{7–11}$$

$$v_l(n+1) = [v_l(n) - \alpha_b(n)\rho_l(n)]^+ \ \forall l \in \mathbb{L} \tag{7–12}$$

where $[x]^+$ denotes $\max(0, x)$ and n is the iteration number. $\alpha_l(n)$, $\alpha_e(n)$ and $\alpha_b(n)$ are the current stepsizes while $\zeta_l(n)$, $\xi_e(n)$ and $\rho_l(n)$ are random variables. More precisely, they are named the *stochastic subgradient* of the dual function $g(\lambda, \mu)$ and the following

requirements need to be satisfied

$$\mathfrak{E}\{\zeta_l(n)|\lambda(1),\cdots,\lambda(n)\} = \partial_{\lambda_l} g(\lambda,\mu,\mathbf{v})\ \forall l \in \mathbb{L} \tag{7–13}$$

$$\mathfrak{E}\{\xi_e(n)|\mu(1),\cdots,\mu(n)\} = \partial_{\mu_e} g(\lambda,\mu,\mathbf{v})\ \forall e \in \mathbb{E} \tag{7–14}$$

$$\mathfrak{E}\{\rho_l(n)|\mathbf{v}(1),\cdots,\mathbf{v}(n)\} = \partial_{v_l} g(\lambda,\mu,\mathbf{v})\ \forall l \in \mathbb{L} \tag{7–15}$$

where $\mathfrak{E}(.)$ is the expectation operator and $\lambda(1),\cdots,\lambda(n)$, $\mu(1),\cdots,\mu(n)$ and $\mathbf{v}(1),\cdots,\mathbf{v}(n)$ denote the sequences of solutions generated by (7–10), (7–11) and (7–12), respectively. By Danskin's Theorem [162], we can obtain the subgradients as

$$\zeta_l(n) = d_l - \sum_{k\in\mathbb{P}_l} \tilde{r}_l^k(n)\ \forall l \in \mathbb{L} \tag{7–16}$$

$$\xi_e(n) = c_e^s(n) - \tilde{f}_e(n)\ \forall e \in \mathbb{E} \tag{7–17}$$

$$\rho_l(n) = b_l - \sum_{k\in\mathbb{P}_l} \tilde{r}_l^k(n) \sum_{e\in P_l^k} l_e^s(\tilde{f}_e(n), c_e^s(n))\ \forall l \in \mathbb{L} \tag{7–18}$$

where $\tilde{r}_l^k$ is the optimum solution of (7–7). Note that $c_e^s(n)$ denotes the instantaneous channel capacity on link e at iteration n.

We next show how to calculate $\mathcal{M}^s(\lambda,\mu,\mathbf{v})$ in (7–7), i.e., finding the optimum solution, denoted by $\tilde{\mathbf{r}}$, which maximizes

$$\sum_{l\in\mathbb{L}} \Bigg(U_l(\sum_{k\in\mathbb{P}_l} r_l^k) + \lambda_l(d_l - \sum_{k\in\mathbb{P}_l} r_l^k) + v_l b_l - \sum_{k\in\mathbb{P}_l} r_l^k(\sum_{e\in P_l^k}(v_l l_e^s(f_e, c_e^s) + \mu_e)) \Bigg) + \sum_{e\in\mathbb{E}} \mu_e c_e^s \tag{7–19}$$

Note that when updating the primal variable, i.e., $\mathbf{r}$, the link costs are deterministic which are obtained via the feedback signal, e.g., ACK messages. Therefore, by utilizing the same stochastic subgradient approach, we have

$$r_l^k(n+1) = \left[r_l^k(n) + \alpha_r(n)\eta(n)\right]_0^{d_l} \tag{7–20}$$

where

$$\eta(n) = \frac{\partial U_l}{\partial \sum_{k\in\mathbb{P}_l} r_l^k(n)} - \lambda_l - \sum_{e\in P_l^k} (\mu_e + v_l l_e(f_e, c_e^s)) \tag{7–21}$$

is the stochastic subgradient measured at time n.

Theorem 7.1. *The proposed algorithm converges to the global optimum of $\mathcal{P}_1$ with probability one, if the following constraints of stepsizes are satisfied: (1) $\alpha(n) > 0$, (2) $\sum_{n=0}^{\infty} \alpha(n) = \infty$, and (3) $\sum_{n=0}^{\infty} (\alpha(n))^2 < \infty$, $\forall l \in \mathbb{L}$ and $e \in \mathbb{E}$, where α represents α_e, α_l, α_b and α_r generally.*

Proof. First, let us revisit the updating equations of (7–10), (7–11) and (7–12). Note that in the stochastic subgradient approach, the measured values of $\zeta_l(n)$, $\xi_e(n)$ and $\rho_l(n)$ are considered as the instantaneous observation of the real gradients, denoted by $\overline{\zeta_l(n)}$, $\overline{\xi_e(n)}$ and $\overline{\rho_l(n)}$, respectively. We consider the relationship of $\zeta_l(n)$ and $\overline{\zeta_l(n)}$ for instance. The observation value, i.e., $\zeta_l(n)$, can be rewritten as

$$\begin{aligned} \zeta_l(n) &= \zeta_l(n) - \mathfrak{E}(\zeta_l(n)) + \mathfrak{E}(\zeta_l(n)) - \overline{\zeta_l(n)} + \overline{\zeta_l(n)} \\ &= \overline{\zeta_l(n)} + \mathfrak{E}(\zeta_l(n)) - \overline{\zeta_l(n)} + \zeta_l(n) - \mathfrak{E}(\zeta_l(n)) \\ &= \overline{\zeta_l(n)} + \widetilde{\zeta_l(n)} + \widehat{\zeta_l(n)} \end{aligned} \tag{7–22}$$

where $\mathfrak{E}$ is the expectation operator and

$$\widetilde{\zeta_l(n)} = \mathfrak{E}(\zeta_l(n)) - \overline{\zeta_l(n)} \tag{7–23}$$

$$\widehat{\zeta_l(n)} = \zeta_l(n) - \mathfrak{E}(\zeta_l(n)). \tag{7–24}$$

Note that $\widetilde{\zeta_l(n)}$ is the difference between the expectation of the observations and the real gradient. Hence, it is the biased estimation error term. Next, we examine that

$$\mathfrak{E}(\widehat{\zeta_l(n)} | \widehat{\zeta_l(n-1)}, \cdots, \widehat{\zeta_l(0)}) = 0 \ \forall n. \tag{7–25}$$

Therefore, the series of $\widehat{\zeta_l(n)}$ is a martingale difference sequence [163]. The relationship of (7–22) indicates that the observation value is the real gradient disturbed by a biased estimation error as well as a martingale difference noise. We next investigate the convergence conditions of the stochastic primal-dual approach. For $\widetilde{\zeta_l(n)}$, the following requirement

$$\sum_{n=0}^{\infty} \alpha_e(n) |\mathfrak{E}(\zeta_l(n)) - \overline{\zeta_l(n)}| < \infty \tag{7–26}$$

is satisfied due to the stationary assumption. Similarly,

$$\mathfrak{E}(\widehat{\zeta_l(n)}^2) = \mathfrak{E}\left((\zeta_l(n) - \mathfrak{E}(\zeta_l(n)))^2\right) \tag{7–27}$$

is bounded as well. The similar analysis can be extended to $\xi_e(n)$, $\rho_l(n)$ and $\eta(n)$ in (7–11), (7–12) and (7–20) straightforwardly. Therefore, the standard conditions are satisfied and the convergence result of Theorem 1 follows [8].

It is worth noting that the aforementioned distributed algorithm enjoys the merit of distributed implementation from an engineering perspective. With the current values of dual variables, each source node $S(l)$ optimizes (7–19) according to (7–21) and (7–20). The information needed is either locally attainable or acquirable by the feedback along the paths. For example, the channel states of the intermediate nodes along paths can be piggybacked by the end-to-end acknowledgement messages from the destination node, i.e., the gateway node in our scenario. The source node updates the λ_l and v_l according to (7–10) and (7–12) where the needed information is calculated by (7–16) and (7–18), respectively. For each link e, the current status of (7–17) is measured. Next, the value of μ_e is updated following (7–11). The iteration continues until an equilibrium point is reached. Note that our framework can incorporate the wireless lossy network scenarios by replacing the flow rate with the effective flow rate in the leaky-pipe flow model [164].

7.5 Stochastic Traffic Engineering without Convexity

Thus far, we have considered the scenarios where all the users have concave utility functions. However, in practice, several network applications may possess a non-concave utility function. For example, in a data streaming application, the user is satisfied if the achieved data rate exceeds a threshold, where the utility function is a step function and thus the convexity does not preserve. Therefore, the proposed stochastic primal-dual approach in Section 7.4 cannot be applied here. It is worth noting that we can still formulate the stochastic traffic engineering problem as in $\mathcal{P}_1$ except that the optimization problem is a stochastic non-convex programming, which is NP-hard in general, and computationally prohibitive to solve even in a centralized fashion [165]. In the following section, we will propose an algorithmic solution to the non-convex stochastic traffic engineering problem, based on the *learning automata* techniques. Moreover, we analytically show that the proposed algorithm will converge to the global optimum solution asymptotically, in a decentralized fashion.

We first convert the compact strategy space of each user into a discretized set denoted by $\mathbb{R}$. More specifically, each user, say l, maintains a probability vector $\mathbf{p}_{l,k}$ for each path $k \in \mathbb{P}_l$. The segment of $[0, r^m]$ is quantized into Q sections where r^m is the maximum allowed transmission rate on any path. In other words, the continuous variable r_l^k is transformed into a discrete random variable, $r_{l,k}^q$, within a discretized set $\mathbb{R}$ with $Q+1$ elements. The data rate is randomly selected from $\mathbb{R}$ according to the probability vector of $\mathbf{p}_{l,k}$ where the q-th element, $p_{l,k}^q$, $q = 0, \cdots, Q$, denotes the probability that the l-th user transmits with a rate of $r_{l,k}^q = q \times \frac{r^m}{Q}$ on the k-th path of $\mathbb{P}_l$. Associated with each probability vector $\mathbf{p}_{l,k}$, there is a *weighting vector* $\mathbf{w}_{l,k}$ with the same dimension of $1 \times (Q+1)$. The probability vector $\mathbf{p}_{l,k}$ is uniquely determined by the weighting vector $\mathbf{w}_{l,k}$ by the *softmax function* [166],

$$p_{l,k}^q = \frac{e^{w_{l,k}^q}}{\sum_{q=0}^{Q} e^{w_{l,k}^q}} \; \forall l, k, q \tag{7–28}$$

where $w_{l,k}^q$ is the q-th element of $\mathbf{w}_{l,k}$, $q = 0, \cdots, Q$.

Next, we formulate an *identical interest game* where the players are the $|\mathbb{L}|$ source nodes and the common objective function is the overall network utility, i.e., the summation of the utility functions. In addition, for each source node, a team of learning automata [167] is constructed. At each time step, every source node picks the data rates on its own paths according to the probability vectors, which are determined by the weighting vectors. Based on the feedback signal Ξ, which will be defined shortly, each source node adjusts the weighting vectors and the iteration continues. The executed algorithm on every source node, say l, is provided as follows.

Algorithm:

Repeat:

- For every path, say k, randomly selects a transmission rate $r_{l,k}^j$ from $\mathbb{R}$, according to the current probability vector $\mathbf{p}_{l,k}(n)$ where n denotes the current time slot.
- After receiving the feedback signal $\Xi(n)$ from the gateway node, if the cost constraint is satisfied, the weighting vector $\mathbf{w}_{l,k}$ is updated as

$$w_{l,k}^q(n+1) = \left[w_{l,k}^q(n) + \tau(n)\Xi(n)(1 - \frac{e^{w_{l,k}^q}}{\sum_{q=0}^{Q} e^{w_{l,k}^q}}) + \sqrt{\tau(n)}\varsigma_{l,k}^q(n) \right]_0^{\mathcal{L}} \text{ for } q = j;$$
$$w_{l,k}^q(n+1) = \left[w_{l,k}^q(n) + \sqrt{\tau(n)}\varsigma_{l,k}^q(n) \right]_0^{\mathcal{L}} \text{ for } q \neq j; \quad (7\text{–}29)$$

  Otherwise, the weighting vector remains the same.
- The probability vector $\mathbf{p}_{l,k}$ is then updated, following equation (7–28).

Until:

- $\max(\mathbf{p}_{l,k}(n+1)) > B$ where B is a predefined convergence threshold.

In the algorithm, $\tau(n)$ is the *learning parameter* of the algorithm satisfying $0 < \tau(n) < 1$. $\mathcal{L}$ is a sufficiently large yet finite number which keeps the weighting vector bounded. The sequence of $\varsigma_{l,k}^q(n)$ is a set of i.i.d. random variables with zero mean and a variance of $\sigma^2(n)$. The global feedback signal $\Xi(n)$ is calculated by the gateway node

and sent back to all source nodes, as

$$\Xi(n) = \frac{\sum_{l \in \mathcal{L}} (U_l(\sum_{k \in \mathbb{P}_l} r_l^k))}{\mathcal{J}} \tag{7–30}$$

where $\mathcal{J}$ is a number to normalize the feedback signal. For example, we can set $\mathcal{J}$ to the maximum value of overall utility till n and update this value on the fly. Therefore, the value of $\Xi(n)$ lies within $[0, 1]$. U_l is the non-convex utility function for the l-th user. Note that the utility functions of all users are assumed to be truly acquired by the gateway node [168]. In practice, the value of $\Xi(n)$ can be circulated efficiently by established multicast algorithms such as [169]. Based on the feedback, the learning automata team adjusts the weighting vector in a decentralized fashion. In addition, note that B is the predefined convergence threshold, e.g., $B = 0.999$, which provides a tradeoff between the performance of the algorithm and its convergence speed.

Before analyzing the steady state behavior of the proposed algorithm, we first discuss the following concepts.

Denote the maximum network utility of the original traffic engineering problem, i.e., $\mathcal{P}_1$, as O^*. Next, we define the final outcome of the proposed algorithm as O'. We say that the algorithm provides an ϵ-accurate solution, if for any arbitrarily small $\epsilon > 0$, there exists a Q' such that

$$|O^* - O'| < \epsilon \; \forall Q > Q' \tag{7–31}$$

A potential game [67] is defined as a game where there exists a potential function V such that

$$V(a', a_{-l}) - V(a'', a_{-l}) = U_l(a', a_{-l}) - U_l(a'', a_{-l}) \; \forall l, a', a'' \tag{7–32}$$

where U_l is the utility function for player l and a', a'' are two arbitrary strategies in its strategy space. The notation of a_{-l} denotes the vector of choices made by all players other than l.

A weighted potential game [67] is defined as a game where there exists a potential function V such that

$$(V(a', a_{-l}) - V(a'', a_{-l})) \times h_i = U_l(a', a_{-l}) - U_l(a'', a_{-l}) \tag{7–33}$$

for all l, a', a'' where $h_i > 0$.

According to the definitions, it is apparent that the formulated identical interest game is a special case of weighted potential games. In the following theorem, we will provide the convergence behavior of a more general setting for weighted potential games, and hence the result applies to our specific scenario naturally.

Theorem 7.2. *For an N-person weighted potential game where each person represents a team of learning automata, the proposed algorithm can converge to the global optimum solution asymptotically, which is an ϵ-accurate solution to the original stochastic traffic engineering problem, for sufficient small value of τ and σ.*

Proof. The proof follows similar lines as in [167]. However, we extend the result to a more general setting where the underlying N-person stochastic game is a weighted potential game. Therefore, the proof in [167] can be viewed as a special case. Define V as the potential function of the game. Note that the selected rate is determined by the probability vector which is generated uniquely by the weighting vector. Therefore, we can view the weighting vector as the variable in this case and the objective function is given by $z = \mathfrak{E}(V|\mathbf{w})$. In the updating procedure of (7–29), signal Ξ is replaced by V. We first verify that

$$\frac{\partial z}{\partial w_{l,k}^q} = \frac{\partial \mathfrak{E}(V|\mathbf{w})}{\partial w_{l,k}^q} = \frac{\partial \sum_q p_{l,k}^q \mathfrak{E}(V|\mathbf{w}, r_{l,k}^q)}{\partial w_{l,k}^q} = \sum_q \frac{e^{w_{l,k}^q}}{\sum_{q=0}^{Q} e^{w_{l,k}^q}} (1 - \frac{e^{w_{l,k}^q}}{\sum_{q=0}^{Q} e^{w_{l,k}^q}}) \mathfrak{E}(V|\mathbf{w}(n), r_{l,k}^q).$$

Note that

$$
\begin{aligned}
& \mathfrak{E}(V(1-\frac{e^{w_{l,k}^q}}{\sum_{q=0}^{Q} e^{w_{l,k}^q}})|\mathbf{w}(n)) \\
= & \sum_q p_{l,k}^q (1-\frac{e^{w_{l,k}^q}}{\sum_{q=0}^{Q} e^{w_{l,k}^q}})\mathfrak{E}(V|\mathbf{w}(n), r_{l,k}^q) \\
= & \sum_q \frac{e^{w_{l,k}^q}}{\sum_{q=0}^{Q} e^{w_{l,k}^q}}(1-\frac{e^{w_{l,k}^q}}{\sum_{q=0}^{Q} e^{w_{l,k}^q}})\mathfrak{E}(V|\mathbf{w}(n), r_{l,k}^q) \\
= & \frac{\partial z}{\partial w_{l,k}^q}.
\end{aligned}
$$

Next, it is straightforward to verify that the standard conditions in [170] (Chap.6, Theorem 7) are satisfied. We omit the verifications since they are the similar procedures as in [167]. Thus, we conclude that the above dynamic weakly converges to the following SDE [170, 171]

$$
d\mathbf{w} = \nabla z + \sigma d\mathcal{W} \tag{7–34}
$$

for a sufficiently small $\tau \rightarrow 0$ where σ is the standard deviation of the i.i.d. random variables $\varsigma_{l,k}^q$ and $\mathcal{W}$ is a standard Wiener Process. Note that the SDE (7–34) falls into the category of Langevin equation [172] which is well-known that the probability measure concentrates on the global maximum solution of z for a sufficiently small σ [167, 172]. Therefore, we conclude that in the weighted potential game scenario, the proposed algorithm will converge to the global optimum of the objective function, for the quantized data rate setting. The association of the ϵ-accurate solution to the original stochastic traffic engineering problem of $\mathcal{P}_1$ follows the result of [173].

Note that Theorem 2 establishes the convergence behavior of the aforementioned algorithm with no additional requirement for the problem structure. In contrast, we propose a stochastic primal-dual approach in Section 7.4, which requires the underlying problem to be a stochastic convex programming. The stochastic primal-dual approach cannot be applied efficiently otherwise. However, the aforementioned learning-based algorithm is suitable for almost every aspect such as stochastic

non-convex programming and stochastic mixed-integer programming. The asymptotically convergence result still holds. Therefore, in this work, the proposed algorithms provide two different exemplifying methods for protocol designs under the stochastic environment. However, it is worth noting that for the latter approach, the tradeoff for general applicability is the convergence speed. In other words, in order to achieve an accurate result, i.e., when ϵ is small, the convergence speed may be slow. The actual convergence speed depends on the values of ϵ, Q, τ, σ as well as the inherent structure of the problem and hence is difficult to quantify. Fortunately, in practical applications, achieving a "good enough" result is sometimes satisfactory. This tradeoff can be achieved by utilizing diminishing values of τ and σ, as demonstrated in the simulated annealing literature [78] and [174]. To sum up, if the stochastic traffic engineering problem possesses a nice property of convexity, the algorithm based on the stochastic primal-dual approach in Section 7.4 is recommended due to its nice decomposed structure and computationally efficient solution. However, if the problem is non-convex in nature, the learning automata based algorithm can be utilized to achieve an approximate solution. The tradeoff between the accuracy and convergence speed can be tuned by adjusting the values of τ and σ.

7.6 Performance Evaluation

In this section, we present a simple yet illustrative example to demonstrate the theoretical results. We consider a cognitive wireless mesh network[3] depicted in Figure 7-2. There are three edge routers as the source nodes, denoted by A, B, C, which transmit to the gateway node GW via the relay routers X, Y and Z. Among all feasible

[3] Figure 7-2 only shows the links on the available paths obtained by the signalling mechanisms or manually configurations. The actual physical topology of the network can be potentially larger.

paths, we select the following available paths for edge routers, as summarized in Table 7-1.

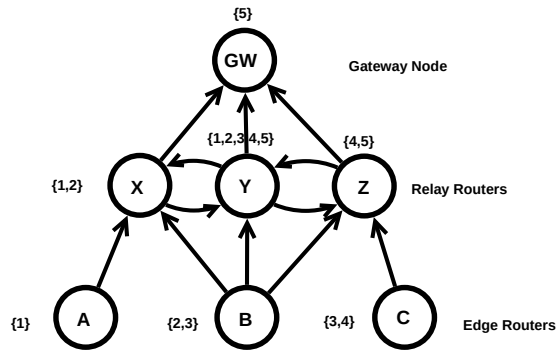

Figure 7-2. Example of cognitive wireless mesh network

Table 7-1. Available paths for edge routers

A	P_A^1:	$\{A \to X \to GW\}$
	P_A^2:	$\{A \to X \to Y \to GW\}$
	P_A^3:	$\{A \to X \to Y \to Z \to GW\}$
B	P_B^1:	$\{B \to X \to GW\}$
	P_B^2:	$\{B \to Y \to GW\}$
	P_B^3:	$\{B \to Y \to X \to GW\}$
	P_B^4:	$\{B \to Y \to Z \to GW\}$
	P_B^5:	$\{B \to Z \to GW\}$
C	P_C^1:	$\{C \to Z \to GW\}$
	P_C^2:	$\{C \to Z \to Y \to GW\}$
	P_C^3:	$\{C \to Z \to Y \to X \to GW\}$

There are five primary users in the area, denoted by $1, 2, 3, 4$ and 5 where each one has a primary band of $10MHz$. The common ISM band is assumed to be $10MHz$. The return probability of the primary users is given as $\varpi = [0.2, 0.3, 0.4, 0.3, 0.3]$. The transmitting power of each node is fixed as $100mW$ and the noise power is assumed to be $3mW$. We consider a model where the received power is inversely proportional to the square of the distance. Note that the transmitting power is uniformly spread on all available bands. In addition, we explicitly specify the affecting primary users for a particular node. We use $\{i, j, k, \cdots\}$ to represent that a particular node is affected by primary user $i, j, k, \cdots$. For example, node X is labeled with $\{1, 2\}$ which indicates that

the transmission of node X will devastate the transmissions of primary user 1 and 2 if the corresponding primary band is utilized. Note that the central node, namely, Y, is most severely affected by all primary users. Intuitively, to achieve an expected optimum solution, the stochastic traffic engineering algorithms are inclined to steer the traffic away from Y. We will demonstrate this *detour effect* next.

We first consider the cognitive wireless mesh network with convexity, e.g., $U_l(x_l) = \log x_l$ to achieve a proportional fairness among the flows [161]. The link cost is assumed to be in the form of $l_e^s(f_e, c_e^s) = \frac{1}{c_e^s - f_e}$, which reflects the delay experienced for a unit flow on link e under the $M/M/1$ assumption [76]. Note that if $f_e \geq c_e$, the cost is $+\infty$. We set the traffic demand of all edge routers as $d_l = 30Mbps$ while the cost budget is $b_l = 5$. The step sizes are chosen as $\alpha = 1/n$ where n is the current iteration step. Figure 7-3A illustrates the trajectories of the rate variables and Figure 7-3B shows the convergence of the network overall utility as well as the individual utility functions[4] . We observe that while the rate variables converge as the iterations go, the overall objective, i.e., the sum of the individual utilities, approaches to the global optimum indicated by the dashed line, which is attained by calculating the steady state distribution following the return probability ϖ.

In addition, Table 7-2 provides the rate on each path after convergence for a sample run of the algorithm. For comparison, we provide the convergence rates when node Y is switched from the most affected node to the *least affected* node, i.e., node Y can utilize all five primary bands all the time, in Table 7-3. From Table 7-2 and 7-3, it is interesting to note that, in the first scenario, each user allocates a relatively small amount of flow on the paths which traverse through node Y. On the contrary, when node Y is less affected, all the flows allocate noticeably larger data rates on paths that traverse through

[4] Note that Figure 7-3B also reflects the evolution of the throughput of each edge router logarithmically.

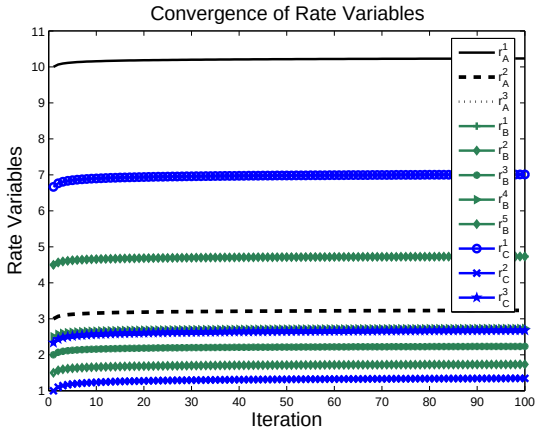

A Trajectories of Rate Variables

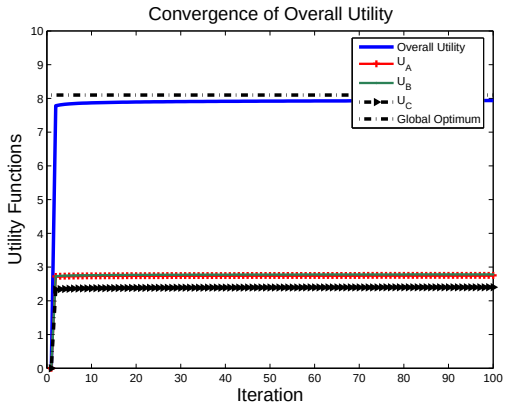

B Trajectories of Utility Functions

Figure 7-3. Cognitive wireless mesh networks with convexity

Y despite the fact that node Y is the central node which is least favorable by traditional traffic engineering solutions. Therefore, our proposed stochastic traffic engineering algorithm is of particular interest for multi-hop cognitive wireless mesh networks due to the capability of steering the traffic away from the severely affected areas automatically, without a prior knowledge of the underlying probabilistic structure, in a distributed fashion.

Table 7-2. Convergence rates when Y is affected by all five primary users

A	P_A^1:	15.3035
	P_A^2:	3.2458
	P_A^3:	2.7362
B	P_B^1:	7.3725
	P_B^2:	1.9584
	P_B^3:	2.1752
	P_B^4:	2.6458
	P_B^5:	5.3489
C	P_C^1:	17.3051
	P_C^2:	2.3792
	P_C^3:	2.5675

Table 7-3. Convergence rates when Y is not affected by any of the primary users

A	P_A^1:	9.6413
	P_A^2:	11.1335
	P_A^3:	9.1861
B	P_B^1:	5.0101
	P_B^2:	6.2625
	P_B^3:	4.9711
	P_B^4:	4.9921
	P_B^5:	8.7878
C	P_C^1:	15.3118
	P_C^2:	9.1042
	P_C^3:	5.6121

We next consider a cognitive wireless mesh network with non-convex utility functions. Specifically, we consider the utility function as

$$U_l(x_l) = \begin{cases} 1, & \text{if } x_l \geq 2Mbps \\ 0, & \text{if } x_l < 2Mbps. \end{cases} \tag{7–35}$$

while other settings are the same as in the previous scenario. Additionally, we utilize diminishing values of τ and σ as $\tau = 1/n$ and $\sigma = 1/n$, where n is the iteration step[5] . Without loss of generality, we set $\mathcal{L} = 100$ and the quantization level $Q = 20$. The

[5] By utilizing diminishing parameters, a tradeoff between the performance and the convergence speed can be achieved by tuning the decreasing speed [78].

maximum allowed rate r^m is assumed to be 10. Therefore, the discretized data rate set is given by $\mathbb{R} = [0.5, 1.0, 1.5, \cdots, 9.0, 9.5, 10.0]$. Figure 4 illustrates the evolution of the probability vector of $\mathbf{p}_{A,1}$. Note that as the iterations evolve, the probability of $p^{20}_{A,1}$, i.e., the probability that router A chooses the twentieth data rate (r^m in this case), excels others and approaches to 1 asymptotically. We plot the evolutions of the probability vectors of other paths in Figure 5 collectively. For each path, the probability of selecting one particular data rate soon excels others. We observe that router A selects the twentieth, the first and the fourth date rate on its three paths asymptotically. Meanwhile, router B inclines to choose the eighth, the second, the first, the fourth and the twentieth data rate on its paths. The steady state data rates for router C is the twentieth, the first and the first element in $\mathbb{R}$, as depicted in Figure 5. It is interesting to notice that all the routers automatically detour the traffic from the severely affected node Y by allocating more data rate on other paths.

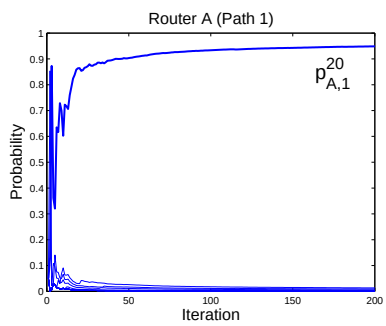

Figure 7-4. Trajectory of the probability vector of router A's first path

7.7 Conclusions

In this chapter, we investigate the stochastic traffic engineering (STE) problem in cognitive wireless mesh networks. To harness the randomness induced by the unpredictable behaviors of primary users, we formulate the STE problem in a stochastic network utility maximization framework. For the cases where convexity holds, we derive a distributed algorithmic solution via the stochastic primal-dual approach, which provably converges to the global optimum solution. For the scenarios where convexity is not

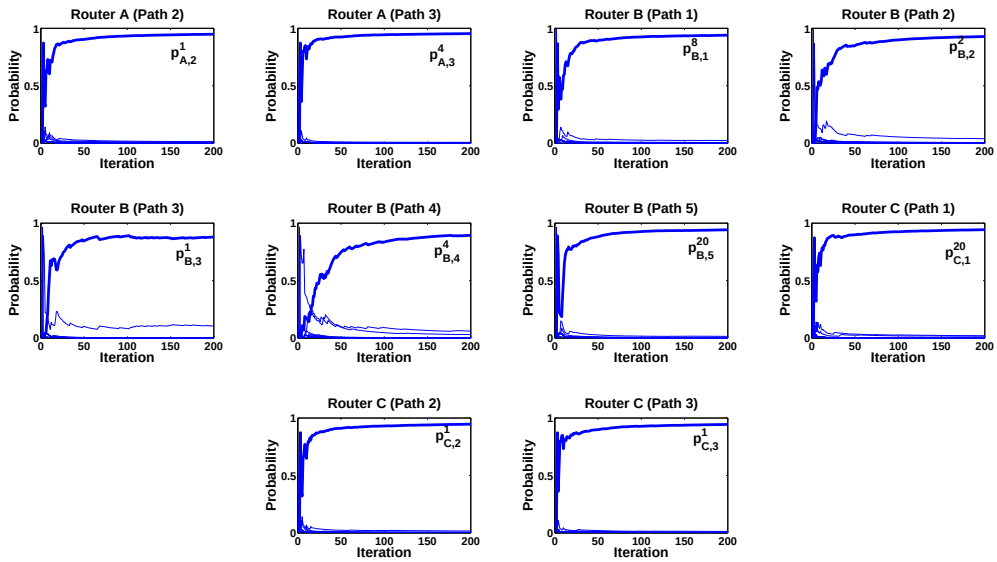

Figure 7-5. Trajectories of the probability vectors on other paths

attainable, we propose an alternative decentralized algorithmic solution based on the learning automata techniques. We show that the algorithm converges to the global optimum solution asymptotically, under certain conditions.

In our work, we restrict ourself in a single gateway scenario. The extension to the multiple gateway scenario seems interesting and needs further investigation. In addition, in this work, we consider a cooperative case where all the edge routers attempt to maximize the overall network performance. In the cases where the edge routers are non-cooperative, each player is interested in its own utility rather than the social welfare. Stochastic game theory provides a feasible tool to address the non-cooperative case, which remains as future research. We also assume a negligible delay for the feedback signal while in a more general case, the impact of feedback delay needs further investigation. One feasible solution is to utilize the distributed robust optimization framework [175] where the worst case performance is maximized given that the feedback delay/error is within a reasonable range. Our work initiates a first step to investigate the impact of unpredictable returns of primary users, on the stochastic traffic engineering problem in cognitive wireless mesh networks.

CHAPTER 8
CONCLUSIONS

In this dissertation, we provide efficient and effective solutions to a number of dynamic resource allocation and optimization problems in wireless networks with time-varying channel conditions.

For wireless ad hoc networks, we first develop a dynamic pricing scheme which can achieve a network-wide stability while maximizing the accumulated revenue with a controllable tradeoff with the average delay. In addition, a service differentiation solution can be achieved by prioritizing the flows according to their QoS requirements. We also propose a minimum energy scheduling algorithm which minimizes the overall energy consumption in the network without decreasing the throughput region. For wireless mesh networks, we investigate the joint frequency and power allocation problem among multiple access points in a game theoretical framework. The proposed negotiation-based algorithm can achieve the optimal frequency and power allocation with arbitrarily high probability. The price of anarchy in non-cooperative wireless mesh networks is also studied. For wireless sensor networks, we propose a constrained queueing model to capture the complex cross layer interactions among multiple sensor nodes. We also study the stochastic network utility maximization problem and propose a cross layer solution which solves the problems of admission control, load balancing, dynamic scheduling and routing in a collective fashion. For wireless local area networks, we study the thresholds-based rate adaptation algorithms from a reverse engineering perspective, where the implicit objective function is revealed. We also investigate the stochastic traffic engineering problem in multi-hop cognitive radio networks, where distributed algorithms are developed to maximize the overall network utility.

REFERENCES

[1] G. R. Gupta and N. Shroff, "Delay analysis for multi-hop wireless networks," *IEEE INFOCOM*, 2009.

[2] M. Andrews and L. Zhang, "Satisfying arbitrary delay requirements in multi-hop networks," *IEEE INFOCOM*, 2008.

[3] M. Chiang, "Balancing transport and physical layer in wireless multihop networks: Jointly optimal congestion control and power control," *IEEE Journal on Selected Areas in Communications*, pp. 104–116, 2005.

[4] M. Chiang, S. H. Low, A. R. Calderbank, and J. C. Doyle, "Layering as optimization decomposition: A mathematical theory of network architectures," *Proceedings of the IEEE*, pp. 255–312, Mar. 2007.

[5] A. Eryilmaz and R. Srikant, "Fair resource allocation in wireless networks using queue-length-based scheduling and congestion control," *IEEE INFOCOM*, 2005.

[6] F. Kelly, A. Maulloo, and D. Tan, "Rate control for communication networks: Shadow prices, proportional fairness and stability," *Journal of the Operational Research Society*, pp. 237–252, 1998.

[7] S. H. Low and D. E. Lapsley, "Optimization flow control, i: Basic algorithm and convergence," *IEEE/ACM Transactions on Networking*, pp. 861–875, 1999.

[8] J. Zhang, D. Zheng, and M. Chiang, "The impact of stochastic noisy feedback on distributed network utility maximization," *IEEE Transactions on Information Theory*, 2008.

[9] S. Boyd and L. Vandenberghe, *Convex Optimization*. Cambridge University Press, 2003.

[10] R. Srikant, *The Mathematics of Internet Congestion Control*. Birkhauser Boston, 2003.

[11] S. Shakkottai and R. Srikant, *Network Optimization and Control*. Foundations and Trends in Networking, 2008.

[12] L. Tassiulas and A. Ephremides, "Stability properties of constrained queueing systems and scheduling policies for maximum throughput in multihop radio networks," *IEEE Transactions on Automatic Control*, pp. 1936–1949, 1992.

[13] M. J. Neely, E. Modiano, and C. E. Rohrs, "Dynamic power allocation and routing for time-varying wireless networks," *IEEE Journal on Selected Areas in Communications*, pp. 89–103, Jan. 2005.

[14] M. J. Neely, “Dynamic power allocation and routing for satellite and wireless networks with time varying channels,” Ph.D. dissertation, Masssachusetts Institute of Technology, LIDS, 2003.

[15] M. J. Neely, E. Modiano, and C.-P. Li, “Fairness and optimal stochastic control for heterogeneous networks,” *IEEE/ACM Transactions on Networking*, pp. 396–409, April 2008.

[16] M. J. Neely, “Energy optimal control for time varying wireless networks,” *IEEE Transactions on Information Theory*, pp. 2915–2934, July 2006.

[17] L. Georgiadis, M. J. Neely, and L. Tassiulas, *Resource Allocation and Cross-Layer Control in Wireless Networks*. Foundations and Trends in Networking, 2006.

[18] Y. Xi and E. M. Yeh, “Distributed algorithms for spectrum allocation, power control, routing, and congestion control in wireless networks,” *ACM MOBIHOC*, 2007.

[19] ——, “Node-based optimal distributed power control, routing, and congestion control in wireless networks,” *IEEE Transactions on Information Theory*, pp. 4081–4106, 2008.

[20] Y. Song, C. Zhang, and Y. Fang, “Routing optimization in wireless mesh networks under uncertain traffic demands,” *ICST Fifth International Conference on Quality of Service in Heterogeneous Wired/Wireless Networks (QShine)*, 2008.

[21] M. Andrews, K. Kumaran, K. Ramanan, A. Stolyar, P. Whiting, and R. Vijayakumar, “Providing quality of service over a shared wireless link,” *IEEE Communications Magazine*, 2001.

[22] A. Stolyar, “Control of end-to-end delay tails in a multiclass network: Lwdf discipline optimality,” *The Annals of Applied Probability*, 2003.

[23] T. B. Reddy, I. Karthigeyan, B. S. Manoj, and C. S. R. Murthy, “Quality of service provisioning in ad hoc wireless networks: A survey of issues and solutions,” *Ad Hoc Networks*, 2006.

[24] B. Zhang and H. T. Mouftah, “Qos routing for wireless ad hoc networks: Problems, algorithms, and protocols,” *IEEE Communications Magazine*, 2005.

[25] M. A. Zafer and E. Modiano, “A calculus approach to minimum energy transmission policies with quality of service guarantees,” *IEEE INFOCOM*, 2005.

[26] W. Chen, M. J. Neely, and U. Mitra, “Energy-efficient transmissions with individual packet delay constraints,” *IEEE Transactions on Information Theory*, pp. 2090–2109, 2008.

[27] L. He and J. Walrand, “Pricing differentiated internet services,” *IEEE INFOCOM*, 2005.

[28] T. Basar and R. Srikant, “Revenue-maximizaing pricing and capacity expansion in a many-users regime,” *IEEE INFOCOM*, 2002.

[29] R. K. Lam, D.-M. Chiu, and J. C. Lui, “On the access pricing and network scaling issues of wireless mesh networks,” *IEEE Transactions on Computers*, pp. 1456–1469, 2007.

[30] Shakkottai and R. Srikant, “Economics of network pricing with multiple isps,” *IEEE/ACM Transactions on Networking*, 2006.

[31] N. J. Keon and G. Anandalingam, “Optimal pricing for multiple services in telecommunications networks offering quality-of-service guarantees,” *IEEE/ACM Transactions on Networking*, pp. 66–80, 2003.

[32] Z. Zhang, D. Dey, and Y. Tan, “Pricing communication services with delay guarantee,” *INFORMS Journal on Computing*, pp. 248–260, 2007.

[33] L. Huang and M. J. Neely, “The optimality of two prices: Maximizaing revenue in a stochastic network,” *Proc. Allerton Conf. of Comm, Control, and Computing*, 2007, invited paper.

[34] A. Stolyar, “Maximizing queueing network utility subject to stability: Greedy primal-dual algorithm,” *Queueing Systems*, pp. 401–457, 2005.

[35] A. Brzezinski, G. Zussman, and E. Modiano, “Distributed throughput maximization in wireless mesh networks via pre-partitioning,” *IEEE/ACM Transactions on Networking*, 2008.

[36] C. Joo, “A local greedy scheduling scheme with provable performance guarantee,” *ACM MOBIHOC*, 2008.

[37] A. Gupta, X. Lin, and R. Srikant, “Low-complexity distributed scheduling algorithms for wireless networks,” *IEEE INFOCOM*, 2007.

[38] A. Stolyar, “Dynamic distributed scheduling in random access networks,” *Journal of Applied Probability*, pp. 297–313, 2008.

[39] N. B. Chang and M. Liu, “Optimal channel orobing and transmission scheduling for opportunistic spectrum access,” *ACM MOBICOM*, 2007.

[40] X. Lin and N. Shroff, “The impact of imperfect scheduling on cross-layer rate control in wireless networks,” *IEEE INFOCOM*, 2005.

[41] B. Radunovic, C. Gkantsidis, D. Gunawardena, and P. Key, “Horizon: Balancing tcp over multiple paths in wireless mesh network,” *ACM MOBICOM*, 2008.

[42] U. Akyol, M. Andrews, P. Gupta, J. Hobby, I. Saniee, and A. Stolyar, “Joint scheduling and congestion control in mobile ad-hoc networks,” *IEEE INFOCOM*, 2008.

[43] A. Warrier, S. Janakiraman, and I. Rhee, “Diffq: Practical differential backlog congestion control for wireless networks,” *IEEE INFOCOM*, 2009.

[44] Y. Yi, A. Proutiere, and M. Chiang, “Complexity in wireless scheduling: Impact and tradeoffs,” *ACM MOBIHOC*, 2008.

[45] E. Modiano, D. Shah, and G. Zussman, “Maximizing throughput in wireless networks via gossiping,” *ACM SIGMETRICS*, 2006.

[46] L. Jiang and J. Walrand, “A distributed csma algorithm for throughput and utility maximization in wireless networks,” *Proc. Allerton Conf. of Comm, Control, and Computing*, 2008.

[47] S. Rajagopalan and D. Shah, “Reversible networks, distributed optimization, and network scheduling: What do they have in common?” *Proc. Conf. on Information Sciences and Systems (CISS)*, 2008.

[48] X. Wu, R. Srikant, and J. Perkins, “Scheduling efficiency of distributed greedy scheduling algorithms in wireless networks,” *IEEE Transactions on Mobile Computing*, 2007.

[49] C. Joo, X. Lin, and N. Shroff, “Understanding the capacity region of the greedy maximal scheduling algorithm in multi-hop wireless networks,” *IEEE INFOCOM*, 2008.

[50] T. Hou, Y. Shi, and H. D. Sherali, “Rate allocation in wireless sensor networks with network lifetime requirement,” *ACM MOBIHOC*, 2004.

[51] I. F. Akyildiz and X. Wang, “A survey on wireless mesh networks,” *IEEE Communications Magazine*, no. 9, pp. S23–S30, 2005.

[52] H.-J. Ju and I. Rubin, “Backbone topology synthesis for multiradio mesh networks,” *IEEE Journal on Selected Areas in Communications*, Nov. 2006.

[53] J. Zhu and S. Roy, “802.11 mesh networks with two-radio access points,” *IEEE ICC*, pp. 3609–3615, 2005.

[54] [Online]. Available: http://moment.cs.ucsb.edu/meshnet/

[55] A. K. Das, R. Vijayakumar, and S. Roy, “Static channel assignment in multi-radio multi-channel 802.11 wireless mesh networks: Issues, metrics, and algorithms,” *IEEE GLOBECOM*, 2006.

[56] R. Vedantham, S. Kakumanu, S. Lakshmanan, and R. Sivakumar, “Component based channel assignment in single radio, multi-channel ad hoc networks,” *ACM MOBICOM*, pp. 378–389, 2006.

[57] A. H. M. Rad and V. W. S. Wong, “Joint channel allocation, interface assignment and mac design for multi-channel wireless mesh networks,” *IEEE INFOCOM*, 2007.

[58] C. Eklund, R. B. Marks, K. L. Stanwood, and S. Wang, “Ieee standard 802.16: A technical overview of the wirelessman-tm air interface for broadband wireless access,” *IEEE Communications Magazine*, pp. 98–107, 2002.

[59] C.-C. Chen, E. Seo, H. Luo, N. H. Vaidya, and X. Wang, “Rate-adaptive framing for interfered wireless networks,” *IEEE INFOCOM*, 2007.

[60] C. Na, J. K. Chen, and T. S. Rappaport, “Measured traffic statistics and throughput of ieee 802.11b public wlan hotspots with three different applications,” *IEEE Transactions on Wireless Communications*, pp. 3296–3305, Nov. 2006.

[61] X. Yang, G. Feng, and D. S. C. Kheong, “Call admission control for multiservice wireless networks with bandwidth asymmetry between uplink and downlink,” *IEEE Transactions on Vehicular Technology*, Jan. 2006.

[62] Q. Pang, S. C. Liew, and V. C. M. Leung, “Performance improvement of 802.11 wireless network with tcp ack agent and auto-zoom backoff algorithm,” *IEEE Vehicular Technology Conference*, pp. 2046–2050, 2005.

[63] S. W. Kim, B.-S. Kim, and Y. Fang, “Downlink and uplink resource allocation in ieee 802.11wireless lans,” *IEEE Transactions on Vehicular Technology*, Jan. 2005.

[64] J. Proakis, *Digital Communication*. McGraw-Hill Science/Engineering/Math (4 edition), 2000.

[65] C. Peng, F. Yang, Q. Zhang, D. Wu, M. Zhao, and Y. Yao, “Impact of power and rate selection on the throughput of ad hoc networks,” *IEEE ICC*, pp. 3898–3902, 2006.

[66] J. Neel, J. Reed, and R. Gilles, “Game models for cognitive radio algorithm analysis,” *SDR Forum Technical Conference*, 2004.

[67] D. Monderer and L. Shapley, “Potential games,” *Journal of Games and Economic Behavior*, pp. 124–143, 1996.

[68] V. Srivastava, J. Neel, A. Mackenzie, R. Menon, L. Dasilva, J. Hicks, J. H. Reed, and R. Gilles, “Using game theory to analyze wireless ad hoc networks,” *IEEE Communications Surveys and Tutorials*, pp. 46–56, 2005.

[69] J. Neel, “Analysis and design of cognitive radio networks and distributed radio resource management algorithms,” Ph.D. dissertation, Virginia Polytechnic Institute and State University, 2006.

[70] J. Marden and G. Arslan, “Joint strategy fictitious play with inertia for potential games,” *IEEE Conference on Decision and Control*, 2005.

[71] N. Nie, C. Comaniciu, and P. Agrawal, “A game theoretic approach to interference management in cognitive networks,” *In Proceeding of IMA*, 2006.

[72] N. Nie and C. Comaniciu, “Adaptive channel allocation spectrum etiquette for cognitive radio networks,” *IEEE DySPAN*, 2005.

[73] J. Neel and J. Reed, “Performance of distributed dynamic frequency selection schemes for interference reducing networks,” *IEEE MILCOM*, 2006.

[74] G. Arslan, M. F. Demirkol, and Y. Song, “Equilibrium efficiency improvement in mimo interference systems: A decentralized stream control approach,” *IEEE Transactions on Wireless Communications*, pp. 2984–2993, 2007.

[75] H. P. Young, *Individual Strategy and Social Structure*. Princeton, NJ: Princeton University Press, 1998.

[76] D. Bertsekas and R. Gallager, *Data Networks*. Prentice Hall; 2 edition, 1991.

[77] L. Kleinrock, *Queueing Systems, Volume 1, Theory*. Wiley-Interscience; 1 edition, 1975.

[78] P. J. M. V. Laarhoven and E. H. L. Aarts, *Simulated Annealing: Theory and Applications*. Holland: Reidel, 1987.

[79] R. K. Lam, D.-M. Chiu, and J. C. S. Lui, “On the access pricing issues of wireless mesh networks,” *IEEE ICDCS*, 2006.

[80] G. Debreu, “A social equilibrium existence theorem,” *Proceedings of the National Academy of Sciences*, pp. 886–893, 1952.

[81] J. Yee and H. Pezeshki-Esfahani, “Understanding wireless lan performance trade-offs,” *Communication Systems Design*, Nov. 2002.

[82] A. Goldsmith, *Wireless Communications*. Cambridge University Press, 2005.

[83] H. Viswanathan and S. Mukherjee, “Throughput-range tradeoff of wireless mesh backhaul networks,” *IEEE Journal on Selected Areas in Communications*, Mar. 2006.

[84] I. F. Akyildiz and I. H. Kasimoglu, “Wireless sensor and actor networks: Research challenges,” *Elsevier Computer Networks*, 2004.

[85] J. Yick, B. Mukherjee, and D. Ghosal, “Wireless sensor network survey,” *Elsevier Computer Networks*, 2007.

[86] A. Stolyar, “Large deviations of queues under qos scheduling algorithms,” *Proc. Allerton Conf. of Comm, Control, and Computing*, 2006.

[87] X. Lin, “On characterizing the delay performance of wireless scheduling algorithms,” *Proc. Allerton Conf. of Comm, Control, and Computing*, 2006.

[88] Y. Song and Y. Fang, “Distributed rate control and power control in resource-constrained wireless sensor networks,” *IEEE MILCOM*, 2007.

[89] L. Ying, S. Shakkottai, and A. Reddy, “On combining shortest-path and back-pressure routing over multihop wireless networks,” *IEEE INFOCOM*, 2009.

[90] W. F. Trench, *Introduction to Real Analysis*. Prentice Hall, 2003.

[91] A. B. Sharma, L. Golubchik, R. Govindan, and M. J. Neely, “Dynamic data compression in multi-hop wireless networks,” *ACM SIGMETRICS*, 2009.

[92] D. Qiao and S. Choi, “Fast-responsive link adaptation for IEEE 802.11 WLANs,” *IEEE ICC*, 2003.

[93] P. Chevillat, J. Jelitto, A. N. Batteto, and H. L. Truong, “A dynamic link adaptation algorithm for IEEE 802.11a wireless LANs,” *IEEE ICC*, 2003.

[94] M. Lacage, M. H. Manshaei, and T. Turletti, “IEEE 802.11 rate adaptation: A practical approach,” *ACM MSWiM*, 2004.

[95] J. Kim, S. Kim, S. Choi, and D. Qiao, “CARA: Collision-aware rate adaptation for IEEE 802.11 WLANs,” *IEEE INFOCOM*, 2006.

[96] S. H. Y. Wong, H. Yang, S. Lu, and V. Bharghavan, “Robust rate adaptation for 802.11 wireless networks,” *ACM MOBICOM*, 2006.

[97] B. Sadeghi, V. Kanodia, A. Sabharwal, and E. Knightly, “Opportunistic media access for multirate ad hoc networks,” *ACM MOBICOM*, 2002.

[98] S. Pal, S. R. Kundu, K. Basu, and S. K. Das, “IEEE 802.11 rate control algorithms: Experimentation and performance evaluation in infrastructure mode,” the University of Texas at Arlington, Tech. Rep., 2006.

[99] Q. Pang, V. C. M. Leung, and S. C. Liew, “A rate adaptation algorithm for IEEE 802.11 WLANs based on MAC-layer loss differentiation,” *IEEE BroadNets*, 2005.

[100] H. Jung, K. Cho, Y. Seok, T. Kwon, and Y. Choi, “RARA: Rate adaptation using rate-adaptive acknowledgement for IEEE 802.11 WLANs,” *IEEE CCNC*, 2008.

[101] G. Judd, X. Wang, and P. Steenkiste, “Low-overhead channel-aware rate adaptation,” *ACM MOBICOM (Extended Abstract)*, 2007.

[102] J. C. Bicket, “Bit-rate selection in wireless networks,” Master’s thesis, Massachusetts Institute of Technology, 2005.

[103] G. Holland, N. Vaidya, and P. Bahl, “A rate-adaptive mac protocol for multi-hop wireless networks,” *ACM MOBICOM*, 2001.

[104] K. Ad and M. Leo, “WaveLAN(C)-II: a high-performance wireless LAN for the unlicensed band,” *Bell Labs Technical Journal*, pp. 118–133, 1997.

[105] I. Haratcherev, K. Langendoen, R. Lagendijk, and H. Sips, “Hybrid rate control for IEEE 802.11,” *ACM MOBIWAC*, 2004.

[106] [Online]. Available: http://madwifi.org/browser/madwifi/trunk/ath_rate/onoe

[107] J.-H. Yun and S.-W. Seo, "Novel collision detection scheme and its applications for IEEE 802.11 wireless LANs," *Computer Communications*, 2007.

[108] S.-C. Wang and A. Helmy, "BEWARE: Background traffic-aware rate adaptation for IEEE 802.11 MAC," *IEEE WoWMoM*, 2008.

[109] [Online]. Available: http://secure.enterasys.com/products/wireless/RBTBG-AW

[110] J. Choi, K. Park, and C. kwon Kim, "Cross-layer analysis of rate adaptation, DCF and TCP in multi-rate WLANs," *IEEE INFOCOM*, 2007.

[111] S. Rayanchu, A. Mishra, D. Agrawal, S. Saha, and S. Banerjee, "Diagnosing wireless packet losses in 802.11: Separating collision from weak signal," *IEEE INFOCOM*, 2008.

[112] J. Choi, J. Na, K. Park, and C. kwon Kim, "Adaptive optimization of rate adaptation algorithms in multi-rate WLANs," *IEEE ICNP*, 2007.

[113] F. Kelly, A. Maulloo, and D. Tan, "Rate control in communication networks: shadow prices, proportional fairness and stability," *Journal of Operation Research Society*, pp. 237–252, 1998.

[114] S. H. Low and D. E. Lapsley, "Optimization flow control — I: basic algorithm and convergence," *IEEE/ACM Transactions on Networking*, no. 6, pp. 861–874, 1999.

[115] T. G. Griffin, F. B. Shepherd, and G. Wilfong, "The stable paths problem and interdomain routing," *IEEE/ACM Transactions on Networking*, pp. 232–243, 2002.

[116] J.-W. Lee, A. Tang, J. Huang, M. Chiang, and A. R. Calderbank, "Reverse-engineering MAC: A non-cooperative game model," *IEEE Journal on Selected Areas in Communications*, Jun. 2007.

[117] F. Cali, M. Conti, and E. Gregori, "Dynamic tuning of the IEEE 802.11 protocol to achieve a theoretical throughput limit," *IEEE/ACM Transactions on Networking*, 2000.

[118] P. Glasserman, *Gradient Estimation Via Perturbation Analysis*. Springer, 1991.

[119] C. G. Cassandras and S. Lafortune, *Introduction to Discrete Event Systems (Second Edition)*. Springer, 2008.

[120] X.-R. Cao, "A basic formula for online policy gradient algorithms," *IEEE Transactions on Automatic Control*, 2005.

[121] ——, *Stochastic Learning and Optimization: A Sensitivity-Based Approach*. Springer, 2007.

[122] Y. Xing and R. Chandramouli, "Price dynamics in competitive agile spectrum access markets," *IEEE Journal on Selected Areas in Communications*, Mar. 2007.

[123] M. A. Haleem and R. Chandramouli, "Adaptive downlink scheduling and rate selection: A cross layer design," *IEEE Journal on Selected Areas in Communications*, Jun. 2005.

[124] S. Kiran and R. Chandramouli, "An adaptive energy-efficient link layer protocol using stochastic learning control," *IEEE ICC*, 2003.

[125] Y. Xing and R.Chandramouli, "Distributed discrete power control for bursty transmissions over wireless data networks," *IEEE ICC*, 2004.

[126] G. I. Papadimitriou, M. Sklira, and A. S. Pomportsis, "A new class of ϵ-optimal learning automata," *IEEE Transactions on Systems, Man, and Cybernetics*, pp. 346–354, 2004.

[127] M. A. L. Thathachar and P. S. Sastry, "Varieties of learning automata: An overview," *IEEE Transactions on Systems, Man, and Cybernetics*, Dec. 2002.

[128] ——, *Networks of Learning Automata - Techniques for Online Stochastic Optimization*. Kluwer Academic Publishers, 2004.

[129] T. S. Rappaport, *Wireless Communications Principles and Practices*. Prentice Hal, 2002.

[130] J. del Prado Pavon and S. Choi, "Link adaptation strategy for IEEE 802.11 WLAN via received signal strength measurement," *IEEE ICC*, 2003.

[131] I. F. Akyildiz, L. W. Y., V. M. C., and M. S., "Next generation/dynamic spectrum access/cognitive radio wireless networks: A survey," *Elsevier Computer Networks*, Sep. 2006.

[132] K. Xing, X. Cheng, L. Ma, and Q. Liang, "Superimposed code based channel assignment in multi-radio multi-channel wireless mesh networks," *ACM MOBICOM*, pp. 15–26, 2007.

[133] H. T. Cheng, H. Jiang, and W. Zhuang, "Distributed medium access control for wireless mesh networks," *Wireless Communications and Mobile Computing*, pp. 845–864, 2006.

[134] [Online]. Available: http://www.sharedspectrum.com

[135] C. Ghosh and D. P. Agrawal, "Channel assignment with route discovery (card) using cognitive radio in multi-channel multi-radio wireless mesh networks," *IEEE SECON*, 2006.

[136] T. Chen, H. Zhang, G. M. Maggio, and I. Chlamtac, "Cogmesh: A cluster-based cognitive radio network," *IEEE DySPAN*, 2007.

[137] A. AL-Fuquha, B. Khan, A. Rayes, M. Guizani, O. Awwad, and G. B. Brahim, "Opportunistic channel selection strategy for better qos in cooperative networks with cognitive radio capabilities," *IEEE Journals on Selected Areas in Communications (JSAC)*, pp. 156–167, Jan. 2008.

[138] K. R. Chowdhury and I. F. Akyildiz, "Cognitive wireless mesh networks with dynamic spectrum access," *IEEE Journal on Selected Areas in Communications (JSAC)*, pp. 168–181, Jan. 2008.

[139] [Online]. Available: http://wirelessman.org/le/

[140] [Online]. Available: http://www.ece.gatech.edu/research/labs/bwn/mesh/

[141] D. Awduche, L. Berger, D. Gan, T. Li, V. Srinivasan, and G. Swallow, "Rsvp-te: Extensions to rsvp for lsp tunnels," RFC 3209.

[142] B. Jamoussi, L. Andersson, R. Callon, R. Dantu, L. Wu, P. Doolan, T. Worster, N. Feldman, A. Fredette, M. Girish, E. Gray, J. Heinanen, T. Kilty, and A. Malis, "Constraint-based lsp setup using ldp," RFC 3212.

[143] D. Mitra and Q. Wang, "Stochastic traffic engineering for demand uncertainty and risk-aware network revenue management," *IEEE/ACM Transactions on Networking*, pp. 221–233, Apr. 2005.

[144] H. Wang, H. Xie, L. Qiu, Y. R. Yang, Y. Zhang, and A. Greenberg, "Cope: Traffic engineering in dynamic networks," *ACM SIGCOMM*, 2006.

[145] A. Elwalid, C. Jin, S. Low, and I. Widjaja, "Mate: Mpls adaptive traffic engineering," *IEEE INFOCOM*, pp. 1300–1309, 2001.

[146] J. He, M. Bresler, M. Chiang, and J. Rexford, "Towards robust multi-layer traffic engineering: Optimization of congestion control and routing," *IEEE Journal on Selected Areas in Communications (JSAC)*, Jun. 2007.

[147] Q. Wang and H. Zheng, "Route and spectrum selection in dynamic spectrum networks," *IEEE DySPAN*, 2005.

[148] C. Xin, B. Xie, and C.-C. Shen, "A novel layered graph model for topology formation and routing in dynamic spectrum access networks," *IEEE DySPAN*, 2005.

[149] Y. Shi and T. Hou, "Optimal power control for programmable radio networks," *IEEE INFOCOM*, 2007.

[150] T. Hou, Y. Shi, and H. Sherali, "Optimal spectrum sharing for multi-hop software defined radio networks," *IEEE INFOCOM*, 2007.

[151] ——, "Spectrum sharing for multi-hop networking with cognitive radios," *IEEE Journal on Selected Areas in Communications (JSAC)*, pp. 146–155, Jan. 2008.

[152] Y. Shi and T. Hou, “A distributed optimization algorithm for multi-hop cognitive radio networks,” *IEEE INFOCOM*, 2008.

[153] J.-W. Lee, R. R. Mazumdar, and N. B. Shroff, “Opportunistic power scheduling for dynamic multi-server wireless systems,” *IEEE Transactions on Wireless Communications*, Jun. 2006.

[154] ——, “Joint opportunistic power scheduling and end-to-end rate control for wireless ad-hoc networks,” *IEEE Transactions on Vehicular Technology*, Mar. 2007.

[155] A. A. Abidi, “The path to the software-defined radio receiver,” *IEEE Journal of Solid-State Circuits*, pp. 954–966, 2007.

[156] P. G. Cook and W. Bonser, “Architectural overview of the speakeasy system,” *IEEE Journal on Selected Areas in Communications (JSAC)*, pp. 650–661, 1999.

[157] F. K. Jondral, “Software-defined radio - basics and evolution to cognitive radio,” *EURASIP Journal on Wireless Cmmunications and Networking*, pp. 275–283, 2005.

[158] H. Kim and K. G. Shin, “In-band spectrum sensing in cognitive radio networks: Energy detection or feature detection?” *ACM MOBICOM*, 2008.

[159] P. Kyasanur, J. So, C. Chereddi, and N. H. Vaidya, “Multi-channel mesh networks: Challenges and protocols,” *IEEE Wireless Communications*, Apr. 2006, invited paper.

[160] A. R. S. Bahai, B. R. Saltzberg, and M. Ergen, *Multi-carrier Digital Communications: Theory and applications of OFDM*. Springer, 2004.

[161] M. Chiang, “To layer or not to layer: Balancing transport and physical layers in wireless multihop networks,” *IEEE INFOCOM*, 2004.

[162] D. P. Bertsekas, *Nonlinear Programming*. Athena Scientific, 1999.

[163] H. J. Kushner and G. G. Yin, *Stochastic Approximation and Recursive Algorithms and Applications*. Springer, 2003.

[164] Q. Gao, J. Zhang, and S. V. Hanly, “Cross-layer rate control in wireless networks with lossy links: Leaky-pipe flow, effective network utility maximization and hop-by-hop algorithms,” *IEEE INFOCOM*, 2008.

[165] M. H. Van der Vlerk, “Stochastic programming bibliography,” 1996-2007.

[166] K. Swingler, *Applying Neural Networks: A Practical Guide*. Morgan Kaufmann, 1996.

[167] M. A. L. Thathachar and P. S. Sastry, *Networks of Learning Automata*. Kluwer Academic Publishers, 2004.

[168] D. Lehmann, L. I. Ocallaghan, and Y. Shoham, “Truth revelation in approximately efficient combinatorial auctions,” *Journal of the ACM (JACM)*, pp. 577 – 602, 2002.

[169] G. Zeng, B. Wang, Y. Ding, L. Xiao, and M. Mutka, “Multicast algorithms for multi-channel wireless mesh networks,” *IEEE ICNP*, 2007.

[170] H. J. Kushner, *Approximation and Weak Convergence Methods for Random Processes*. MIT Press, 1984.

[171] P. Billingsley, *Convergence of Probability Measures*. Wiley, New York, 1968.

[172] F. Aluffi-Pentini, V. Parisi, and F. Zirilli, “Global optimization and stochastic difference equations,” *Journal of Optimization Theory and Applications*, pp. 1–26, 1985.

[173] A. S. Poznyak and K. Najim, *Learning Automata and Stochastic Optimization*. Springer, 1997.

[174] Y. Song, C. Zhang, and Y. Fang, “Throughput maximization in multi-channel wireless mesh access networks,” *IEEE ICNP*, 2007.

[175] K. Yang, Y. Wu, J. Huang, X. Wang, and S. Verdu, “Distributed robust optimization for communication networks,” *IEEE INFOCOM*, 2008.

BIOGRAPHICAL SKETCH

Yang Song received his Bachelor and Master of Science degrees from Dalian University of Technology and the University of Hawaii in 2004 and 2006, respectively. Since August 2006, he has been working as a Research Assistant with the Wireless Networks Laboratory in the Department of Electrical and Computer Engineering at the University of Florida. His research topics include routing, scheduling and cross layer design in wireless networks, optimization and control in complex networks, applied network economics, efficient algorithmic design in information networks, and social computing.